

MASTER

Tensairity arch

in what way can a rapidly deployable, demountable Tensairity arch be realised with optimal structural properties?

Zwarts, S.H.C.

Award date:
2015

[Link to publication](#)

Disclaimer

This document contains a student thesis (bachelor's or master's), as authored by a student at Eindhoven University of Technology. Student theses are made available in the TU/e repository upon obtaining the required degree. The grade received is not published on the document as presented in the repository. The required complexity or quality of research of student theses may vary by program, and the required minimum study period may vary in duration.

General rights

Copyright and moral rights for the publications made accessible in the public portal are retained by the authors and/or other copyright owners and it is a condition of accessing publications that users recognise and abide by the legal requirements associated with these rights.

- Users may download and print one copy of any publication from the public portal for the purpose of private study or research.
- You may not further distribute the material or use it for any profit-making activity or commercial gain

Tensairity arch

End colloquium report

Ing. S.H.C. (Sander) Zwarts
3 December 2015

Colophon

Tensairity arch

In what way can a rapidly deployable, demountable Tensairity arch be realised with optimal structural properties?

End colloquium report

This report represents the results of the graduation project, conducted by Sander Zwarts at Buitink Technology.

Graduation committee

Ir. S.R. de Vries	Buitink Technology B.V.
Ir. A.D.C. Pronk	University of Technology Eindhoven
Prof. Dr. Ing P.M. Teuffel	University of Technology Eindhoven
Ir. A.P.H.W. Habraken	University of Technology Eindhoven

Graduate student

Ing. S.H.C. (Sander) Zwarts
0811180
Master Architecture, Building and Planning
Building Technology – Product Development
University of Technology Eindhoven
The Netherlands

3 December 2015
Duiven, the Netherlands

Summary

The goal of structural engineering of tent structures is to find an optimal balance between tension and compression. This balance is optimized with Tensairity. The original Tensairity beam consists of a compression element, a cylindrical low pressure air beam and a tensioned cable connected to the ends of the compression element. The cables close the force flow between the cables and the compression element. These compression elements determine the load bearing capacity of the structure. The air beam prevents the compression element from buckling. Further development of the Tensairity principle led to the transformation of the cylindrical air beam to a cigar shaped air beam, enhancing the stiffness of the beam. The addition of vertical/triangular webbing enhanced the stability of the Tensairity beams and made it possible to remove the cables.

Buitink Technology developed an interesting Tensairity concept of a Tensairity arch with a triangular web in collaboration with Tentech and ABT. The concept was never further developed, while a lot of progress had to be made in order to actually produce and use it. This became the basis for this graduation project. The main goal of this project was to develop and build an optimal Tensairity arch.

Multiple designs of the arch were created based on a tent structure designed during this project. The fabric hull of the final design consisted of a PVC coated Polyester outer layer, PVC coated Aramid webs and PU-foil inflatable bags. The compression elements were made of aluminium tubes. The different layers of fabric were connected through fabric sleeves, where the compression elements were slid in. The arch was connected to two steel impositions, which were anchored to the ground.

The Tensairity arch was tested after construction. Three different tests were performed: a load in the middle¹, a load at a quarter² and a load distributed over five points³. The deformation of the arch was tested. The arch was asymmetric, which gave altered results. The overall results were quite expected, except for a plastic deformation of the arch. The first test was done again in order to verify this conclusion.

The Tensairity arch was designed in Oasys GSA, where the three tests were simulated. The deformation of the arch, the forces in the fabric and the bending stress in the compression elements were investigated and compared with the physical tests. The simulation showed similar type of deformation for the first two test, but deformed much less than the physical test situation. The simulation results were quite different from the physical test results in the third test. The differences in the tests are accounted to the fact that the physical arch was asymmetric and plastically deformed during each test. Some inaccuracies in the simulation model were also present, which made the exact simulation results less reliable.

It can be concluded that the optimal Tensairity arch was not found during this project. The fabrication of the arch was very complex and time consuming. The plastic deformation was also an undesired result. Further development is necessary in order to create an optimal Tensairity arch. Insight in the Tensairity principle was gained and bottlenecks with detailing have become clear and will be beneficial for future development.

Preface

The end colloquium is the final assessment of the graduation process. It is an elaboration on the mid colloquium presented in May 2015. The student presents the results obtained during the entire project.

The graduation project is the end part of the master program of Building Technology within the faculty of Architecture, Building and Planning at University of Technology Eindhoven. The main subject of this project is the designing, engineering, simulating, realisation and testing of a rapidly deployable, demountable Tensairity arch.

First of all I would like to give special thanks to Rienk de Vries for giving me the opportunity to build the Tensairity arch at Buitink Technology. I would also like to thank Marnix Bakker, Harry Bleumink and Roel Bloemberg from Buitink Technology for sharing their knowledge and their assistance. Finally I would like to thank the employees at the production hall of Buitink Technology for assisting me during the production. I especially want to thank Ratna Ho and Joffrey van Santen for stitching and welding the arch.

I also want to thank my graduation committee, Patrick Teuffel, Arno Pronk and Arjan Habraken for their input in the project. I especially want to thank Arjan Habraken, who helped me out a lot with the simulations in Oasys GSA.

S.H.C. Zwarts
Arnhem 3 December 2015

Table of Contents

Introduction	6	Test set-up	45
Project description	7	Test results	45
Alteration content project	7	Reason of plastic deformation	51
Research questions	7	Comparison with study by R. Maffei	51
Research methodology	7	Comparison with study (Crettol, Gauthier, Luchsinger, & Vogel, 2010)	53
Buitink Technology	7	Simulation of Tensairity arch in Oasys GSA	56
Ho Mulder Design Factory	7	Design in Oasys GSA	57
Literature study	8	Permanent loads	57
Fabric structures	9	Start situation	58
Production process of fabrics	10	Comparison of simulations	59
Fabric materials	10	Final simulations	60
Production methods	12	Comparison of test and simulation	64
European regulations for tent structure	13	Comparison of start situation	65
Tensairity principle	13	Comparison of test one	65
Tensairity projects	16	Comparison of test two	66
Design structure	18	Comparison of test three	66
Mind map and program of requirements	19	Verifying effect asymmetry of beam on test results	67
Preliminary design	19	Conclusion and Discussion	68
Alternative design	19	Design of the tent structure	69
Final design	21	Design, production and end result of the arch	69
Design Tensairity arch	24	Test Results	69
Design arch overall	25	Simulation results	70
Preliminary design section Tensairity arch	25	Comparison of test and simulation	70
Final design section Tensairity arch	29	End conclusion	71
Detail imposition	32	Bibliography	72
Division compression elements	33	Appendix A	75
Self-weight of Tensairity arch	33	Appendix B	76
Building of Tensairity arch	34	Appendix C	77
Building steel impositions	35	Appendix D1	78
Connection of aluminium compression elements	35	Appendix D2	79
Building inflatable bags	36	Appendix E	80
Building fabric hull	36	Appendix F	82
Construction of Tensairity arch	39	Appendix G	83
Testing of connections	41	Appendix H1	84
Conclusion of testing	43	Appendix H2	85
Testing of Tensairity arch	44	Appendix H3	86

Appendix H4	87
Appendix I	88
Appendix J	91
Appendix K1	93
Appendix K2	94
Appendix K3	95
Appendix L1	96
Appendix L2	97
Appendix L3	98
Appendix M	100
Appendix N	102

Introduction

This graduation project is the final part of the master program of building technology on the University of Technology Eindhoven. The project consists of three phases and four assessments. This report describes the process and results of all three phases of this project.

The chapters in this report describe the activities and results of the project in chronological order in which they were conducted. Conclusions and recommendations are made in the end.

This chapter describes the subject, research questions and approach of this project. It describes the collaboration with Buitink Technology as well. This chapter is a summary of the graduation plan with several alterations, which was submitted in October 2014.

Project description

Buitink Technology, Tentech and ABT designed a tent structure with Tensairity arches. It was never further developed than a preliminary design. The preceding project by Buitink Technology contained several gaps in the design and needed improvement. This graduation project was an elaboration on that project, due to a profound interest in lightweight structures. More information on the preceding project by Buitink Technology can be found in the literature study.

The objective of this graduation project was to improve the Tensairity arch from Buitink and to determine its load bearing capacities. This was achieved by designing, simulating, building and testing of the arch. The results will be used for further research and possible marketing purposes by Buitink Technology.

Alteration content project

The content of the graduation project was altered during phase two. Phase one consisted of the literature study, creation of a graduation plan and the creation of a preliminary design of the structure. In consultation with the graduation supervisors, it became clear that the content of the project had to be reduced during phase two. A single Tensairity beam was designed, built and tested during the remaining two phases. The preliminary design of the tent structure was used for the design of the arch.

Research questions

The main goal of this project was to develop and build an optimal Tensairity arch. This was formulated in a main research question, which was answered with the help of several sub research questions.

Main research question

In what way can a rapidly deployable, demountable Tensairity arch be realised with optimal structural properties?

Sub research questions

- In what way can a Tensairity arch be applied in a structure, which meets all demands and regulations?
- In what way can a Tensairity arch be designed which meets all demands and regulations?
- In what way can a good balance between costs, sustainability and structural properties be made?
- To what extent do the simulation and physical testing match?

Research methodology

This project was directed through a predefined designing methodology (Appendix A), which had the function of organising the graduation process and providing an overview of the phases for the structure of the report. This methodology was derived from the design methodology from Van den Kroonenberg (1974) and Zeiler (1994). It was a serial process consisting of five main steps: analysis, synthesis, selection, designing and construction. This design methodology was an iterative process, which means that during a decision point the student had to decide whether he continues with the next step or redoes the previous one(s). The progress was evaluated during the entire process, in cooperation with the supervisors.

Buitink Technology

This graduation project was conducted at Buitink Technology in Duiven (the Netherlands). Colleagues at Buitink Technology supervised and assisted during the entire project. The physical arch was produced by colleagues at Buitink, assisted and supervised by the student.

Ho Mulder Design Factory

Ho Mulder Design Factory is creating an inflatable tent structure in cooperation with Buitink Technology. Conventional inflatable arches are used instead of Tensairity arches. A collaboration was started during this graduation project, because the projects were quite similar. Tent structure designs were exchanged during the project, complementing this graduation project.

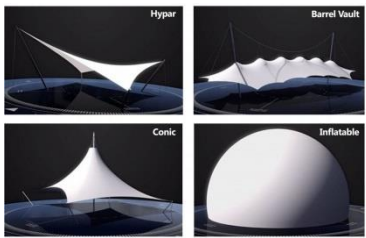






Literature study

A literature study was performed at the start of this graduation project. The following subjects were researched:

- Fabric structures,
- Production process of fabrics,
- European regulations for tent structure,
- Tensairity principle,
- Tensairity projects.

Fabric structures

Fabrics give many advantages (Lightweight, transportability, etc.), but wind and other loads can bring complications to the structure. In order to withstand these loads, all structures need to comply to NEN-EN 13782; Temporary structures; Tents; Safety (2005). It states all requirements regarding load bearing, fire safety, etcetera which have to be met. Several methods are available to meet these requirements, which mostly requires steel cables and aluminium (or steel) frames as support. Eight main structural types are distinguished:

<ul style="list-style-type: none"> ▪ Tensile structures 	<p>Characterized by tensioning fabric or pliable material system to provide the structural support to the structure. Three main shapes are distinguished: Hypar, Barrel Vault and Conic.</p>	
<ul style="list-style-type: none"> ▪ Cable-net structures 	<p>Single-layer anticlastic surface made of two sets of cables that are orthogonal to one another. The net usually supports a fabric or pliable material.</p>	
<ul style="list-style-type: none"> ▪ Frame supported fabric structure 	<p>A structure consisting of a frame that forms a load-bearing structure and fabric which only has a covering function.</p>	
<ul style="list-style-type: none"> ▪ Tensegrity structures 	<p>A planar or curvilinear structure composed of short discontinuous compression elements connected by tensile members to form a coherent configuration.</p>	
<ul style="list-style-type: none"> ▪ Geodesic domes 	<p>Spherical, single- or double-layered shells made up of hexagons and pentagons.</p>	
<ul style="list-style-type: none"> ▪ Grid-shell structures 	<p>A curvilinear surface (synclastic or anticlastic) composed of linear elements configured to form squares, triangles, and/or parallelograms.</p>	
<ul style="list-style-type: none"> ▪ Air-inflated structures 	<p>A structure that uses air-pressurized membrane beams, arches, or other elements to enclose space.</p>	

- Air-supported structures

A structure that attains its shape by air pressure.



(Big Span structures, N.D.)

Production process of fabrics

The production of textile fabrics consists of two steps: interlacing of Warp and Weft threads and coating of fabric (Figure 1). The Warp thread follows the longitudinal direction of fabric, and the Weft thread the transverse direction. The Warp thread is kept under tension during the weaving process. The

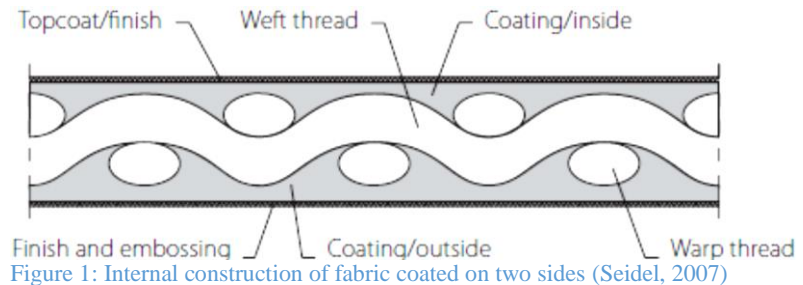


Figure 1: Internal construction of fabric coated on two sides (Seidel, 2007)

Weft thread is interlaced with the Warp thread using a rapier loom. The textile fabrics are subject to numerous of structural, chemical and biological influences. It is therefore necessary to treat the fabric after the weaving process is finished. The fabrics are coated and a top coating/finish is applied on the surface of the fabric. (Seidel, 2007)

Fabric materials

There are several materials used for fabric structures. The choice of material depends on multiple factors, of which the most important factors are:

- Type of structure
- Size of the structure
- Temporary or permanent structure
- Structural or aesthetical function

The most used fabrics are PVC coated Polyester, PTFE coated Fiberglass and ETFE foil. Many other materials exist, like PCV coated Aramid and PU-foil. These are less common in fabric structures.

A comparison of some of the most important properties was made in order to gain insight of the qualities of these fabrics (Table 1).

PVC coated Polyester

Poly-Vinyl-Chloride (PVC) coated polyester is one of the most frequently used base material for multiple products and applications. This is due to its strength, durability, costs and stretch. Even though PTFE coated fiberglass has better overall properties, PVC coated polyester has the big advantage of being much cheaper compared to PTFE coated fiberglass. (Buitink Technology, N.D.), (Son, 2007),

PTFE coated Fiberglass

Poly Tetra Fluoro Ethylene or Teflon (PFTE) coated glass cloth is one of the most used materials for tensile structures. It has qualities that exceed most of the other materials used in tensile architecture. It is often the material of choice for stadium domes (both air- and cable-supported) and many other permanent structures, due to its excellent properties (high tensile strength, great life expectancy, thermal performance.). (Architen Landrell, 2010), (Son, 2007).

ETFE foil

Ethylene Tetra Fluoro Ethylene (ETFE) is a copolymer that is extruded into thin films which can be used as a single-layer membrane or as a multi-layer cushion. The cushions require an additional frame and must be pressurised continually by an inflation unit. ETFE can be transparent, which makes it for example perfect for skylights and other applications where transparency is preferred. It has a high life expectancy (Wilson, 2013), (Buitink Technology, 2011) (Son, 2007).

	PTFE coated fiberglass	PVC coated polyester	ETFE foil
Weight	800 – 1500 g/m ²	600-1450 g/m ²	85 – 350 g/m ²
Panel size	Width: 1,5 – 2,5 m.	Width: 2,5 m	Width 1,5m, thickness 25-250 μm
Tensile strength	3500MPa	350 to 1200 MPa	0.1mm thick = 225 N/5cm
Fire performance	Inherent non-flammable.	Flame retardant	Flame retardant
Solar performance	Light transmission rate: 12-16%, 75% reflection, 10% absorption.	Light translucency up to 22%	Single layer approx. 85% light transmission, Transmission across UV-range approx. 83-88%, Absorbs a large proportion of IR light transmitted
Thermal performance	U-value = 4-5 W/m ² K.	U value = 5,5 =6,5 W/m ² K	Single ply ETFE membrane U-value = 5.6 W/m ² K, Three layer cushion U-value = 1.96 W/m ² K.
Acoustics	Acoustically relatively transparent, but provide a degree of absorption and noise attenuation.	Weakening index = 14 dBA	High insulation value depending on amount of layers
Maintenance	Little need of maintenance due to cleaning action of rain on the Teflon outer layer.	Top layer erodes over time, so it can become dirty	Water washes away any dirt. Harsh dirt can be cleaned with light PH neutral detergents.
Life expectancy	Over 30years	10-15 years	Over 25 years
Costs	400 to 800 €/m ²	75 to 100 €/m ²	single layer: 15-25 €/m ²

Table 1: Comparison of fabric materials (Buitink Technology, 2011), (Architen Landrell, 2010), (Son, 2007), (Buitink Technology, N.D.)

Production methods

There are two main production methods used in fabric architecture: welding and sewing. The production method partially depends on the type of joint. Several joint types are possible, shown in Figure 2.









Joint type/production	Erection method	Connecting element	Connection function	Location of load introduction
Welding	—	 fabric or foil	bonding	surface
Glueing	—	 fabric or foil	bonding	surface
Sewing	—	 fabric or foil, seam	mechanical	surface
Welding or sewing	—	 fabric, webbing (sewing thread)	bonding or mechanical	surface or edge
Welding	pull-through	 fabric, rope or tube	form-fit	edge
Welding	hanging clamping bolting	 fabric or foil, keder, clamping plate, bolts, clip, rope or tube	form-fit mechanical	edge
Welding	pull-through	 fabric or foil, keder, keder rail	form-fit	surface or edge
Welding	hanging clamping bolting	 fabric or foil, keder, clamping plate, bolts	form-fit mechanical	surface or edge

Figure 2: Joint Types (Seidel, 2007)

Welding

Welding basically happens in two possible ways: hot air welding (Figure 3) or high-frequency welding (Figure 4). (Seidel, 2007)

Hot air machines heatens the fabric, making it possible to weld the two surfaces together. Hot air machines provide fast, decent seams. However it requires the right movement speed and temperature, because it can result in fabric burns (moving too slowly / too high temperature), or weak seams (moving too fast / too low temperature).

High frequency machines weld through pressure and heat. High-frequency radiation causes fabrics to heathen between two electrodes. The seam has to cool off under pressure in order to harden the material. The quality of the seam depends on the temperature and pressure during the welding process and the time taken for the process.



Figure 3: Hot air welding (Ascent Roofing LTD, N.D.)



Figure 4: High frequency welding (Forsstrom, N.D.)

Sewing

Sewing is a traditional method of joining two pieces of fabric (Figure 5). Fast and strong connections can be made with sewing. Special care has to be taken on the tidiness. Disproportionate sewing speeds causes the sewing needle to heat up and burn holes in the fabric (Seidel, 2007).



Figure 5: Sewing machine (Seidel, 2007)

There are three main type of seams (Figure 6, Figure 7 and Figure 8), while several derived types also exist. Some of these seams hide the end of the seam from sight (turned-in seam and hem-seam). (Seidel, 2007)



Figure 6: Flat seam (Seidel, 2007)



Figure 7: Turned-in seam (Seidel, 2007)



Figure 8: Hem-seam (Seidel, 2007)

European regulations for tent structure

The leading regulation in the fabric architecture is the ‘NEN-EN 13782:2005; Temporary structures – Tents- Safety’. These regulations are mainly made to secure the safety of the user. The European regulation states several requirements on different aspects. Aspects like ‘design and manufacture criteria’ and ‘use and operation criteria’ (Annex C and D) have a direct influence in the design of the tent structure and are used in a preliminary stage of this project. Aspects like load bearing capacity, stability and strength of components (chapter one to Annex B) are used in a later stage of the project.

Tensairity principle

The main principle

The goal of structural engineering with tent structures is to find an optimal balance between tension and compression. This balance is optimized with Tensairity. A basic Tensairity beam contains a compression element (different materials possible), a cylindrical low pressure air beam and a tensioned cable connected to each end of the compression element (Figure 9). The cables close the force flow between the cables and the compression element. These elements determine the load bearing capacity of the structure. The air beam prevents the compression element from buckling, creating a stabilizing function for the beam, giving it the possibility to operate with low pressured air (Figure 10). This enables minimisation of the dimensions of the compression element and the cables, which makes it possible to create a lightweight design (R.H. Luchsinger, 2004).

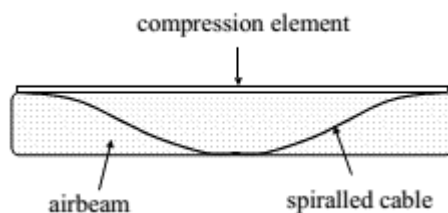


Figure 9: Tensairity principle (R.H. Luchsinger, 2004)

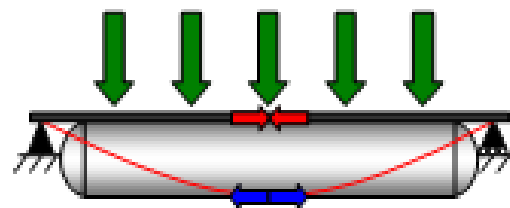


Figure 10: Tensairity principle (EMPA, N.D.)

Advantages of Tensairity

Tensairity is an interesting concept, due to the many important properties it has gained from both pneumatic structures and cable-strut structures (Figure 11). Its most important advantages are that it is lightweight while still being able to bear heavy loads. It is rapidly deployable, and has a small transport volume.

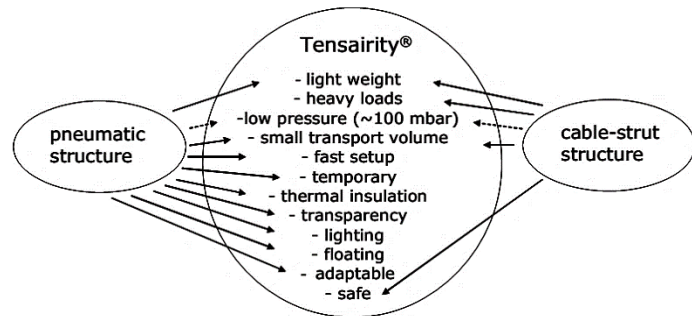


Figure 11: properties of Tensairity (Luchsinger & Crettol, N.D.)

Shapes of Tensairity

Various shapes of the Tensairity beams have been developed since the first cylindrical shape, because theoretical and numerical results made clear that improvements of the system were possible. The addition of a second cable was the first improvement (Figure 12a), because the first cable doesn't counteract the load at the first quarter of the beam. The second improvement was changing the shape of the compression element and the air beam into a cigar shape, due to the fact that it is the best shape for carrying load over a given span using compression only (Figure 12b). The third improvement involved the cable curvature radius. The larger the radius, the larger the cable force for a given contact force. The best possible curve is therefore a straight line. By degenerating the tube ends into points, the cable spiral reduces to a bended line (Figure 12c). Straightening the cables gives an asymmetric shape, which is even more favourable (Figure 12d). These improvements have led to a substantial gain in stiffness. The beam of Figure 12d deflects six times less than the original beam of Figure 12a under the same load (Figure 13). (Pedretti, Steingruber, Pedretti, & Luchsinger, N.D.)

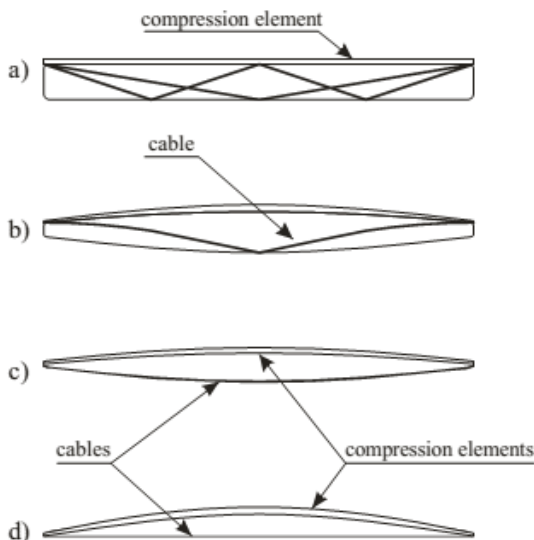


Figure 12: different shapes of Tensairity beam (Pedretti, Steingruber, Pedretti, & Luchsinger, N.D.)

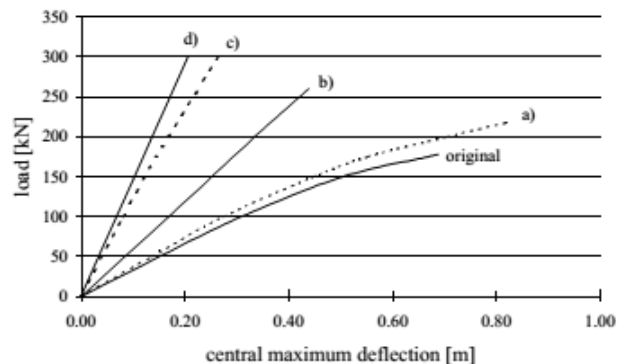


Figure 13: Load deflection diagram of different shapes (Pedretti, Steingruber, Pedretti, & Luchsinger, N.D.)

A study in 2008, performed by T.E. Wever, concluded that adding internal webbing improves the structural behaviour of the Tensairity beam (Figure 14). It however has several disadvantages: material deficiency, more complex fabrication and less slender structures. (Wever, 2008)

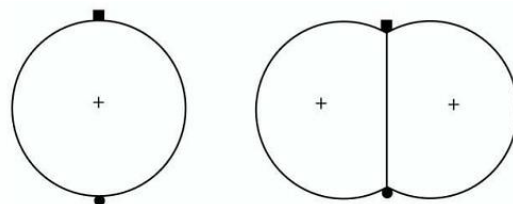


Figure 14: left: Tensairity without webbing, right: Tensairity with webbing (Wever, 2008)

Further development on the internal webbing introduced triangular webbing instead of a single vertical web (Figure 15). It has improved structural behaviour compared to the webbed beam in Figure 14. It is now more stable and can bear more load in three directions instead of two. Even though it has improved structural behaviour, it also has the disadvantage of more complex fabrication, material deficiency and an even less slender structure. (Wever, 2008)

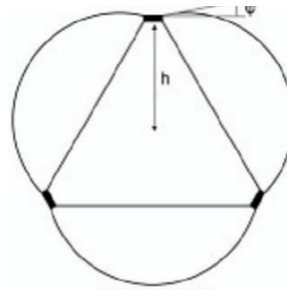


Figure 15: Tensairity with triangular webbing (Wever, Plagianakos, Luchsinger, & Marti, 2010)

Another development within the Tensairity concept was the replacement of conventional compression elements (like aluminium) into water filled tubes (Figure 16). This has the advantage of reduced weight and transport volume (Pronk, Maffei, & Martin, 2009). It has however a big disadvantage of reduced safety, because a single leak in the element would cause the element to fail under its load.

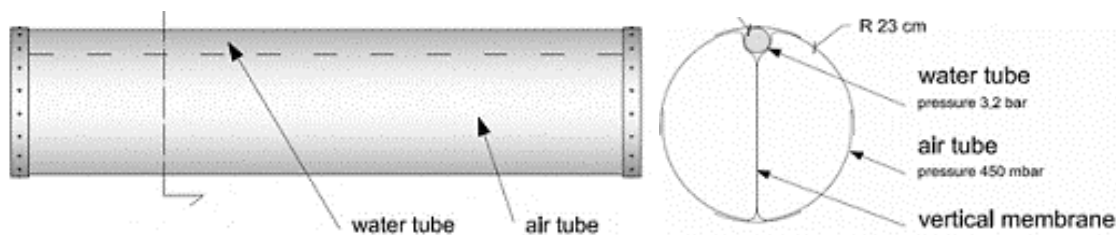


Figure 16: Combination of Tensairity with water compression elements (Pronk, Maffei, & Martin, 2009)

As mentioned earlier, Buitink Technology developed a Tensairity concept in collaboration with Tentech and ABT (Figure 17). This is an elaboration on the triangular webbing shown in Figure 15. It uses eight spindle shaped Tensairity arches with a free span of 42.5 meters as structure. Each arch contains three aluminium extrusion profiles supported by the air beam. The beam is both welded and clamped (discontinuous) at the compression elements. Cables are placed perpendicular to the Tensairity arches, in order to stabilize the structure in the transverse direction. The arches are supported by a steel triangular frame (Buitink Technology, N.D.). This concept was the basis for this graduation project.

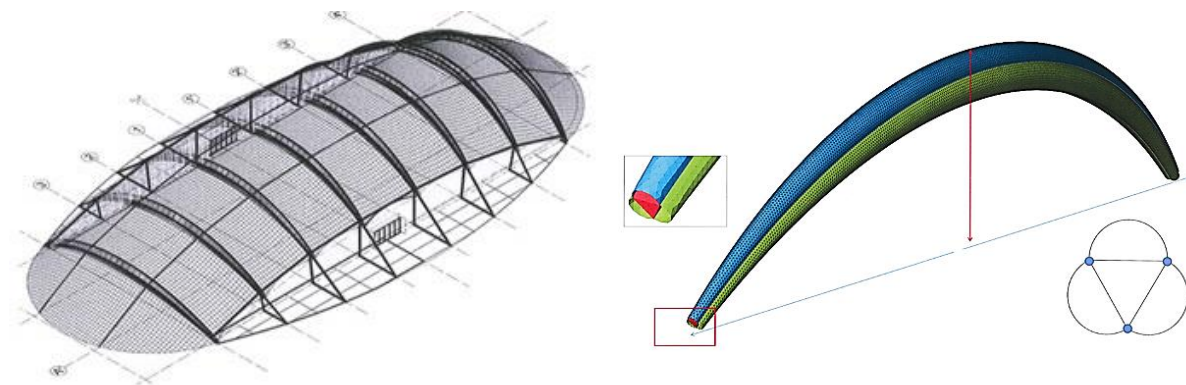


Figure 17: Elaboration Tensairity concept (Buitink Technology, N.D.)

Tensairity projects

Canopy parking garage

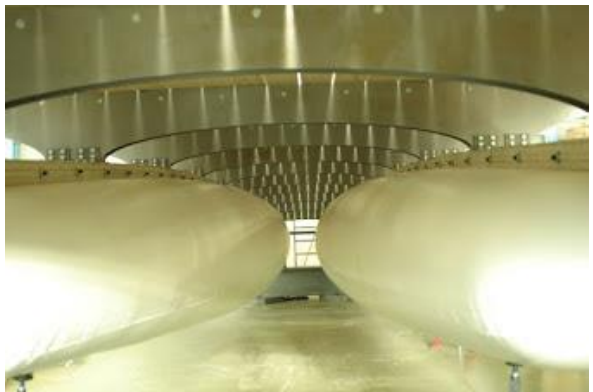
This project is a canopy for a parking garage in Montreux, Switzerland, developed by Airlight Ltd and Luscher Architectes. It is one of the most famous projects built with the Tensairity concept. Twelve spindle shaped Tensairity beams with a span up to 28 meter support the fabric roof. Integrated lighting in the beams create an amazing effect (Technet Alliance, N.D.).



(Technet Alliance, N.D.) and (Detail inspiration, N.D.)

Tensairity Bridge

The Tensairity principle was also used to develop a 52 meter span bridge structure in Lanslevillard, France. Two spindle shaped beams support the steel bridge frame. It is developed by the Swiss company Airlight Ltd. (Empa, N.D.).



(Dieterle, 2008)

Design structure

This chapter describes the design process of the tent structure. This occurred after the literature study. A mind map and program of requirements were created prior to the designing. The designs were first drawn on paper, then it was improved in Rhinoceros 5. The rendering images were made with Artlantis Studio 5.

The best preliminary designs are highlighted in this chapter. Several designs were made in collaboration with P. Mulder from Ho Mulder Design Factory. The inflatable arches in those designs were designed as conventional inflatables, but it could be transformed into Tensairity arches with minor adjustments. More designs and information on the designs can be found in the start colloquium report and the mid colloquium report.

The decision for the final design was made with help of the program of requirements and in collaboration with Buitink Technology.

The chosen design will have special attention, because it was the basis for the design of the final Tensairity arch that was tested.

Mind map and program of requirements

The mind map shown in Appendix B was created before the development of the program of requirements (Appendix C). It contained three main subjects (structural, sustainable, economical), and was divided in several categories. The mind map was used for the creation of the program of requirement. The content of the program of requirements was used as a guide for the design of the tent structure in the first phase of the project.

Preliminary design

The preliminary design was made prior to the final design (Figure 18). It had a hexagon floorplan with six arch arches intersecting at the top. The arches were supported by steel frames and walls could be included between the arches.

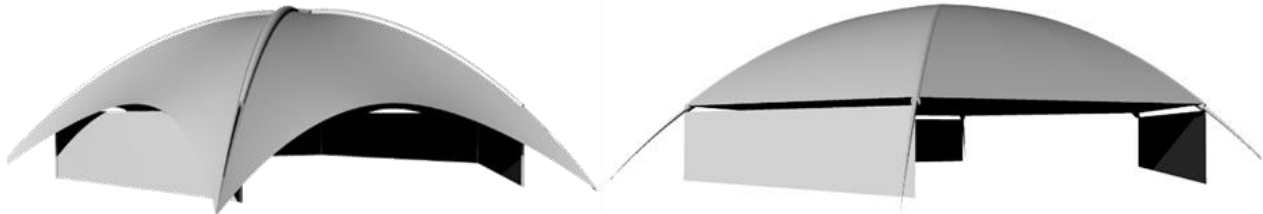


Figure 18: Preliminary design

This design had a problem with the junction in the top of the structure (Figure 19). The arches should have the largest diameter in the top, because the largest loads would come in the top. Due to the ending of the arches in the top, it was ideal to use a small diameter to create an airtight beam. However, this was not an option, because the arches wouldn't give enough stability.

Another problem with this design was the lifting of the structure. Buitink Technology made the requirement to lift the structure up from the ground. In this case it would require a special external structure / mechanism that costs a lot of money. This would affect the feasibility of the project.

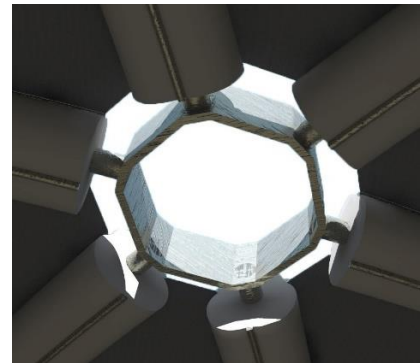


Figure 19: Top junction Tensairity arches

Alternative design

Four alternative designs were made. They showed other possibilities for the tent structures which might be interesting for future developments. The first two designs were produced prior to the final design. The last two designs were made in collaboration with P. Mulder from Ho Mulder Design Factory. They were designed as conventional inflatable arches, but minor adjustments change it into a Tensairity arch.

First alternative design

This first alternative design (Figure 20) consisted of four Tensairity arches, creating a square floor plan. A membrane was tensioned between these arches.

Water drainage in the top of the structure might need special attention. This depends on the slope of the membrane. Stability cables perpendicular to the arches towards the ground would be required.



Figure 20: First alternative design

Second alternative design

The second alternative design consisted of a hexagon floor plan with a Tensairity arch from each corner towards the centre of the structure. A tensioned membrane was placed between the arches. Two variants (Figure 21) were created: the left variant had the arches come together centred at the bottom. The right variant had a pole in the centre, where the Tensairity arches joined in the top.



Figure 21: Second alternative design (left: arches join at bottom, right: arches join at top)

Third alternative design

The third alternative design (Figure 22) had four arches from the centre, each going to a corner. Two variants of this design were created: the first variant had the tensioned membrane over the complete arch, while the other had a membrane only at the top. The structural idea of this concept was that the membrane holds the arches up. Additional cables might be required for extra stability.



Figure 22: Third alternative design

Fourth alternative design

The last alternative design (Figure 23) consisted of four inflatable arches which were rotated 60 degrees from one another. A membrane was tensioned between these arches. Two of these structures were placed next to each other, with a membrane portal to both structures. Altering the entrance of the structure could give multiple variants of this design.



Figure 23: Fourth alternative design

Final design

The base structure consisted of three Tensairity arches, which were rotated 30° from each other. These three arches were mirrored in order to get the total structure (Figure 24). Cables were added, to attain the necessary stability in transverse direction. Membranes were placed between the arches, creating an ellipsoid dome. It was possible to remove the bottom pieces of fabric, creating a different design (Figure 25).

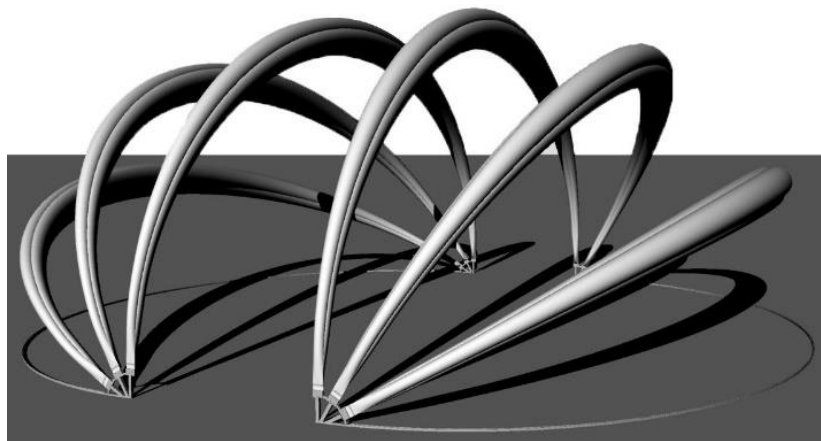


Figure 24: Configuration of arches in final design

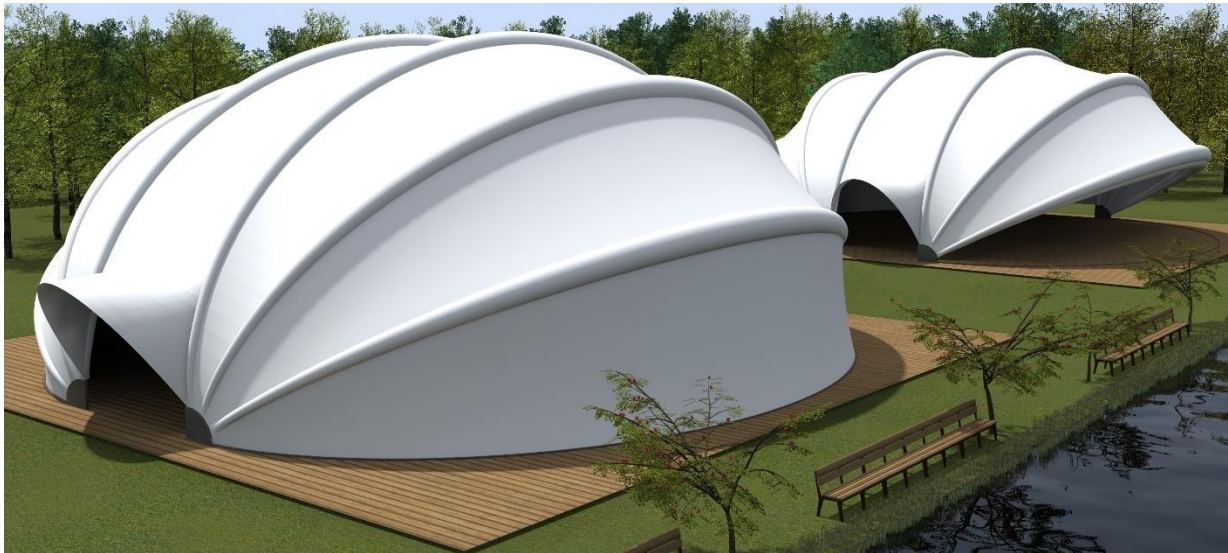


Figure 25: Final design

The beams could rotate during construction. The rotation centre would occur at the steel impositions of the arches. Cables would be used for the lifting. The construction consists of five steps (Figure 26):

- Fixation of arches to impositions, mounting of compression element to the hull, fixation of stability cables to beams, inflation of hull.
- Lifting first Tensairity arch up. Fixation of arch at the right angle.
- Lifting second Tensairity arch up. Fixation of arch at the right angle.
- Lifting third Tensairity arch up. Fixation of arch at the right angle.
- Placement of membrane between Tensairity arches.

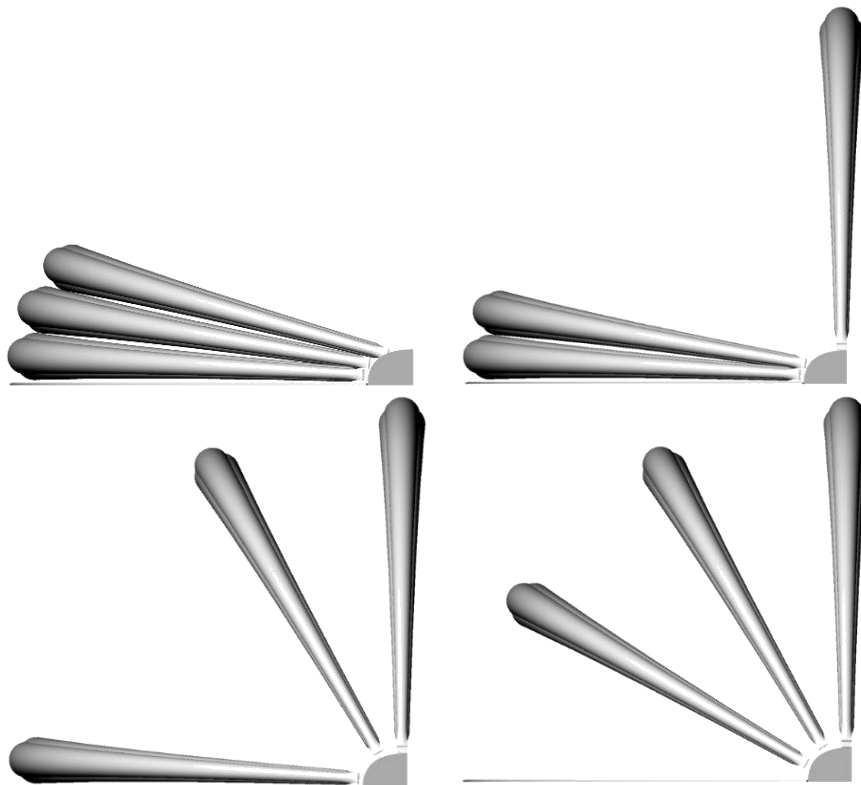


Figure 26: Construction method (resp. left to right, top to bottom)

The detailing of the Tensairity arch was aligned with this structure. Unlike the tent structure, the physical arch wasn't able to rotate in transverse direction, because the focus was on the testing of the arch.

Design Tensairity arch

This chapter describes the design process of the Tensairity arch. The drawings were created with Rhinoceros 5, Grasshopper, Autocad and IxCube.

Several designs of the Tensairity arch were made for this project. The chosen design was developed into a final design. Every aspect of the final design (compression elements, tensioned fabric, inflatable beams and impositions) is described in this chapter. This information was used for the production of the physical arch.

The final design was created in collaboration with and under supervision of several colleagues at Buitink Technology. The designs were discussed with Tentech. The final drawings of the fabric sleeves and the patterning of the fabric were done by colleagues at Buitink Technology under my supervision.

Design arch overall

The Tensairity arch (Figure 27) was a combination of a cigar and a parabola. The arch had a span of 11 meter and a height of 5 meter. These dimensions were chosen, because the testing was done in the fabrication hall at Buitink Technology, which didn't allow a much higher structure. Future Tensairity arches could have larger dimensions.

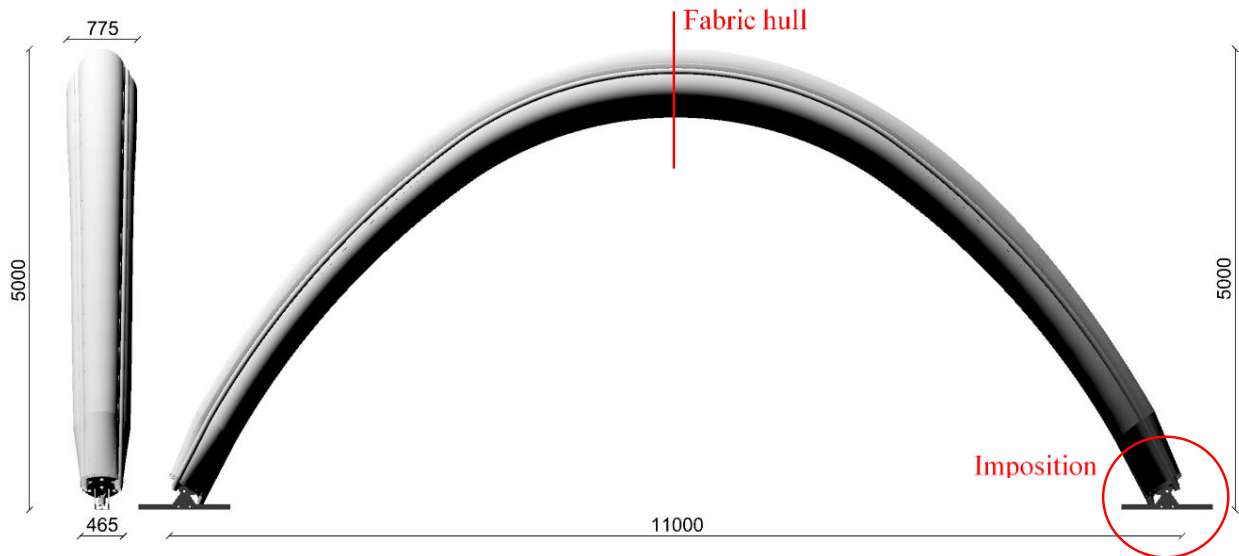


Figure 27: Dimensions and shape Tensairity arch

Shape of arch

The Tensairity arches had a catenary shape. The force line is in the shape of a parabola, when there is a uniformly distributed load on an arch. When the arch follows the curvature of this parabola, there will only be compressive stresses, as long as the horizontal forces can be provided (Vink, 1998). A catenary shape is similar to a parabola (Figure 28). It was assumed that a catenary only has compressive stresses, because it barely deviates from the curvature of a parabola. The catenary follows a more vertical angle towards the end, which was preferable for the impositions of the beams.

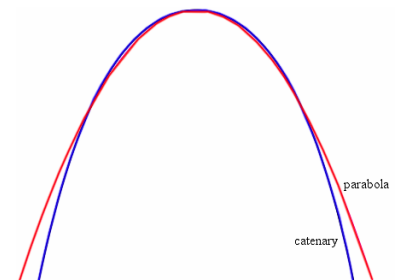


Figure 28: Parabola and Catenary

Preliminary design section Tensairity arch

Many variants of the compression element were made. Two main principles were investigated for the compression elements:

- Clamping the pieces of fabric together with the compression elements,
- Sliding the compression elements in fabric sleeves.

Clamping compression elements

At first the clamping principle was investigated. Several versions of these compression elements were developed, of which the most important variants are discussed in this paragraph. More variants can be found in the mid-colloquium report.

The first design (Figure 29) consisted of two separate identical parts that were fixed to each other with a single bolt and nut. The fabric was clamped between these pieces.

On top of the compression element was a bent piece of aluminium mechanically fixed with bolts and nuts, where cables could be mounted on for transverse stability.

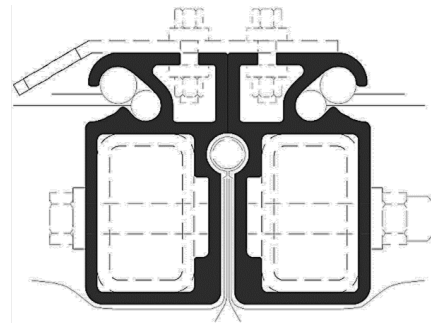


Figure 29: Compression element (first variant)

The extrusion profile contained an improved provision to fix the membrane to the compression elements, originally invented by H. Kaliwoda, used in the Polliniferous project (World in a Shell, N.D.) (Figure 30). This “zipper system” is a cavity with a variable width, which is big enough to place two tendons with different diameters. First the membrane with a smaller tendon is loosely placed between two Tensairity arches. Then a second (bigger) tendon with a small piece of fabric will be slid into the profile to lock the first tendon.

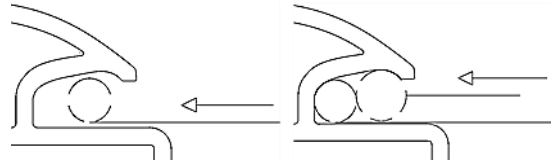


Figure 30: Placing membrane original version

The improved version of the “zipper-system” (Figure 31) was integrated in the extrusion profile for the external membrane. The tendons might deform when large forces are applied, giving the opportunity of slipping out of the “original zipper”. The small tendon in the improved version pushed the bigger tendon up, preventing it to slip out the “zipper”.

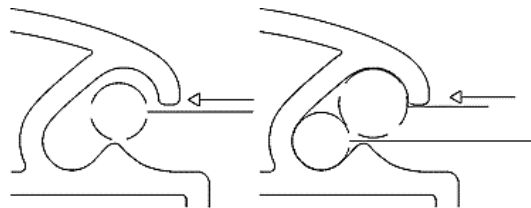


Figure 31: Placing membrane improved version

This design was very time consuming during construction. There were a large amount of bolts and nuts necessary for the clamping of the pieces. This amount of bolts and nuts had to be reduced in order to minimize construction time.

Another problem existed with bending. It had to be bent on a stiff axis (red line in Figure 32) and in two directions, because of the shape of the arch. The section was nearly impossible to bend without deforming the chambers of the section. The bending process would have been very expensive.

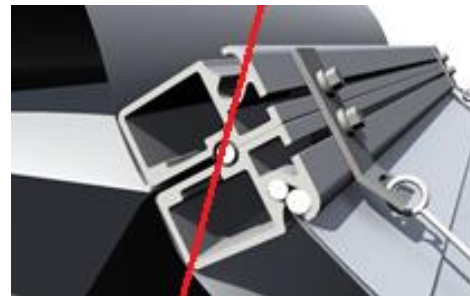


Figure 32: Stiff bending axis compression element (red line) (first variant)

The second design tackled the bending problem by using a circular section and an external piece of aluminium. There were two types of this section: one for the upper elements (Figure 35) and one for the bottom element (Figure 36). Figure 33 shows the locations of the different elements and Figure 34 shows the full section of the beam.

The clamping was done by the external piece of aluminium which was bolted on to the tube. This clamping profile was different for the two elements, because the external membrane was only connected to the upper elements. This clamping profile was a combination of a keder profile and the zipper-system mentioned earlier. The bottom element consisted of an aluminium strip. These external elements would bent by bolting it onto the circular tube, because it would be limp enough when the bending axis is on the limb side.

This design would still be too time consuming during construction. By combining the bolt and nut for the stability cable and the clamping, the time could have been reduced a little.

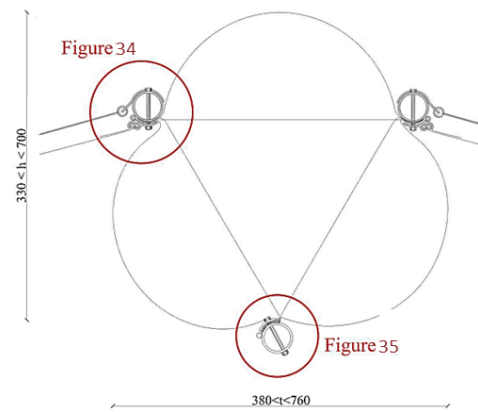


Figure 33: Location compression elements

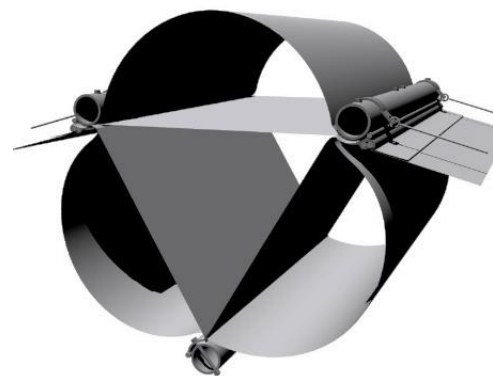


Figure 34: Full section of Tensairity beam (second variant)

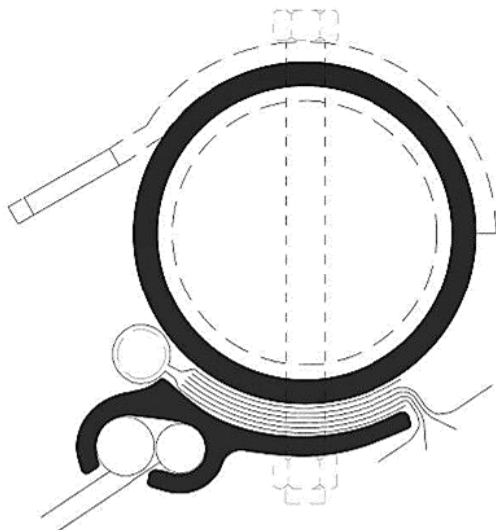


Figure 35: Compression element top (second variant)

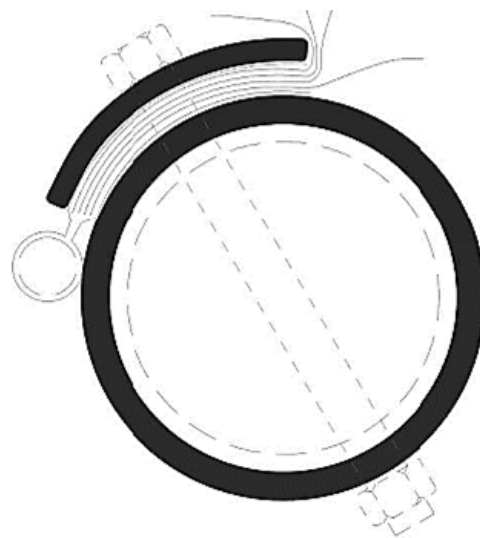


Figure 36: Compression element bottom (second variant)

Fabric sleeves

A meeting with Tentech resulted in a major change of the design of the arch. The clamping principle in its current design could not be (de-)constructed rapidly, due to the high amount of bolts and nuts needed for fixation. Changing this design should made it possible to reduce the building time. It would however be more difficult to create an airtight situation when the beam is not clamped, because the several layers of fabric would peel easily.

More research on inflatable projects gave insights in the possibility of creating an airtight situation with only welding and using pockets for the compression elements (Wever, 2008) (Figure 37). However, the inner layers in this situation might still peel of the outer hull, which could not occur in reality.

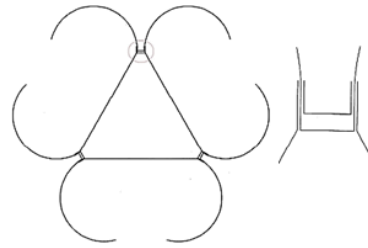


Figure 37: Possible welding package

An improved variant of this situation was made (Figure 38). Just like the version of Wever, it had a continuous outer hull, and separate inner layers. This variant however had the inner web reinforced with another piece of fabric, preventing it from peeling. Another piece of fabric was added to the sleeve, with a tendon to add a double keder profile for the external membrane. The compression element was reduced to an aluminium tube with a diameter of 70 mm and a wall thickness of 5 mm.

The sleeve might still have peeled in this variant, when there were active forces on the compression element. It was therefor required to look for other options.

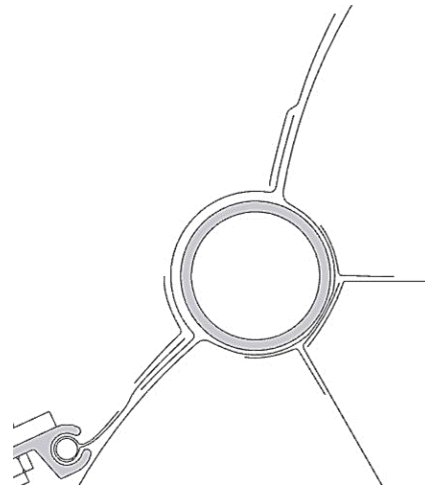


Figure 38: Welding package third variant

A brainstorm session with colleagues at Buitink Technology gave insight in a new variant, which would resolve the peeling problem (Figure 39). The compression element was reduced to an aluminium tube of 50×3 mm. This section used three corner joints made out of one piece of fabric. Multiple flaps were created with this piece of fabric. They were stitched and reinforced with a strip of fabric to prevent peeling. The fabric web and fabric outer layer of the fabric hull were welded onto these flaps. The fabric wouldn't peel, because the flaps were flexible and followed the line of the fabric layers. This was favorable, because the diameter of the Tensairity hull declined towards the imposition. Another flap with a tendon and double keder profile could attach the external membrane onto the Tensairity arch. The fabrication of this detail would not be easy, and required further development.

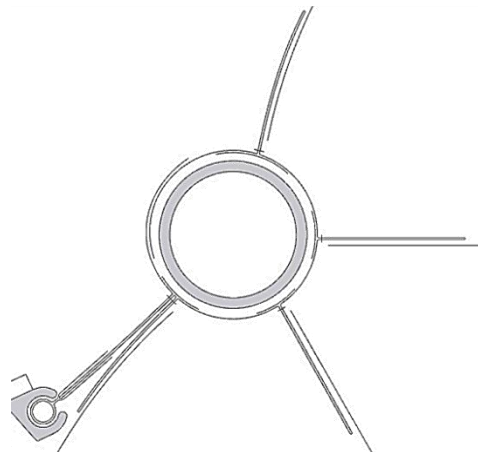


Figure 39: Fourth variant welding package

Alternative variant section

The fourth variant of the corner joint (Figure 39) was discussed during the mid-colloquium presentation. The graduation committee thought that the fabrication would be unnecessarily difficult, and that a variation on the second variant (Figure 35) would be much easier.

Because of the inflatable bag, it wasn't essential that the fabric hull was airtight. This created the possibility to weld or mechanically fix keder profiles onto the compression element, creating an easy instalment by simply sliding tendons in the keder profiles (Figure 40). Welding these keder profiles would be hard according to Buitink Technology. This variant required the keder profiles to be bent. This gave a deformation problem with the two keders on the sides because the holes would deform, which was prohibited. The inflatable bag would also be more vulnerable to rupture.

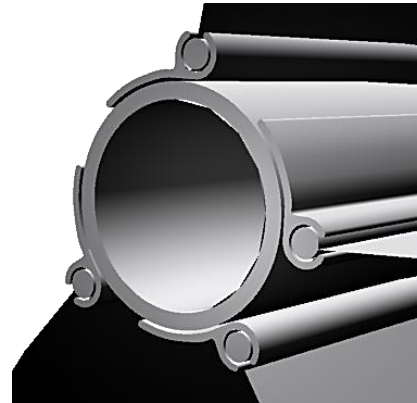


Figure 40: Variant discussed during mid-colloquium

Final design section Tensairity arch

The fabric hull (Figure 41) existed of three sleeves for the aluminium compression elements made of PVC coated Polyester¹, a triangular fabric web made of PVC coated Aramid², three fabric outer layers made of PVC coated Polyester³ and an inflatable bag made of PU-foil in each compartment.

The inflatable bags created an airtight situation, while the other fabric layers were used for the protection of the bag and were used for structural purposes.

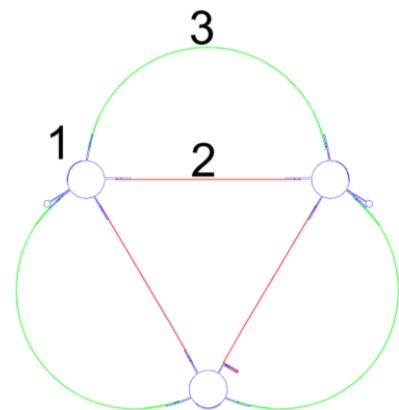


Figure 41: Section fabric hull

Sleeves for aluminium compression elements¹

In collaboration with Buitink Technology, it was decided to continue with the fourth variant (Figure 35). It was however impossible to create the entire sleeve out of one piece of fabric. A colleague at Buitink Technology created a variant of this design under my supervision (Figure 42 and Figure 43). There were two types of this design: a bottom sleeve (Figure 42) and top sleeves (Figure 43). It now consisted of five pieces of fabric instead of one piece. These pieces were stitched, because that was faster to produce than welding. Double stitching it made the connection stronger. The sleeves were closed by welding the C-pieces for the bottom sleeve and the G-pieces for the top sleeves (Figure 42, Figure 43, Appendix D1, and Appendix D2). The top sleeves also contained a tendon with a diameter of 10 mm, for fixing a keder profile to the arch. The fabric web and fabric outer layers were also double stitched onto the sleeves.

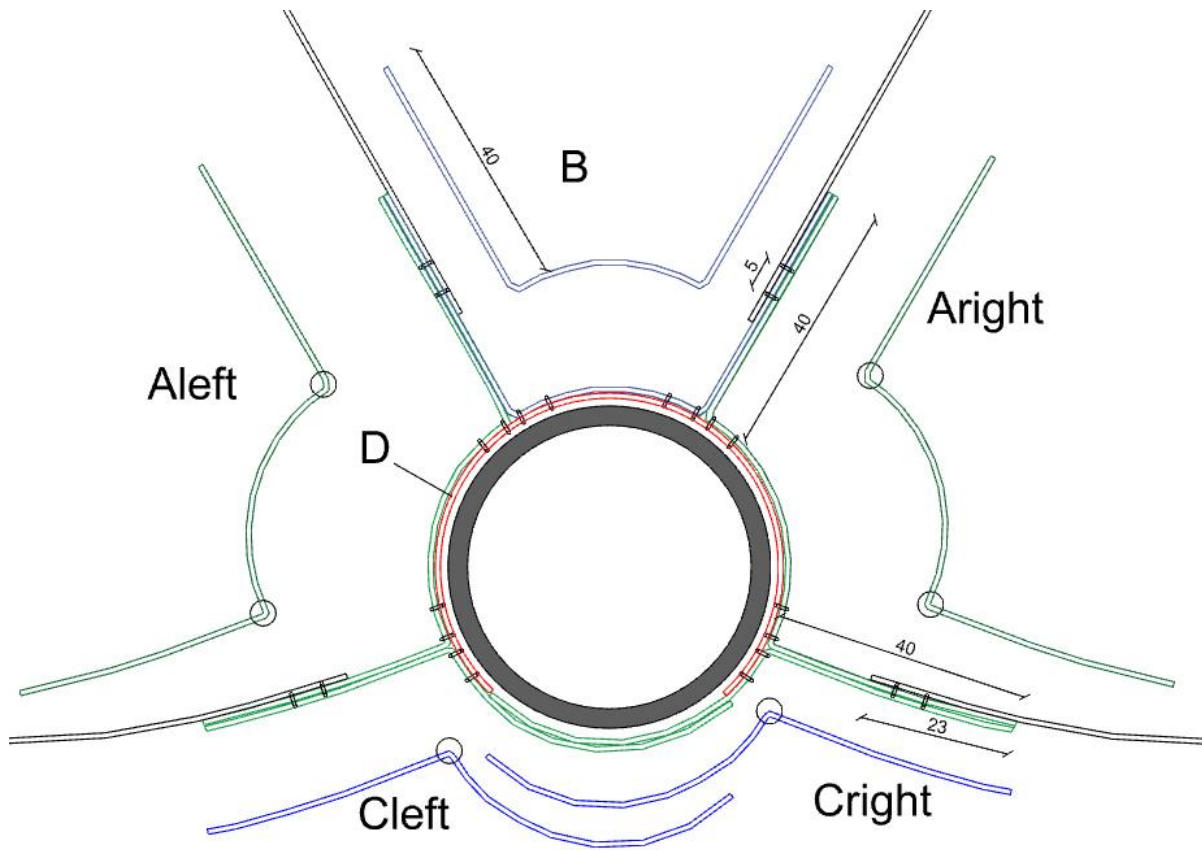


Figure 42: Section bottom fabric sleeve

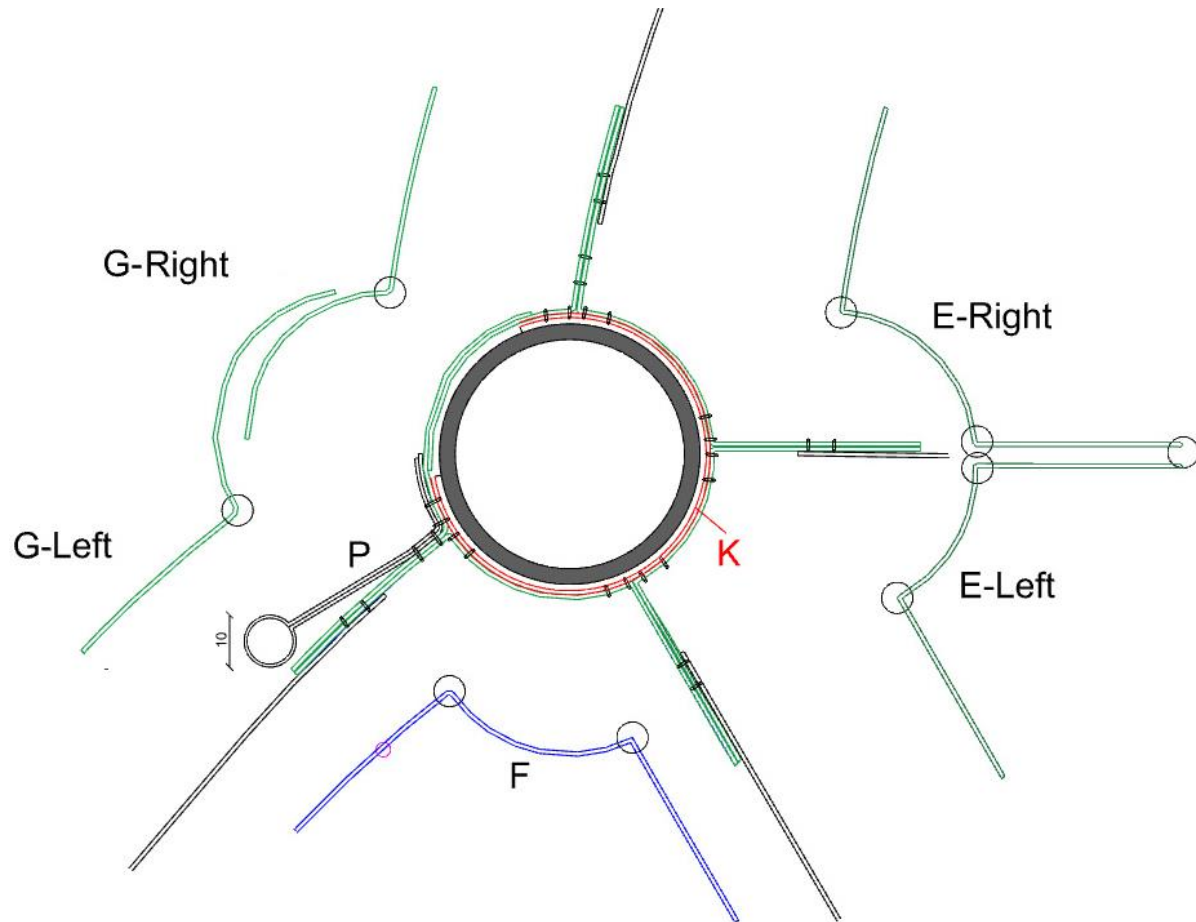


Figure 43: Section top fabric sleeves

Triangular fabric web²

The triangular fabric web gave additional stiffness to the Tensairity arch. The PVC coated Aramid had the great advantages that it does not stretch, which improved the structural integrity of the arch.

Each part of the web consisted of one piece in lateral direction. In order to create decent fabric patterns, it was required to divide each web in four pieces (Figure 44). The different pieces were stitched together, with an overlap of 15 mm. This was done with yarn that is equally strong compared to the PVC coated Aramid.

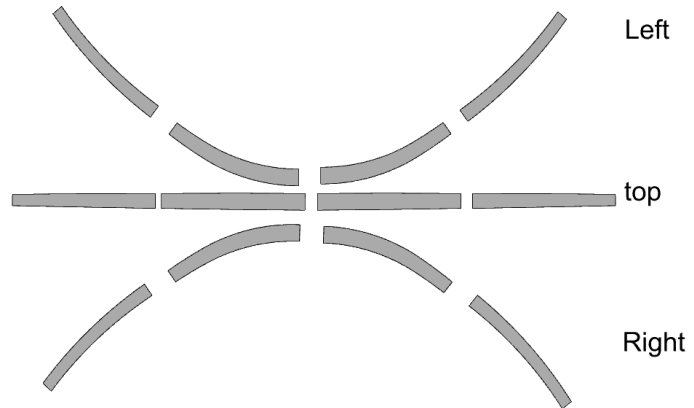


Figure 44: Patterns fabric web

Fabric outer layers³

The fabric outer layers mainly protected the inflatable bags against influences from outside. The inflatable bags introduced forces in the fabric outer layer, which the outer layer had to be able to withstand. PVC coated Polyester was strong enough for these functions.

The section of these parts were divided in three pieces in transverse direction (Figure 45) and in three pieces in longitudinal direction (Figure 46). These pieces were stitched with an overlap of 15 mm. The long side of the patterns were on the warp direction of the fabric roll.

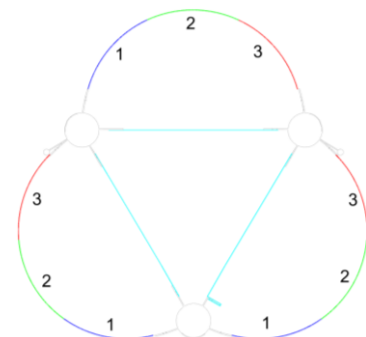


Figure 45: Division outer fabric layer

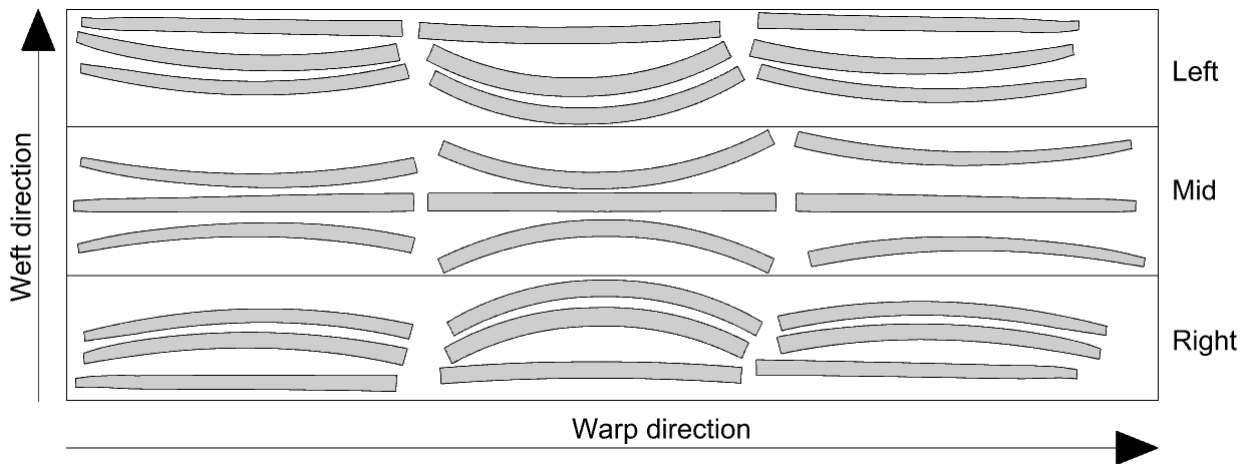


Figure 46: Patterns fabric outer layers

Inflatable bag

Four inflatable bags were inserted in each compartment (Figure 47). These bags were made out of one straight rectangular piece of 200 μ thick PU-foil, that entirely filled each compartment. It had the length of the arch including an over length of 250 mm on each side. The piece of foil were folded and a flat seam was created by welding (Figure 48). The flexibility of the foil would cause the inflatable bags to follow the curvature of the arch, when placed in their compartments.

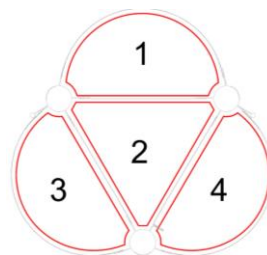


Figure 47: Compartments



Figure 48: flat welding seam

A pressure valve (Figure 49) was inserted at both ends of the bag. These valves were connected to the steel impositions (Figure 50).

It is customary to inflate Tensairity beams with pressures in a range of fifty mbar to a few hundred mbar (Luchsinger, Pedretti, Steingruber, & Pedretti, N.D.). The exact pressure was determined during the construction and testing of the Tensairity arch, but 100 mbar was used as a guideline for the construction and simulation.



Figure 49: Aluminium pressure valve

Detail imposition

The steel impositions (Figure 50, Appendix E) were a crucial part of the design. It connected the aluminium compression elements and the fabric and transferred the loads to the ground. It also closed the fabric hull.

The impositions were completely made out of steel and consisted of several parts.

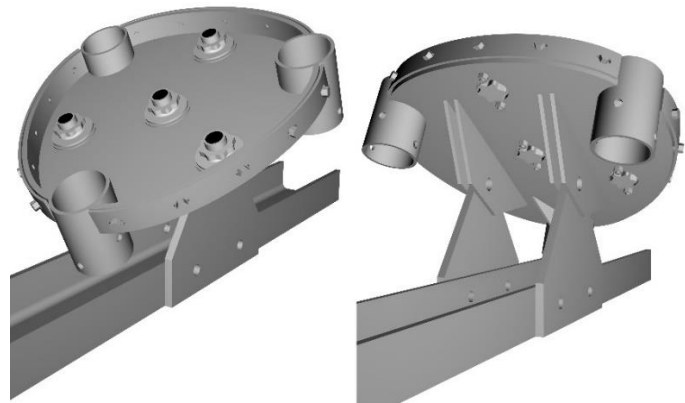


Figure 50: Steel imposition

The custom endplate contained three closing plates¹, four hinge plates² and three connection tubes for the compression elements³ (Figure 51). The border of the endplate corresponded with the end section of the fabric outer layer. The closing plates¹ followed the curvature of the endplate and were welded onto the endplate. They were used to clamp the fabric outer layer with an additional clamping plate (Figure 52, part a), creating a closed arch.

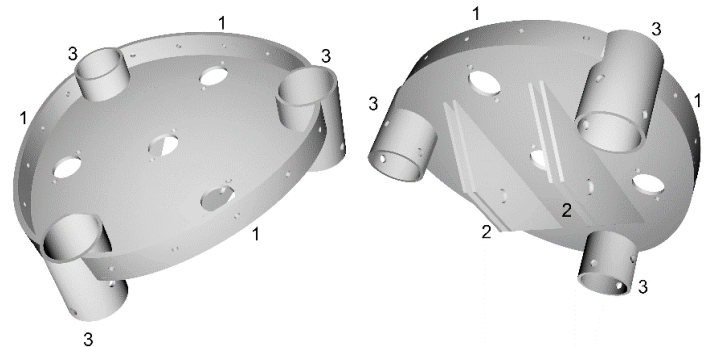


Figure 51: Custom endplate with closing plates¹, hinge plates² and connection tubes³

The arch was hingedly connected to a U-profile (Figure 52, part b). Four hinge plates² were welded onto the endplate in order to establish this connection. These hinge plates were hingedly connected to two external hinge plates (Figure 52, part c), which were mechanically connected to the U-profile. The steel tubes were welded under an angle corresponding with the angle of each of the three compression elements. These three compression elements were fixed mechanically to the tubes, in order to transfer the loads to the ground. The endplate contained holes where the pressure valves of the inflatable bags (Figure 52, part d) can be fixed onto, so they would not move within the fabric hull and the pressure within the bags could be regulated after construction.

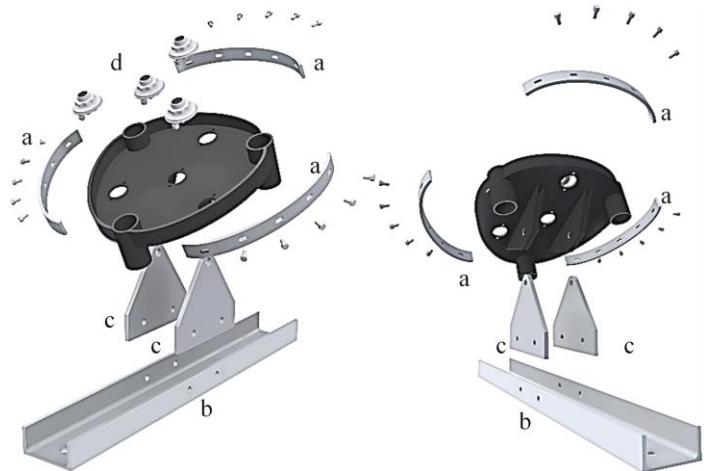


Figure 52: Exploded view of imposition (clamping plates^a, U-profile^b, hinge plates^c and pressure valves^d)

Division compression elements

The compression elements were approximately 14 and 15 meters long. The compression elements were available in trade lengths of 6 meter, which required the compression elements to be divided in three parts. These parts were mechanically fixated with countersunk bolts and nuts. This improved the demountability and decreased the size of transportation. The compression element parts were connected through steel tubes with a smaller diameter and a length of 300 mm (Figure 53).

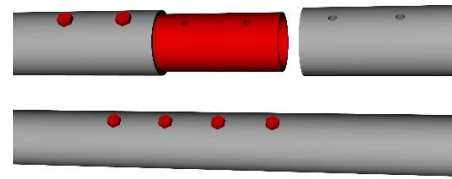


Figure 53: connection pieces of compression elements

Self-weight of Tensairity arch

The full calculation of the self-weight of the Tensairity arch can be found in Appendix F. The arch weighted approximately 8.5 kg per square meter. The weight of bolts, nuts and the impositions were not taken into account.

Weight aluminium compression elements	53 kg	
Weight steel connector	8.2 kg	
Weight fabric	64.3 kg	+
<hr/>		
Total weight arch	126 kg	

Building of Tensairity arch

This chapter describes the production process of the Tensairity arch. It discusses the following aspects of the arch:

- Production of fabric hull,
- Production of inflatable bags,
- Production of steel impositions,
- Connection of compression elements,
- Final construction of complete arch.

A tensile strength test was performed in order to gain knowledge of the strength of the produced fabric connections. The results are discussed in this chapter.

The Tensairity arch was produced at Buitink Technology. The inflatable bag, the steel imposition and the connections of the compression elements were made with assistance of colleagues at Buitink. The fabric hull was produced by colleagues at Buitink with my assistance and under my supervision.

Building steel impositions

The several parts of the imposition were built at Buitink Technology (Figure 54 and Figure 55). The endplate and the hinge plates² (Figure 51) were laser-cut by an external company. The closing plate¹ and the connection tubes³ (Figure 51) were cut, bent and welded at Buitink Technology. The external clamping plate and the U-profile (Figure 52, part a and part b) were cut and bent at Buitink Technology as well.



Figure 54: Steel endplate with closing plates, hinge plates and connection tubes



Figure 55: Steel imposition

Connection of aluminium compression elements

The aluminium compression elements consisted each of three parts. These parts were connected with steel tubes. The compression elements were slid in the fabric sleeves. In order to protect the sleeves and assure a smooth fit, it was important to prevent the existence of protrusions. The connection of the tubes were therefore made with two M10 screwed inserts (Figure 56). Figure 57 shows the connected compression elements.



Figure 56: Connection of compression elements



Figure 57: Compression elements connected

Building inflatable bags

Four inflatable bags were made of 200 μ thick PU-foil. The straight rectangular pieces were cut by hand. The aluminium pressure valves were connected to the foil after a hole was punched in the foil (Figure 58). A pulse welding machine was used to create flat seams and to secure the airtightness of the bags (Figure 59). The inflation process of a bag is shown in Figure 60. One of the pressure valves was closed with a valve cap, while the other valve was kept under constant pressure during the tests. The middle inflatable bag was inserted in the fabric hull after closing the fabric web. The other bags were inserted prior to the closing of the fabric outer layers.



Figure 58: Pressure valve



Figure 59: Seam inflatable bags



Figure 60: Before, during and after inflation (left to right)

Building fabric hull

The fabric hull consisted, as mentioned in the previous chapter, of three parts. The fabric hull was built in four steps, which are discussed in the subparagraphs below.

Cutting the fabric patterns

Fabric patterns for the sleeves, outer layers and the triangular web were created in collaboration with colleagues at Buitink Technology. The final fabric patterns were made with the programs IxCube, AutoCAD and Rhinoceros 5.

The fabric patterns were marked and cut with a cutting machine (Figure 61).



Figure 61: Fabric patterns cut by cutting machine

Stitching the patterns of the sleeves, fabric outer layers and triangular web

All fabric patterns were stitched in collaboration with R. Ho from Ho Mulder Design Factory. The different patterns were first taped in the right order (Figure 62). This was more convenient during the stitching process.

The patterns of the outer layer and the fabric web were stitched with different yarns (Figure 63). The PVC coated Aramid used for the fabric web is a stronger fabric, which required yarns of higher strength in order to maintain its strength at the seams.

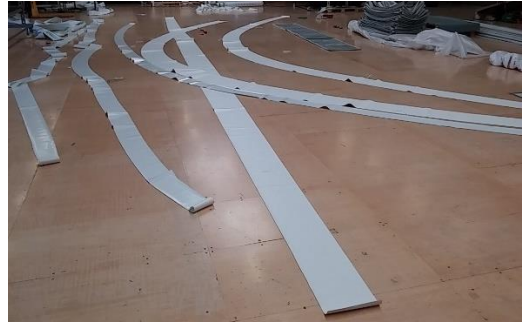


Figure 62: Taping the fabric pieces prior to stitching



Figure 63: left: stitched seam web, right; stitched seam outer layer

The fabric sleeves patterns were first welded with a hot air welding pistol (Figure 3) in longitudinal direction.

The different patterns are stitched together after the welding process has been done (Figure 64). The steps described in Appendix D1 and Appendix D2 were the main guide for the stitching of the sleeves.

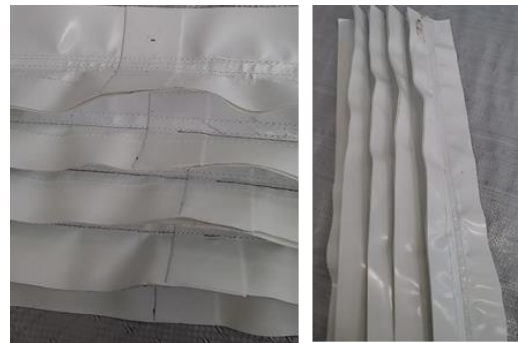


Figure 64: left; stitched patterns at welded seam, right; stitched patterns

Stitching the triangular web and outer layer onto the sleeves

The fabric web and the fabric outer layer were double stitched onto the sleeves. The stitching order is shown below.

- The fabric web was first stitched with a flat seam onto the sleeves (red line in Figure 65 and Figure 66).
- A custom seam was used for the last connection of the web onto the sleeve (blue line in Figure 65 and Figure 67). This was necessary in order to close it. This was not possible with a flat seam.
- The outer layers were stitched with a flat seam onto the sleeves after the web was closed (green and pink line in Figure 65 and Figure 70).

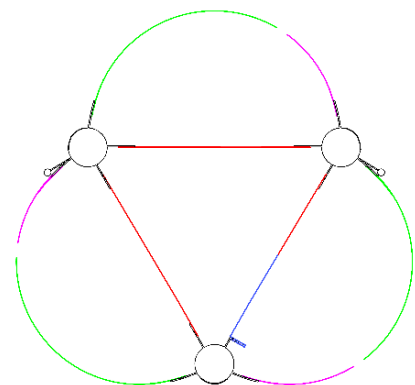


Figure 65: Stitching order (1: red, 2: blue, 3: green and pink)

The stitching was started from the centre of the arch, due to the fact that differences in lengths were present (Figure 69). These differences were enhanced because the patterns had to be stretched unevenly to stitch/weld the patterns straight. Figure 68 shows the end result of the stitching process.



Figure 66: Flat seam between web and sleeve (Figure 65, red line)



Figure 67: Closing seam of web onto sleeve (Figure 65, blue line)



Figure 69: Fabric web closed, overview (Figure 65, red and blue line finished)



Figure 70: flat seam between outer layer and sleeve (Figure 65, green and pink line)



Figure 68: Stitching of fabric hull finished

Welding the outer layer

The outer layers consisted of two patterns, as shown in Figure 65 (green and pink line). These parts were closed by welding with a hot air welding pistol (Figure 3). The inflatable bags were placed in their compartments before closing the fabric outer layers, because this would have been harder afterwards.



Figure 71: welding the outer layer

Welding fabric sleeves

The fabric sleeves (Figure 42 part C and Figure 43 part G) were closed by welding with a hot air pistol (Figure 3) after the fabric hull was closed (Figure 72). The compression elements were placed in the fabric sleeves prior to the welding, due to very tight detailing of the fabric sleeves.



Figure 72: Welding of fabric sleeve with compression element in sleeve



Construction of Tensairity arch

Anchoring steel imposition

The first step was to anchor one of the steel impositions. Four chemical anchors (M12) were drilled in the floor, after which the imposition was slid over the anchors, and fixated with bolts (Figure 73). Two tension belts were mounted between both impositions, creating the option to move the second imposition. This was useful for the placement of the arch in the next phases (Figure 74).

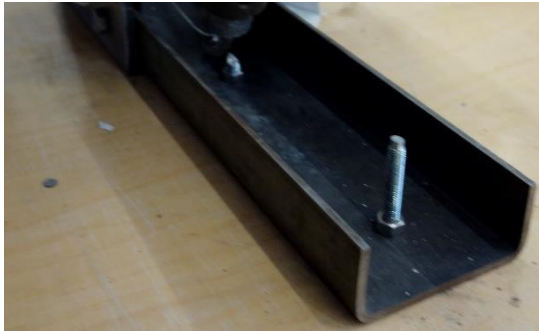


Figure 73: Steel imposition chemically anchored



Figure 74: Tension belt mounted on second imposition

Placing Tensairity arch

The compression elements (thus the entire Tensairity arch) were slid in the tubes of the steel imposition, using a forklift truck. Inaccuracies in the patterns of the fabric sleeves and sag of the compression elements made it hard to place the compression elements in the steel imposition. The compression elements could not be retracted deep enough into the impositions (Figure 75). This was due to the fact that the fabric sleeve got stuck between the imposition and the compression element, creating a barrier. Small incisions were made in the fabric sleeves, making it possible to place the compression elements further in the imposition. The inflatable bags were inflated a little, which was convenient for gaining the correct shape of the arch.



Figure 75: Imposition retracted too little

The two top compression elements went too far in the imposition, pushing the second imposition, that wasn't anchored to the ground, from the ground (Figure 76). In order to push the compression elements in the right position, it was necessary to anchor the second imposition, once it was in the right location. The compression elements being too far in the imposition partially caused the fabric hull to contain a lot of wrinkles (Figure 77 and Figure 78). This might also have been due to inaccuracies in the fabric patterns and uneven stretching of the fabric while stitching/welding.



Figure 76: Imposition pushed from ground



Figure 77: Wrinkles in the fabric prior to heightening the compression elements



Figure 78: shape of arch prior to heightening compression elements (not inflated)

The compression elements were anchored once on the right height with two M10 bolts and nuts each (Figure 79). The outer fabric layer contained large gaps at the ends, which were filled up by welding additional pieces of fabric onto the outer layer (Figure 80). An additional piece of fabric was placed between the inflatable bag and the steel imposition, protecting the inflatable bag (Figure 80). The outer fabric layer was clamped between the imposition and the external with carriage bolts and nuts (Figure 81). The pressure valves and inflation valves were permanently fixated onto the steel impositions, with pressure meters on two of the inflatable bags (Figure 82).



Figure 79: Anchoring of compression element



Figure 80: left; without additional fabric, right; with additional fabric



Figure 81: Clamping of outer fabric layer



Figure 82: left; inflation valves, right; pressure meters

The arch was inflated after the construction seemed finished. There was however a leak in one of the inflatable bags. Unaware of the location of the leak, it was required to remove the leaking bag from the Tensairity hull. This was done by placing a rope on a pressure valve on one side of the arch and pulling on the other side, after making a cut in the outer layer. That pressure valve was disconnected from the leaking bag, giving the opportunity to reattach it after the leak was fixed, pulling the rope and bag back in the hull. The leak was found pretty fast after the bag was inflated (Figure 83). The leak was repaired with ETFE-

tape. The bag was placed back in the hull after it was tested. The incision was patched by welding an additional piece of fabric (Figure 84). The possible cause of this leak was a wooden brace that was placed between the building and the top of the Tensairity arch, in order to increase transverse stability of the arch (Figure 85). The brace was too long, pushing too hard on the hull when the arch was inflated. The wooden brace was removed, eliminating the possibility of rupturing the inflatable bag again.



Figure 83: leak in bag

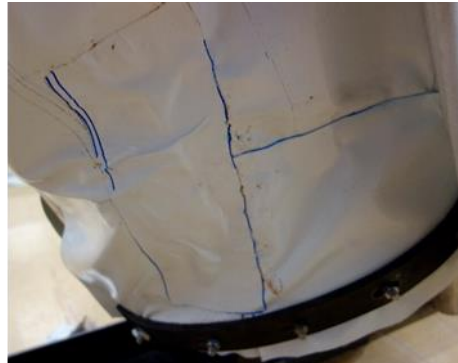


Figure 84: Repaired incision in outer layer



Figure 85: Wooden brace for extra stability

The Tensairity arch was inflated again, once the patch was welded. Figure 86 shows the final result of the construction of the arch. The arch was inflated with 100 mbar. This pressure level removed a few wrinkles, but unfortunately not all. The arch was stable enough without the wooden brace, due to good anchoring.



Figure 86: Construction of tensairity arch completed

Testing of connections

Interest in the strength of the made connections, led to the testing of the stitched connections in a tensile testing machine. The results of the tests are shown in Figure 95.

Test one

The first test was performed in order to create knowledge on the strength of the PVC coated Aramid. The PVC coated Aramid ruptured at a tensile force of approximately 21 kN (Figure 87 and Figure 88).

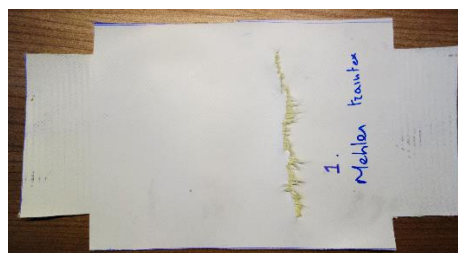


Figure 87: Result test one



Figure 88: Close-up rupture test one

Test two

The integrity of a flat seam between two pieces of PVC coated Aramid was tested in test two. This test refers to the stitching of the fabric web patterns to create the three web parts (Figure 44). The PVC coated Aramid ruptured near the stitches at a tensile force of 4.3 kN (Figure 89 and Figure 90).

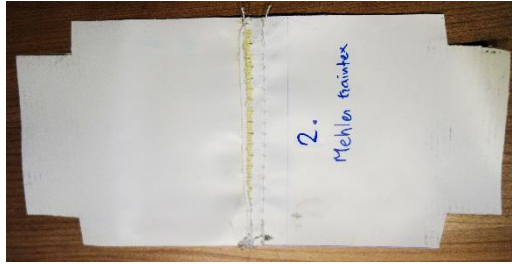


Figure 89: Result test two



Figure 90: Close-up rupture test two

Test three

Test three tested the integrity of a flat seam between a piece of PVC coated Aramid and two pieces of PVC coated Aramid. This connection refers to the stitching between the fabric sleeves and the fabric web. The stitches ruptured at a tensile force of 6.9 kN (Figure 91 and Figure 92).

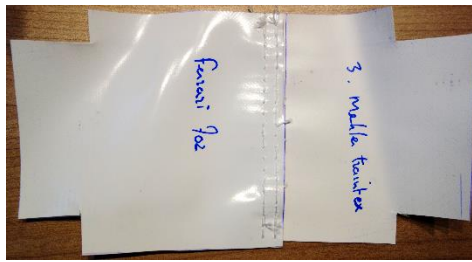


Figure 91: Result test three

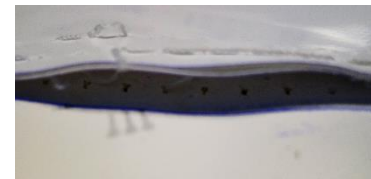


Figure 92: Close-up rupture test three

Test four, five and six

Test four, five and six tested the integrity of a custom seam between a piece of PVC coated Aramid and two pieces of PVC coated Polyester. This connection refers to the last (closing) connection of the fabric web to the fabric sleeve (Figure 67). Test four and five were exactly the same. The connection in test six was created with a different yarn. The stitches ruptured in test four, five and six at a tensile force of approximately 3.5 kN, 3.8 kN 1.4 kN respectively (Figure 93 and Figure 94).

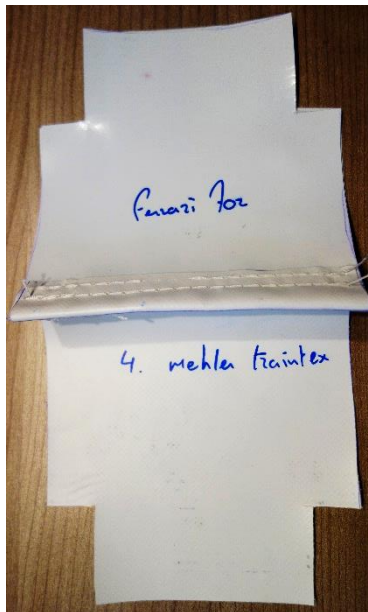


Figure 93: Result test four, five and six



Figure 94: Close-up rupture test four, five and six

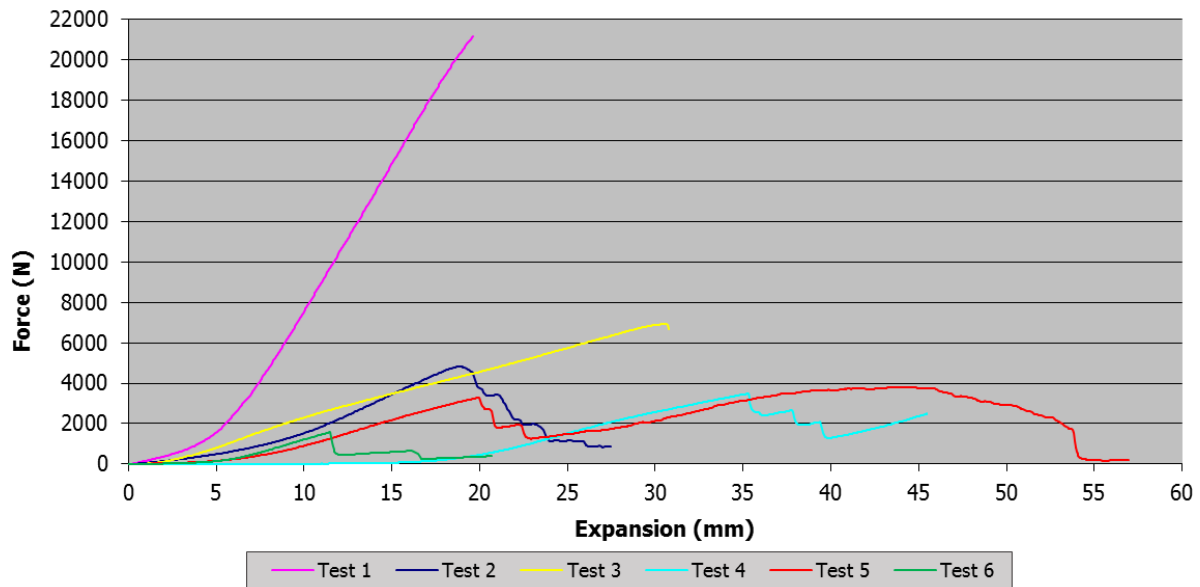


Figure 95: Force-expansion graph tensile strength test

Conclusion of testing

The results showed that the PVC coated Aramid itself could bear much higher tensile force than the connections. The flat seams were stronger than the custom seams, due to the fact that the flat seam introduced much more shear resistance. The yarns in test six were supposed to be stronger than the yarns in test five six, but the stitches in test six ruptured at a lower tensile force. A mistake was probably made with the choice of yarn.

It should be noticed that these tests were not completely comparable with the situation in the Tensairity arch. The tests were tensioned in the same direction as the actual situation, but the pressure given by the inflatable bags were not taken into account, giving more resistance than present in the test. The seams in test four, five and six were also pressed between the inflatable bag and the fabric sleeve / compression element. Nevertheless, the test results of the connection test were disappointing, but experience within Buitink Technology pointed out that it was likely strong enough.

Testing of Tensairity arch

This chapter discusses the testing of the Tensairity arch. The test set-up is described and the test results are analysed. All testing was done at Buitink Technology in Duiven. The testing comprehended four different tests:

- A vertical load in the middle of the arch,
- A vertical load at a quarter of the arch,
- A vertical load distributed over five points,
- A vertical load in the middle of the arch (increasing load till breaking point).

Two comparisons were made, which gave insight in the strength/weaknesses of the two designs and verified results and/or conclusions made earlier in the chapter:

- The third test with a test performed by R. Maffei in 2008-2010.
- The second and third test with tests performed by Crettol et al in 2010.

Test set-up

A set-up was created for the different tests. Two pieces of keder-bolt profiles were anchored on the tendon on each side of the Tensairity arch. An eye-bolt was connected to the keder-bolt profiles for the attachment of tension belts (Figure 96). These tension belts were connected to keder-bolt profiles of 1.5 meters long, which were used as spacers (Figure 97). These spacers created a more realistic situation and prevented unwanted deformation of the section of the hull. Five of these suspension points were distributed over the length of the arch corresponding with Appendix G.



Figure 96: Keder-bolt profile attached on tendon Tensairity arch

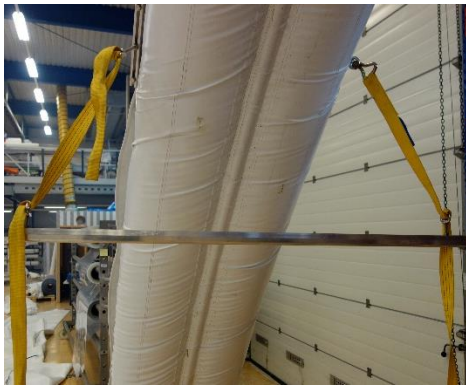


Figure 97: spacers against section deformation



Figure 98: Distribution of suspension points

The load was applied using two different methods. The first method was used for the first three test. This method consisted of IBC tanks (self-weight of 57 kg) attached to the suspension points mentioned earlier. The second method was used in the final test. A chain winch was connected to a completely filled IBC tank in this method. A more specific description of the test is given in the next paragraph.

The height of the bottom compression element was measured before the test, during the test and after the test. A rail profile was placed on top of two ladders, creating a flat surface that didn't move. The measurements were done with a Laser Distance Meter placed on top of the rail profile (Figure 99). The measuring location and target were measured and marked to gain more accurate results during the entire process. The height of the rail-profile was measured prior to each test. This height remained intact during the entire test.



Figure 99: Measurement with Laser Distance Meter

Test results

The results on deformation had an accuracy of measurement of ± 5 mm. This was due to possible sliding of the rail-profile combined with a minor deviation in the Laser Distance Meter. The accuracy of measurement of the weight of the IBC-tanks was ± 15 kg. This was due to the fact that the tanks were not completely levelled out and it was nearly impossible to stop the water at the right amount.

Test zero: start situation

The start situation did not contain any external loads, except for the test set-up (without IBC tanks). The results of the measurements are shown in Table 2. The results showed that the arch was asymmetrical. The difference between point one and five was approximately 3%, while the difference between point two and four was approximately 0.5%. This difference might have been the result of uneven stretching of the fabric during production, or that both ends of the compression elements were not evenly far inserted in the steel impositions. Inaccuracies in measuring could have enlarged the differences, but it is ruled out that this was the sole cause of the differences.

Location	Height
Point 1	2704
Point 2	3820
Point 3	4183
Point 4	3840
Point 5	2775

Table 2: Height bottom compression element start situation

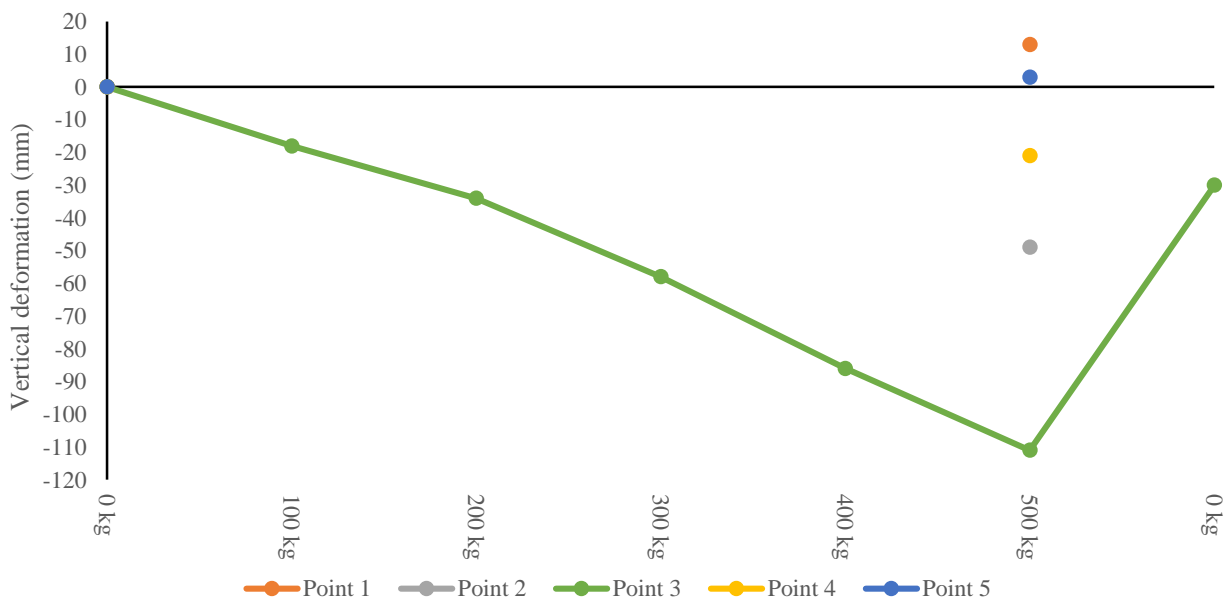
Test one; load in the middle

Test one consisted of one IBC tank hung up on the middle suspension point (Figure 100 and Appendix , point 3). The IBC tank was gradually filled up to 500 kg. Graph 1, Appendix H1 and Appendix I show the results of the first test.

The deformation proceeded quite evenly during the increase of the load. A uniform deformation occurred, where the maximum downward displacement occurred in the middle of the arch. The vertical displacement on points two/four and one/five had different values. This verified that the arch was asymmetric. When looking at the middle of the Tensairity arch, it was clear that the arch did not return to its original state. This was possibly the result of plastic deformation of the aluminium compression elements or that the friction between the inflatable bags and the fabric hull caused the bags to remain in position.



Figure 100: Set-up test one



Graph 1: Vertical displacement arch test one

Test two; load at a quarter

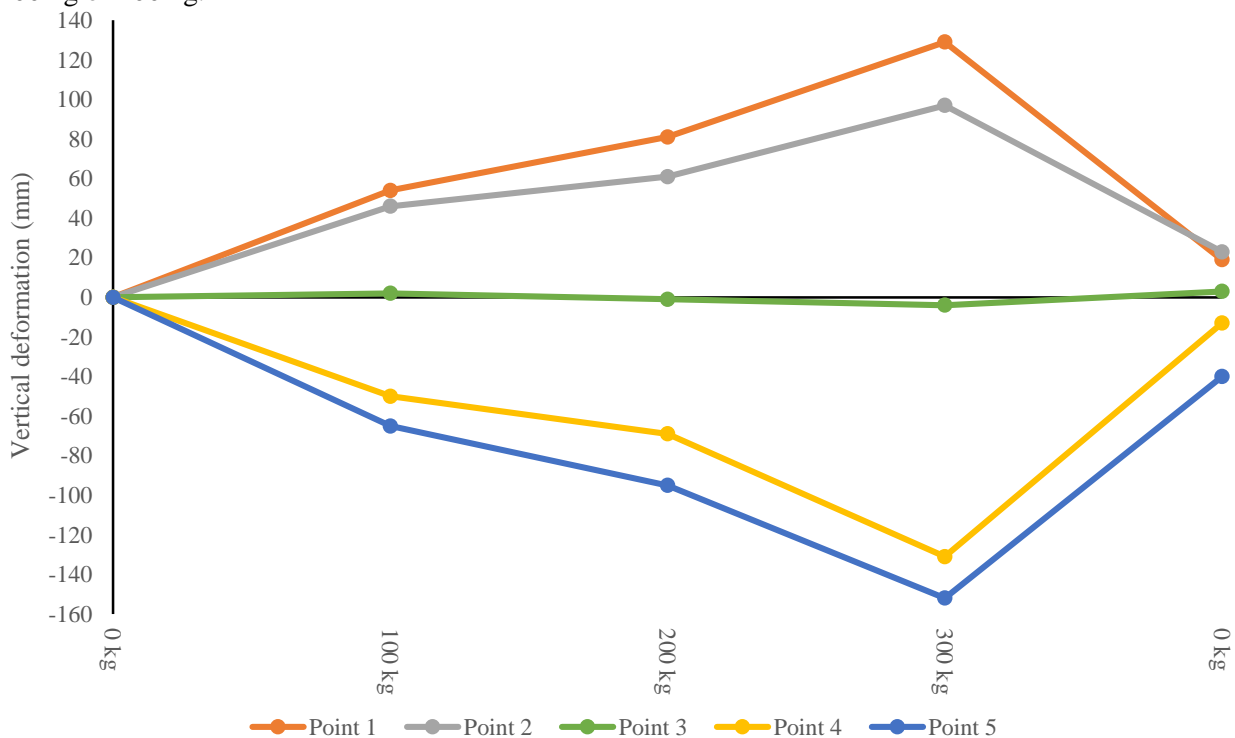
The second test consisted of a IBC tank hung on a quarter of the Tensairity arch (Figure 101 and Appendix , point 4 and 5). The IBC tank was gradually filled up to 300 kg. The tank was not filled up to 500 kg, because the deformation was already large at 300 kg. Continuing the test created the risk that further tests couldn't be performed. Graph 2, Graph 3, Appendix H2 Appendix and Appendix I show the results of the second test.

This deformation did not proceed uniform. Point four and five deformed downwards, while point one and two deformed upwards. Point three remained more or less at the same height during the entire test. The arch had a plastic deformation downwards. The fact that point one plastically vertical deformed less after the test than point two was unexpected, because it deformed more during the test. Point four and five showed a more expected end deformation, looking at the rest of the results. There could have been inaccuracies in the measurement.

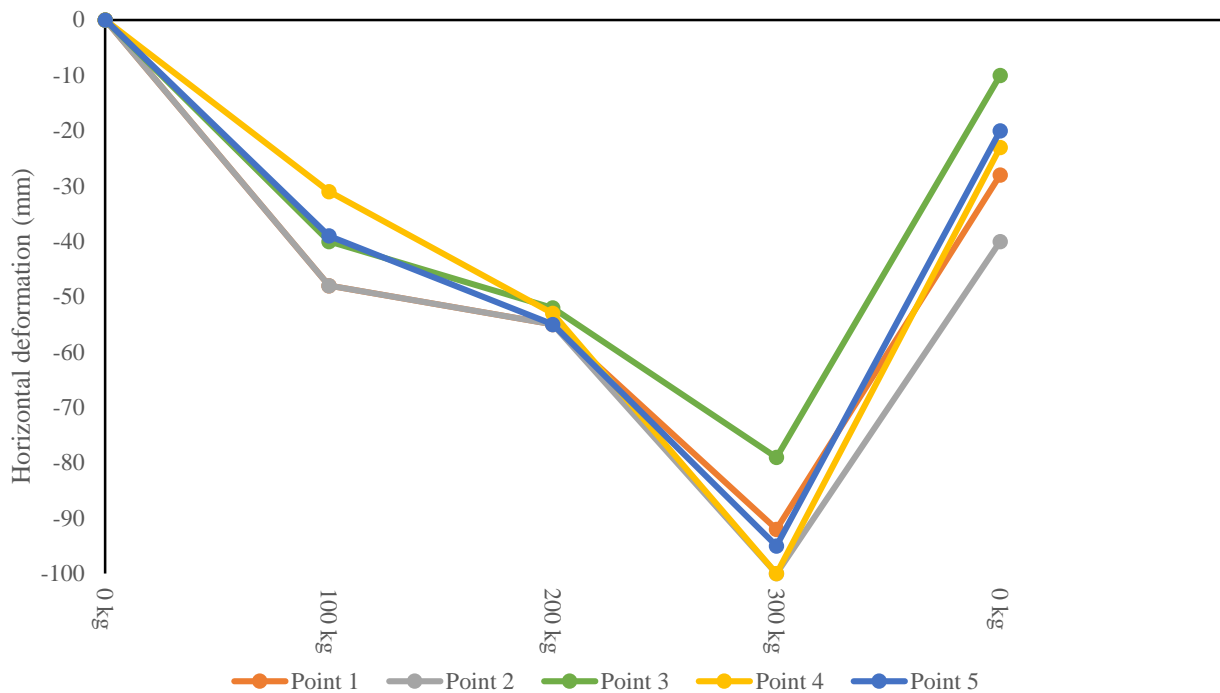
The arch deformed horizontally away from the load (towards point one). There was a minor plastic horizontal displacement. The slopes of the graphs showed unexpected increases/decreases, likely due to a too high load when measuring at 100 kg or 200 kg.



Figure 101: Set-up test two



Graph 2: Vertical displacement arch test two



Graph 3: Horizontal displacement arch test two

Test three; load distributed over five points

The third test consisted of three IBC tanks distributed on the five suspension points of the Tensairity arch (Figure 102 and Appendix G, first tank on point 1 and 2, second tank on point 3, third tank on point 4 and 5). The first and third IBC tank were gradually filled up to 200 kg, while the second IBC tank was filled to 100 kg. The displacement during the test is shown in Graph 4, Graph 5, Appendix H3 and Appendix I.

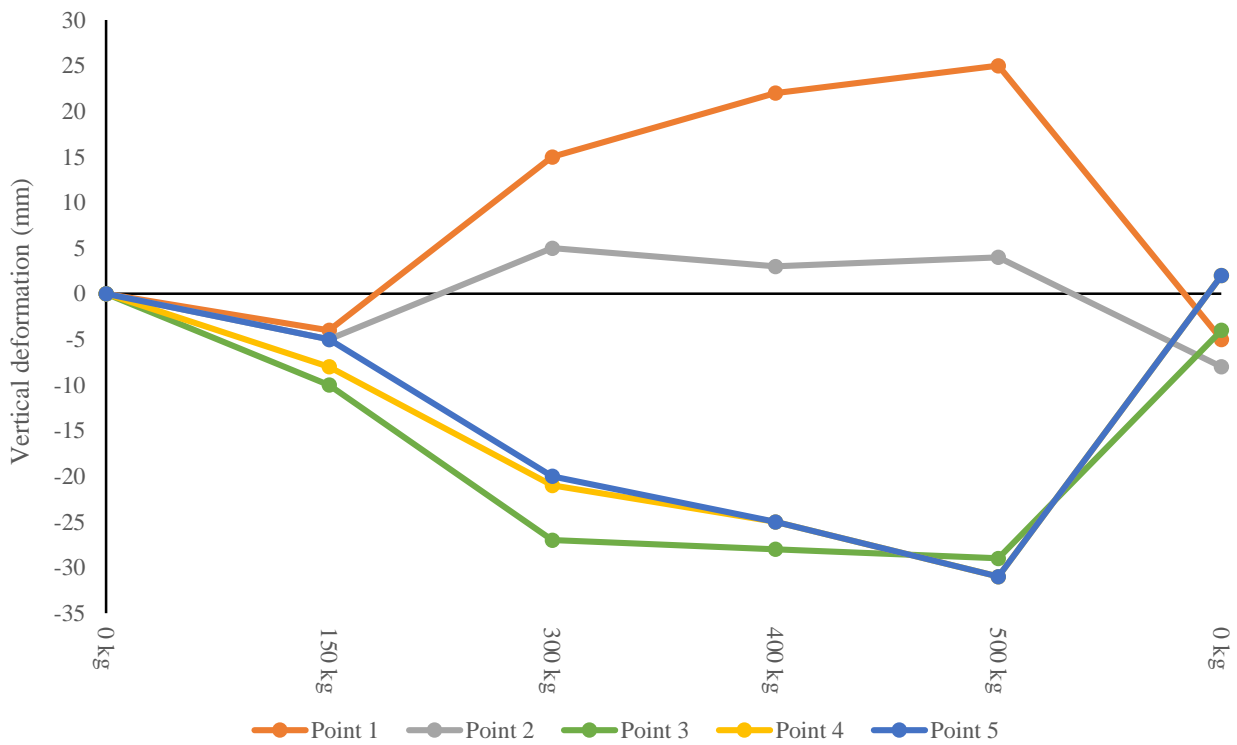


Figure 102: Set-up test three

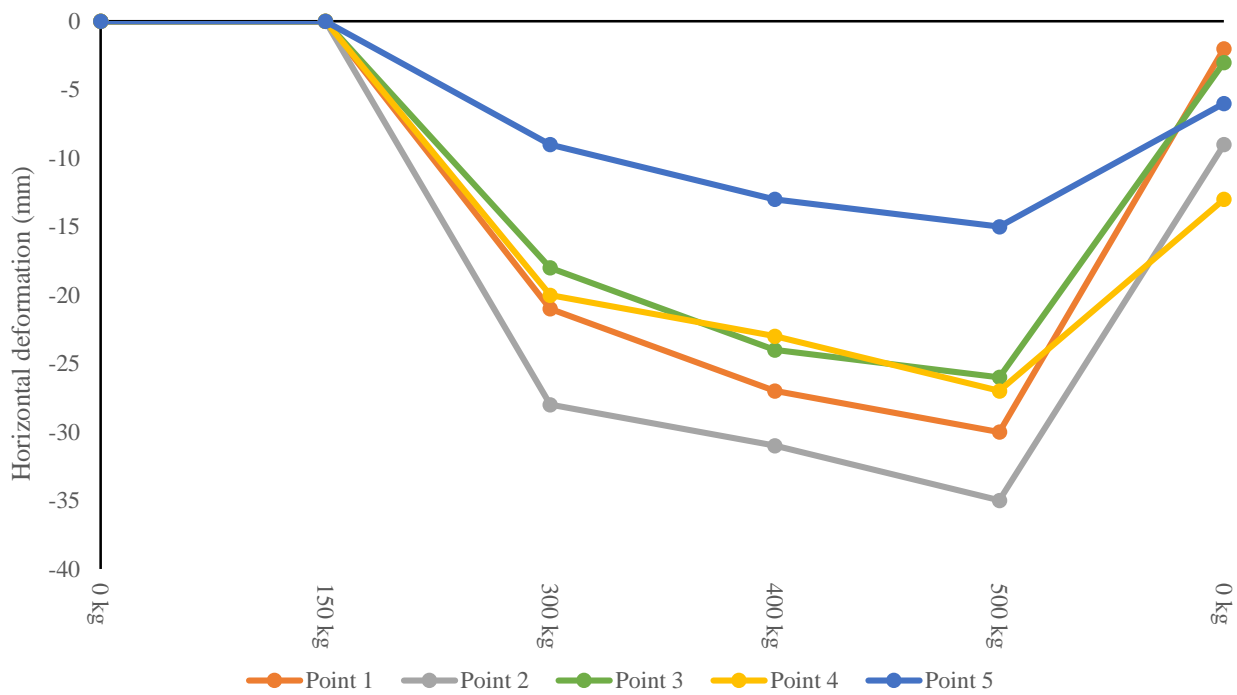
The effect of the second test was visible in the results of the third test. The arch was plastically non-uniform deformed during test two. This effect was further enhanced by test three. Point one and two further deformed upward, while point four and five further deformed downwards. Point three basically didn't vertically deform after the IBC tank on point three was filled up to its end volume. Point one and two had a downward displacement up to 150 kg and then deformed upward. It would be more logical that it would go either upward or downward. This might have been caused by an uneven load value after 150 kg, where the third tank would have been filled more than the first tank. The difference was however much, which made it unlikely that this was the only cause. Point five had an upward plastic deformation, while points one to four had a downward plastic deformation. It was more likely if point one and two plastically deformed upward and point three to five deformed downward. These results were redirected to the fact that point four and five became straighter after test two, while point one and two were still curved. This caused that points four and five deformed more than point one and two.

The arch started to deform horizontally towards point one after 150 kg. Points one to four deformed more than point five. It would be more likely that point five deformed equally much as the other points, like in test two. The arch had a small plastic deformation.

The arch started to deform horizontally towards point one after 150 kg. Points one to four deformed more than point five. It would be more likely that point five deformed equally much as the other points, like in test two. The arch had a small plastic deformation.



Graph 4: Vertical displacement test three



Graph 5: Horizontal displacement test three

Test four; load in the middle

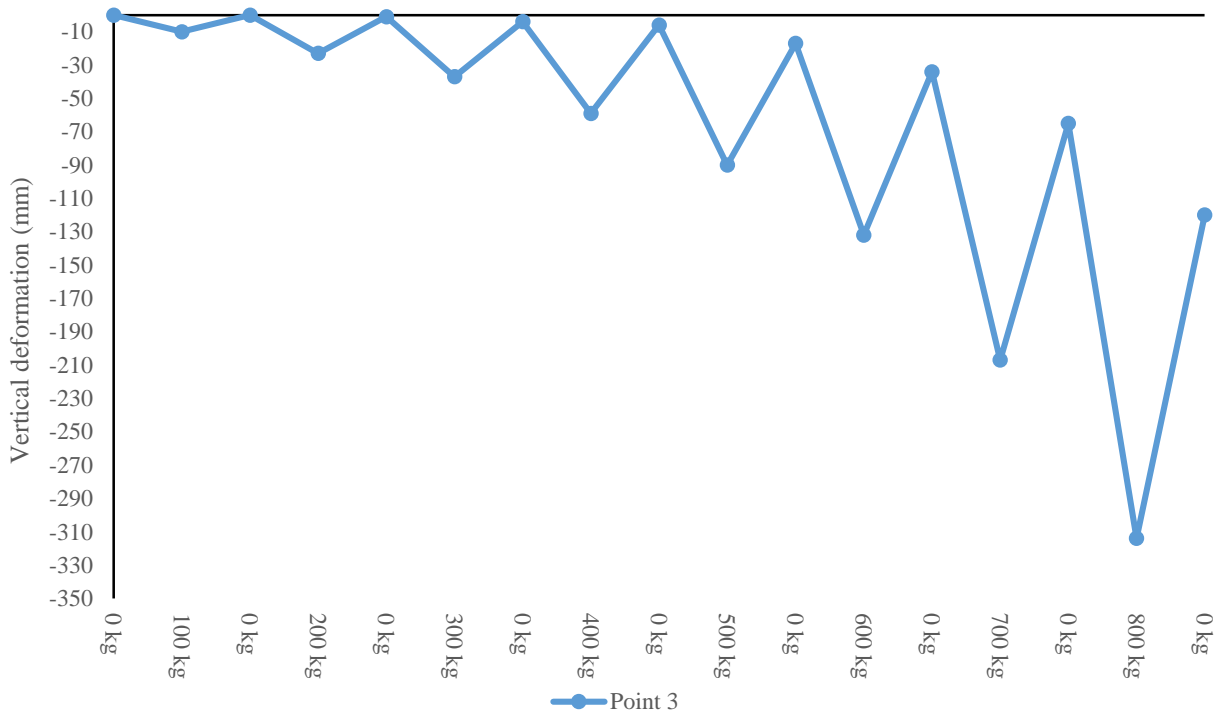
The fourth test consisted of a Chain winch hung up on the middle suspension point. A weight meter was placed between the suspension point and the chain winch in order to measure the weight at all time. The chain winch was connected to an IBC tank, which was completely filled with water (Figure 103 and Appendix G, point 3). The elevation was tested in steps of 100 kg. The load was released after each measurement in order to measure the plastic deformation. Graph 6, Appendix H4 and Appendix I show the results of the third test.

The displacement was measured up to a load of 800 kg. The arch had a large downward displacement at this load. The final plastic deformation was quite large. The arch started to plastically deform after 200 kg. The plastic displacement was however noticeable after 500 kg.

It was unexpected that there was a difference in deformation at 500 kg between test one and four. This difference could be probably the result of the plastic deformation from the previous tests.



Figure 103: Set-up test four



Graph 6: Vertical displacement test four

Reason of plastic deformation

As mentioned during the analysis of the results, the Tensairity arch plastically deformed. This could have been caused by plastic deformation of the aluminium compression elements or that the friction between the inflatable bags and the fabric hull caused the arch to remain in deformed position. The Tensairity arch was deflated and re-inflated, creating the possibility to measure the height of the bottom compression elements again. The results are shown in Table 3. Interesting to see was that the third point went back a little after deflation and re-inflation. This verified the statement that friction between the inflatable bags and the fabric hull partially caused the plastic deformation.

	Point 1	Point 2	Point 3	Point 4	Point 5
Prior to first test	2704	3820	4183	3840	2775
After final test	—	—	4046	—	—
After re-inflation	2738	3740	4062	3788	2792

Table 3: height bottom compression element (before and after testing)

The Tensairity arch was deconstructed at the end of the project. The deconstruction of the arch verified that the aluminium compression elements plastically deformed. Figure 105 shows a large deflection of the top compression elements in the middle of the arch. Figure 104 shows a deflection



Figure 104: Plastic deformation of compression element near connection

of the aluminium compression element at the connection of the different pieces. The deflection of the aluminium started when the steel connection tube ended (Figure 56). This showed that the connection was stronger than the rest of the beam. This could have affected the overall deformation of the beam.



Figure 105: Plastic deformation of compression element in the middle

Comparison with study by R. Maffei

An interesting comparison was made between an arch created by R. Maffei and the arch from this study (Maffei, 2010-2012). The arch created by R. Maffei (Figure 108) had a span of 6.4 meters and a height of 2.4 meters. The span of the arch in this study was 9.7 meters and had a height of 4.18 meter. The arch of R. Maffei had only a vertical web (Figure 106), while the arch in this study had a triangular web (Figure 107). The diameter of the



Figure 106: Section arch R. Maffei

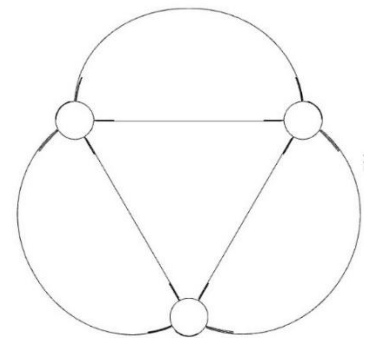


Figure 107: Section arch this study

section is unknown for the arch of Maffei, but it was approximately 400 to 700 mm. This corresponded with the section of the arch of this study. Maffei used aluminium box profiles of 15×6 mm as compression elements. These compression elements were much smaller than used in this study. The arch of Maffei had a simple foundation of wooden blocks where the compression elements were screwed on (Figure 109). A rope connected to both ends of the arch prevented sliding of the arch in longitudinal direction. The arch from Maffei was inflated with 200 / 300 mbar, while it was inflated with 100 mbar in this study.

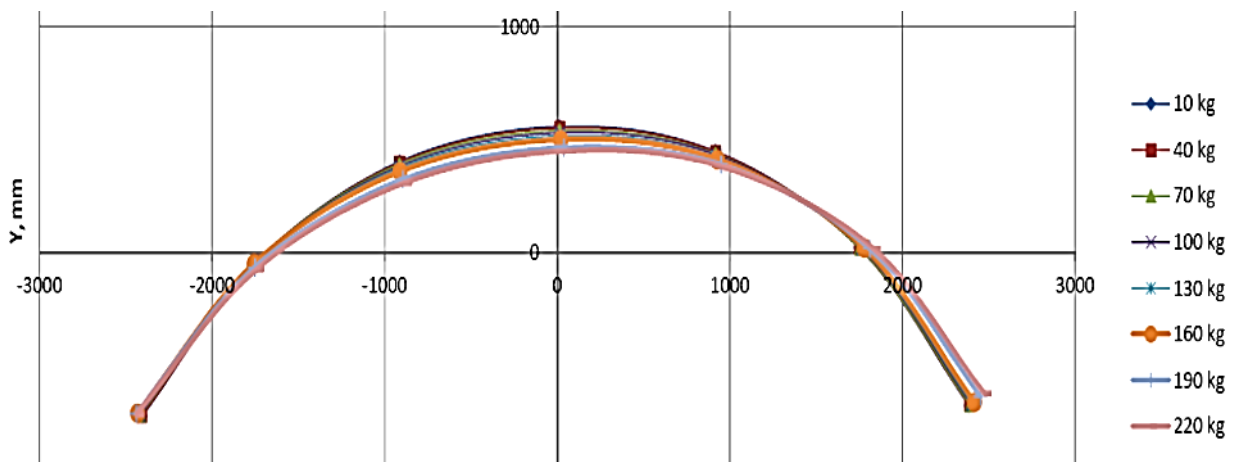


Figure 108: Tensairity arch of R. Maffei



Figure 109: Foundation Tensairity arch R. Maffei

Graph 7 shows the deformation of the Tensairity arch of Maffei when it was inflated with 300 mbar. It can be concluded that both arches deformed in the same way. The right side of the arch from Maffei bent much more compared to the left side (Figure 110, left). This corresponds with the deformation discovered in the results of the tests from this study (Figure 110, right). The arch of Maffei was able to bear a load of 260 kg at 300 mbar, before it buckled. Maffei stated that this was less than calculated in numerical analyses. This was accounted to a production error, because the arch was asymmetric. Another cause for the early buckling was that the load probably wasn't placed fully symmetric. The arch in this study deformed less at a load of 500 kg in test three, compared to what the arch of Maffei deformed at 260 kg. This was expected, because larger compression elements were used. The difference in span to height ratio between the two arch might also had an effect on the results. It has to be noted that it is hard to compare the results due to the fact that many factors are not the same (webbing, dimensions, internal pressure, etcetera).



Graph 7: results deformation Tensairity arch of R. Maffei (300 mbar)

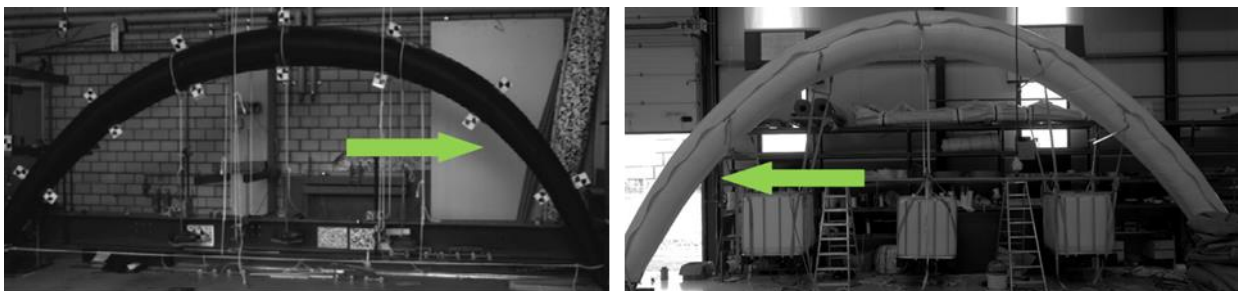


Figure 110: left; deformation arch Maffei, right arch this study

Comparison with study (Crettol, Gauthier, Luchsinger, & Vogel, 2010)

Another interesting comparison was made with a Tensairity arch created by Crettol, et al. They first created a small arch with a span of five meters (Figure 111). The small arch contained two aluminium compression elements with a cross sectional area of $6 \times 50 \text{ mm}^2$, and lacked any form of internal webbing. The test proved that the small arch could bear homogeneous loads up to 1 kN/m using internal pressure above 100 mbar . Further increase of this load would have resulted in collapsing of the arch.



Figure 111: Small arch by Crettol et al

Further optimization of the arch led to a large arch with a span of 10 meter and a constant hull diameter of 500 mm (Figure 112). Aluminium compression elements with a cross sectional area of $60 \times 15 \text{ mm}^2$ and $60 \times 12 \text{ mm}^2$ were used and there was no internal webbing present. Twelve suspension points were used for the load which was applied with a mechanical jack and a whippetree system. A load cell measured the applied load, while a 3D digital image correlation system measured the deformation.



Figure 112: Large arch by Crettol et al

The first test comprehended an asymmetric load of 7.5 kN on one half of the arch (Figure 113). The arch had an internal pressure of 70 mbar . A substantial horizontal deformation occurred. The deformation and the amplitude of the deformation was comparable with the simulation results performed in Abaqus/Explicit.

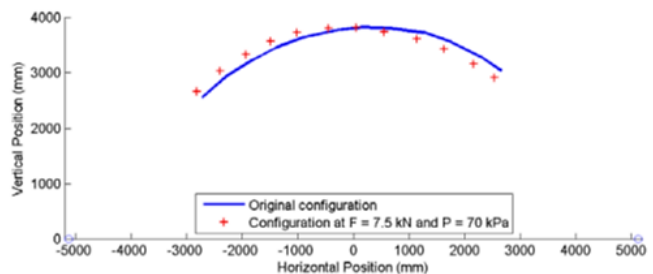


Figure 113: Deformation asymmetric load test by Crettol et al

The second test comprehended a homogeneous distributed load of approximately 35 kN on the entire span of the arch (Figure 114). The arch had an internal pressure of 50 mbar . Small displacements occurred. Minor asymmetry was detected in the arch, which was accounted to residual stresses in the compression elements and to unbalance in the applied load.

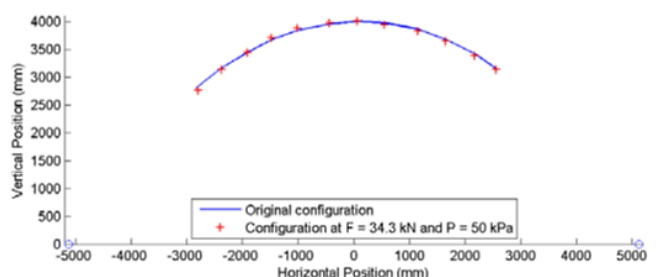


Figure 114: Deformation distributed load test by Crettol et al

The results of these tests correspond with the results of the tests performed in this study. The asymmetry caused by the previous tests dominated the deflection in the following tests in both studies. The arch from Crettol et al performed overall better, whereas it deformed less at higher loads. Crettol et al stated that an increase in internal pressure has more effect and is highly important with arches. This combined with the fact that the Tensairity arch from Crettol et al was optimized for vertical loads, having two compression elements vertically aligned, made it perform better. The triangular configuration of the arch from this study was more structurally balanced, so it should be able to bear out-of-plane forces better, while it functions less in vertical direction. The difference in stiffness of the aluminium compression elements was most likely the cause of the differences in plastic deformation. It is not possible to make a fully trustworthy comparison between both studies, due to the many differences in several variables (internal pressure, webbing, etcetera).

It is very interesting to see that a constant hull diameter resulted in the optimal shape, according to the performed FEM-analyses. This was somewhat unexpected, because previous research stated that a sigar shape was the best shape for Tensairity beams (Pedretti, Steingruber, Pedretti, & Luchsinger, N.D.). It is however possible that this was only the case for straight beams and that the sides of the arches would benefit from the constant hull diameter.

Simulation of Tensairity arch in Oasys GSA

Simulations are useful for predicting the behaviour of structures. A simulation of the Tensairity arch from this project was made in order to verify the results of the physical tests and to gain insights in the forces acting within a Tensairity arch. The simulation of the Tensairity arch was made under supervision of and in collaboration with Ir. A.P.H.W. Habraken from the University of Technology Eindhoven. The simulations are done with Oasys GSA 8.7.

This chapter will discuss the following aspects:

- The design process of the Tensairity arch,
- The start situation, which was the basis of the following simulations,
- A comparison of different variables (alterations in permanent load and material properties),
- The final simulations (start simulation with external loads).

Design in Oasys GSA

The final configuration created in Rhinoceros was first imported into Oasys GSA. The arch was then divided in longitudinal and transverse direction (Figure 115). The remaining quarter of the arch was then further designed, which included:

- Connecting all nodes,
- Aligning 2D element axes,
- Assigning materials for compression element / fabrics,
- Creating rigid constraints at the end of the arch.

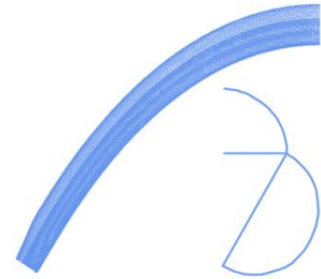


Figure 115: Quarter of the arch

The arch remained divided in transverse direction during the entire simulation process in order to reduce simulation time. This division resulted that half the fabric and one compression element was left out of the simulation. The size of the section of the bottom compression element was reduced, instead of splitting the bottom compression element as well. The new section was 50×1.36 mm. These dimensions were chosen, because the area, second moment of the area and torsion constant were the half of the original size.

The quarter arch was mirrored in longitudinal direction, after it was fully designed (Figure 116). It was important to check if the axes were mirrored correctly and the nodes were all connected.

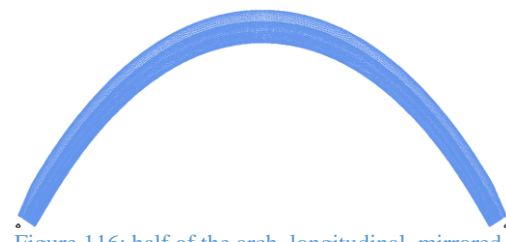


Figure 116: half of the arch, longitudinal mirrored

The PU-foil was not included in the simulation. This might have been beneficial to the physical test a little, because the material itself is very thin and flexible.

Permanent loads

Self-weight

The self-weight of the arch was included in the simulation. This was represented by a gravity load of -1 in Z-direction, appointed to all 2D- and arch-elements (Figure 117).

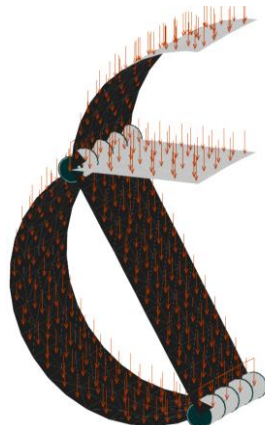


Figure 117: Self-weight

Internal pressure

The internal pressure was represented by a 2D-face load on the 2D-elements (Figure 118). The internal pressure had a value of 10 kN/m^2 (100 mbar). This value corresponded to the air pressure within the inflatable bags.

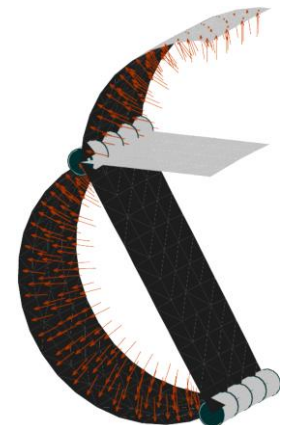


Figure 118: Internal pressure

Start situation

The start situation contained the self-weight of the arch and an internal pressure of 10 kN/m² (100 mbar). The results of the start situation are shown in Figure 119, Figure 120, Figure 121, Figure 122, Figure 123 and Appendix J. The arch transformed in the start situation, with a maximum downward displacement in the middle. The displacement declined towards the imposition, where it was nearly negligible. The fabric outer layer had a higher average 2D force (N_y) than the fabric web. The low 2D forces in the fabric web was assigned to the fact that there was no pretension in the web. There was a difference in 2D-force between the top and the bottom of the section. This was accounted to the fact that the internal pressure counteracted the self-weight in the top, while it accumulated in the bottom of the section. The large displacement / forces at the end-section was dedicated to a sudden angle change / straighter section in the outer layer, which was adjusted more than the rest after inflation (thus a design error).

Unexpected results in the 2D-forces (N_y and N_x) occurred. Points one / five and two / four should have had the same results, because they were mirrored copies of each other. This might have been caused by a design error, or by the fact that the simulations did not completely converge. The differences were however rather small, so it was ignored.

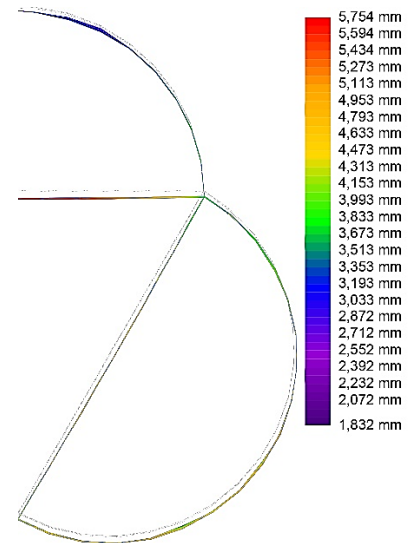


Figure 119: Mid-section deformation start situation (resolved element translation)

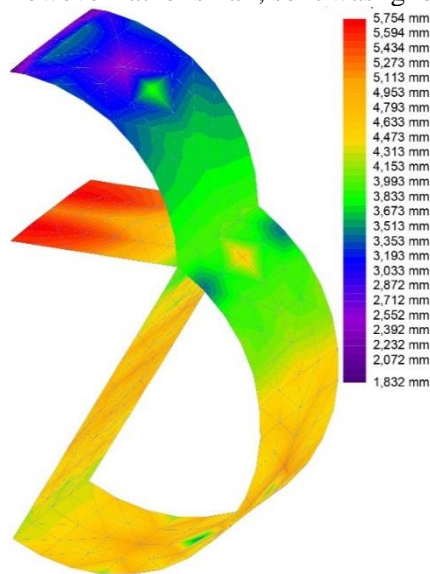


Figure 120: Mid-section start situation (resolved element translation)

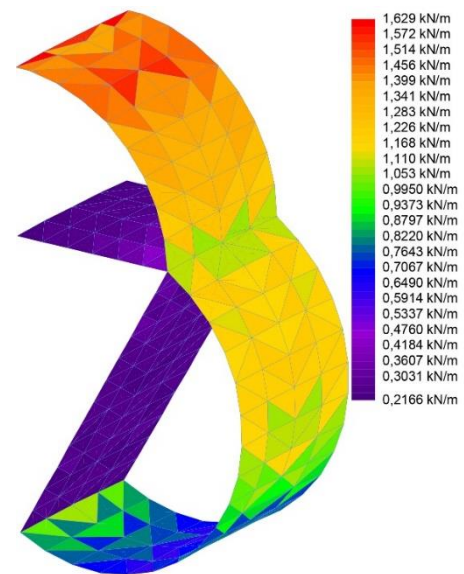


Figure 121: Mid-section start situation (2D-force N_y)

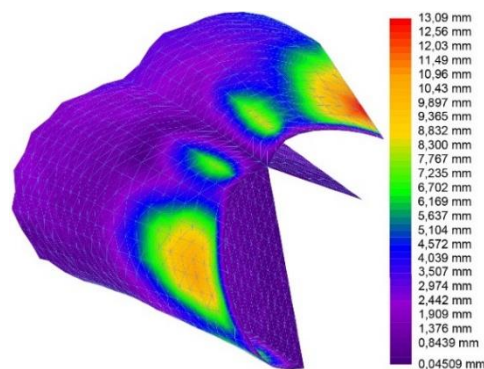


Figure 122: End-section start situation (resolved element translation)

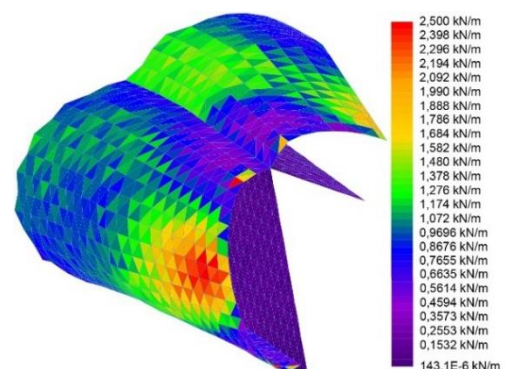


Figure 123: End-section start situation (2D-force N_y)

Comparison of simulations

Appendix K1, Appendix K2, Appendix K3 show the comparisons of the start situation with the different variables. These comparisons gave more insights in the effect of the different variables. Three types of comparisons were made: Resolved Element Translation, 2D-Force (Ny) of fabric outer layer and the 2D-force (Ny) of the fabric web. The Resolved Element Translation comparison checks the effects of the changed variables on the deformation of the mid-section. The 2D-force (Ny) comparison checks the effects of changing variables on the forces in the fabric in transverse direction.

Removal of self-weight

The difference between both simulations were considered negligible. The section had a slightly larger deformation downwards without self-weight. The 2D force (Ny) of the fabric outer layer didn't change. The 2D forces (Ny) in the fabric web declined a little, because there were less forces working on the arch. The internal pressure acting on the fabric outer layer on the other hand had more influence than the self-weight of the arch.

Alteration of internal pressure

The second comparison contained the start situation (10 kN/m²), a situation with a reduced internal pressure (5 kN/m²) and a situation with an increased internal pressure (20 kN/m²). Using a double amount of internal pressure increased the deformation of the section. The 2D-forces (Ny) in the fabric outer layer and the fabric web both doubled when the internal pressure was higher. This was caused by the fact that increasing the internal pressure caused the section to expand, creating more tension in the fabric. Previous studies showed that an increase in internal pressure led to a higher buckling load (Wever, 2008).

Alteration of Poisson ratio of fabric web

“The Poisson ratio of a material is the ratio of transverse strain to axial strain in the direction of stretching force” (Lakes, N.D.). A higher Poisson ratio gives more contraction in lateral direction if the material is stretched in longitudinal direction. This comparison contained the start situation (Poisson ratio of 0.4), a decreased Poisson ratio (0.3) and an increased Poisson ratio (0.5) of the fabric web. The mid-section of the arch deformed more when the Poisson was lower. Increasing the Poisson ratio gave a higher 2D-force (Ny) in the bottom of the section, while it decreased at the top of the section.

Alteration of Warp modulus of fabric web

The Warp modulus of a fabric is the Young's modulus in the Warp direction (Oasys, 1985-2015). “The Young's modulus of a material is the ratio of compressive / tensile stress to compressive / tensile strain in an objects subjected to uniaxial compression / tension.” (University of Cambridge, N.D.) A higher Young's modulus corresponds to a stiffer material. The Warp of the fabric was in longitudinal direction of the Tensairity arch. This comparison consisted of the start situation (Warp modulus of 850 kN/m) a reduced Warp modulus (700 kN/m) and an increased Warp modulus (1000 kN/m) of the fabric web. An increased Warp modulus resulted in a small reduction of the deformation of the section. The 2D forces (Ny) in the fabric outer layer and in the fabric web remained practically the same in the three situations. These results were assigned to the fact that all three situations had high Warp moduli. A variant was therefore simulated with a Warp modulus of 100 kN/m. This variant showed an increase in the 2D-forces (Ny) in the fabric web. It also gave an increase in the 2D-forces (Ny) in the top of the fabric outer layer, while it decreased in the bottom of the fabric outer layer.

Alteration of Weft modulus of fabric web

The Weft modulus of a fabric is the Young's modulus in the Weft direction (Oasys, 1985-2015). A higher Young's modulus corresponds to a stiffer material. The Weft of the fabric was in transverse direction of the Tensairity arch. This comparison contained the start situation (600 kN/m), a reduced Weft modulus (400 kN/m) and an increased Weft modulus (800 kN/m) of the fabric web. A higher Weft modulus gave a decreased deformation of the section. A lower weft modulus gave an increased 2D-force (Ny) in the fabric outer layer and the top fabric web, while it decreased in the bottom fabric web. The differences were

however very small, because the Weft moduli were very high in all situations. Another variant (Weft modulus of 50 kN/m) was simulated, which verified the results.

Alteration of Shear modulus of fabric web

The Shear modulus of a fabric web is the ratio of Shear stress to Shear strain. (Young, Freedman, & Bhathal, 2010) An increased Shear modulus corresponds with a stiffer material. This comparison contained the start situation (45 kN/m), a decreased Shear modulus (30 kN/m) and an increased Shear modulus (60 kN/m) of the fabric web. The section deformed less when the Shear modulus was decreased. A lower Shear modulus gave an increased 2D-force (Ny) in the fabric outer layer and the top fabric web, while it decreased in the bottom fabric web. The differences were very low, because the Shear moduli of all situations were very high. Another variant (Shear modulus of 5 kN/m) was simulated, which verified these results.

Final simulations

The following simulations investigated the effect of external loads on the start situation (with all original values). The load values were cut in half due to the fact that the arch was cut in half in transverse direction. This should however give the same results as the full load in a complete arch. Three tests were performed:

- One point load of 2.5 kN (thus 5 kN) in the top of the Tensairity arch (Figure 124). This corresponded with point three (Appendix G).

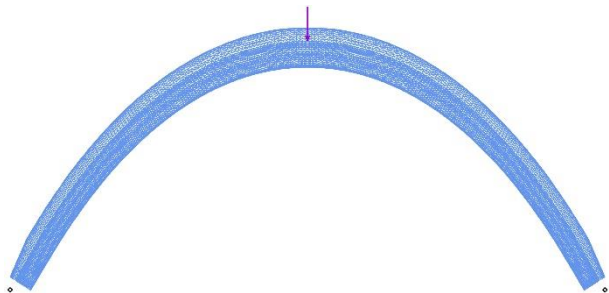


Figure 124: Point load in the top of the arch

- One point load of 1.5 kN (thus 3 kN) at a quart of the span of the Tensairity arch (Figure 125). This point is between point four and five (Appendix G).

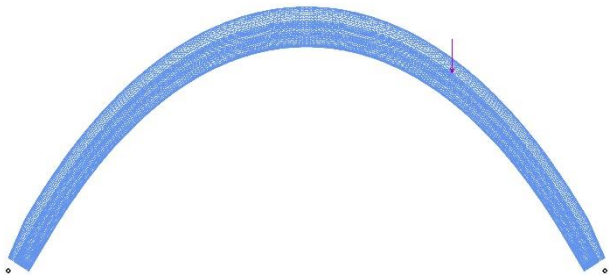


Figure 125: Point load at a quarter of span of the arch

- Five point loads distributed over the span of the Tensairity arch with a total of 2.5 kN (thus 5 kN) (Figure 126). This corresponded with points one to five (Appendix G).

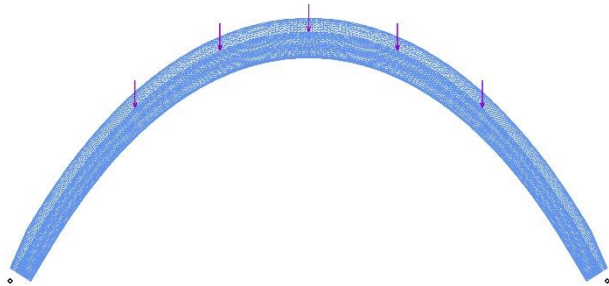


Figure 126: Five point loads distributed over span of the arch

The simulations were investigated at four types of results: Resolved Element Translation, 2D-Force (Ny), 2D-force (Nx) and Bending stress (Bz + ve y). The Resolved Element Translation shows the displacement of the arch. The 2D-force (Ny) shows the forces in the fabric in transverse direction, while the 2D-force (Nx) shows the forces in the fabric in longitudinal direction. The bending stress shows the stress occurring in the compression element as a result of the applied load. The difference in forces between the left and right side of the arch in the start situation was ignored.

Simulation of test one; load in the middle

Appendix L1 shows the results of the first simulation. The arch showed a uniform displacement, with the maximum in the middle of the arch. Point two and four had an equal downward displacement, while point one and five had an equal upward displacement. The arch had a horizontal displacement as well, moving the sides of the arch outward. The 2D-forces (N_y) in the fabric outer layer and the horizontal web was higher compared to the start situation. This was a logical response of the load acting on the arch, moving the top compression elements outward and downward (Figure 127). The tension in the diagonal web on the other hand was lessened, because the distance between the compression elements declined. The sides of the beam expanded outward, creating more forces in the longitudinal directions (2D-force N_x). The top on the other hand contracted more, declining the tension in the fabric. The large difference in bending stress between the top and the sides of the arch was accounted to the fact that the load was in the middle and the compression element distributed the stress over the entire length. The difference in stress between the top and bottom compression element was lower than expected, which means that the web transferred more load than expected.

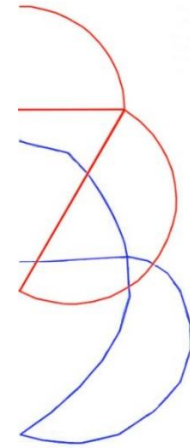


Figure 127: Deformation section middle of arch test one (red = start, blue = deformed) (magnification x10)

Simulation of test two; load at a quarter

The results of the second simulation is shown in Appendix L2. The load is applied between point four and five, which can be seen in the downward displacement at these points. Points one and two had an upward displacement. Point three had no vertical deformation. Horizontal deformation towards points one occurred. The difference in 2D-force (N_y) was very small. The only mentionable difference was in the diagonal web at the location of the load. The top compression element had a downward deformation, declining the tension in the diagonal web (Figure 128). The 2D-force (N_x) was larger at the point of the load compared to the start situation. The 2D-force (N_x) in the rest of the web remained more or less the same. Interesting is the fact that the top outer layer showed larger forces than the bottom outer layer, which was due to the fact that the expansion was larger in the top outer layer. The compression

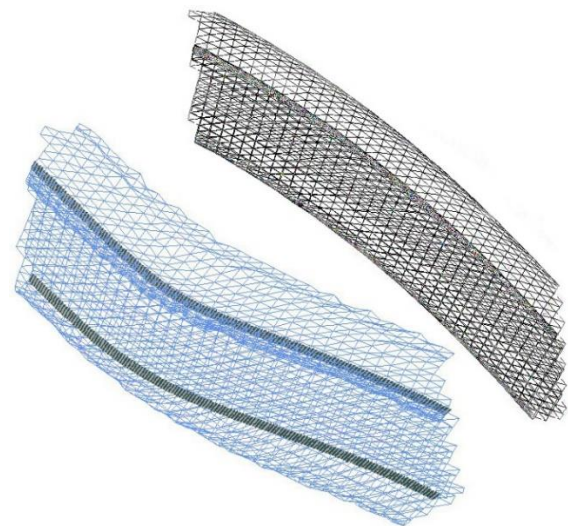


Figure 128: Deformation section quarter of arch test two (black = start, blue = deformed) (magnification x40)

elements showed a large negative bending stress at the location of the load, while the rest of the beam showed a positive bending stress. The stress values weren't expected, but can be explained by the fact that the load was at the quarter of the arch and the compression element distributed the stress over the entire length. The difference in stress between the top and bottom compression element was also lower than expected, which means that the web transferred more load than expected.

Simulation of test three; load distributed over five points

The results of the third simulation can be seen in Appendix L3. The arch showed evenly distributed results for both vertical and horizontal displacement. The middle of the arch showed a maximum downward displacement. Points two and four also showed a downward displacement, while point one and five deformed upward. All points had a horizontal displacement moving outward, except for the middle of the arch. When comparing these results with the simulation of test one, it can be concluded that the load on points one, two, four and five counteracted on the load on point three, decreasing the deformation on all points. There was very little difference in 2D-force (N_y) in the outer layer and the top web compared to the start situation. The 2D-force (N_y) decreased in the diagonal web at the location of the loads compared

to the rest of the arch. The differences were however smaller compared to the first test, which is due to the fact that the loads were much lower. A small increase in 2D-force (N_x) was found in the middle of the bottom outer layer and the quarter of the diagonal web. The difference was however smaller due to the counteracting effect of the other loads. The top outer layer and the top web showed minor differences. A clear relation between the first and third test is visible looking at the bending stress of the compression elements. A negative bending stress occurred at the locations of the arch with the max bending stress in the middle. The rest of the arch showed a positive bending stress. The negative bending stresses at the loads were smaller than with the first test, which is mostly due to the fact that each load was only 1 kN instead of 5 kN. The loads also counteracted each other, because the bending stresses were opposites between the point of the load and the rest of the arch, as shown in test one and two. The five load points deformed the arch downward, reducing the upward deformation of the rest of the arch.

Simulation of test one with increased internal pressure (200 mbar)

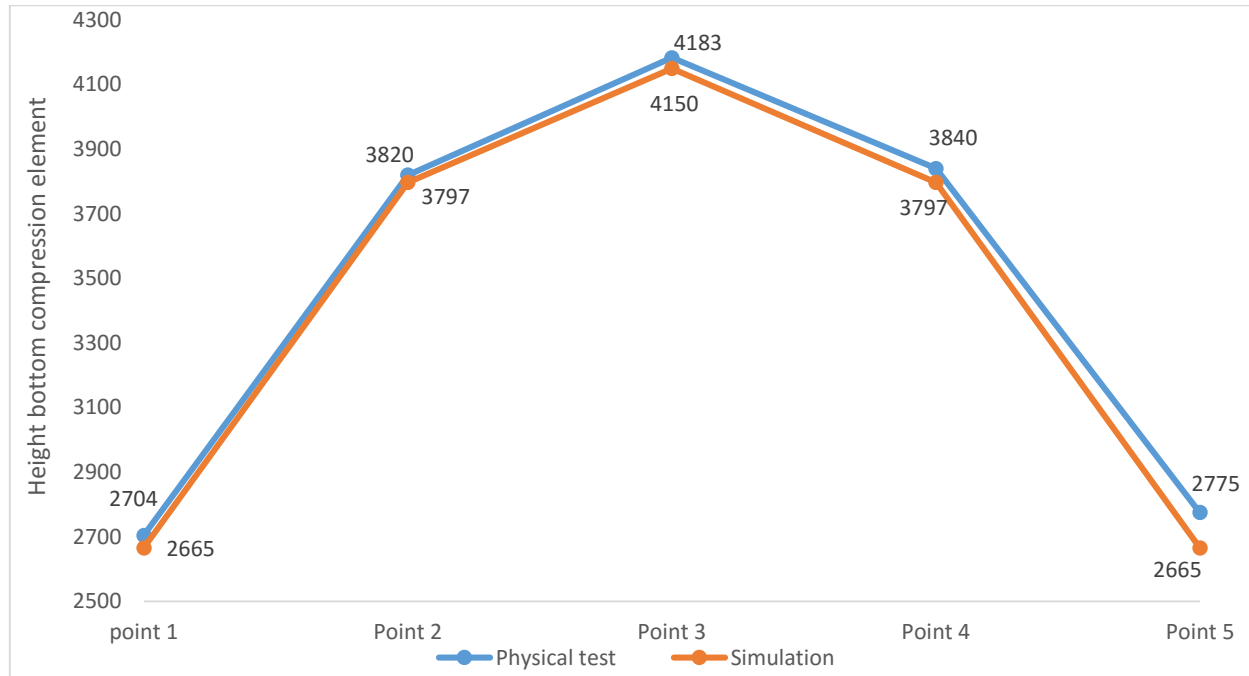
Changing the internal pressure had a noticeable effect on the deformation and forces in the fabric, as mentioned in the paragraph “Comparison of simulations”. The extent of effect on the deformation with an external load present was however unknown. Test one was therefore repeated with an increased internal pressure (200 mbar). The results are shown in Appendix M. There was a minimal difference in deformation in the arch compared to the original situation. The forces in the warp and weft direction of the fabric outer layer and the fabric web increased much. This is a logical result, because the internal pressure pushed harder on the outer layer. The minor difference in deformation is somewhat unexpected, because literature stated that increasing the internal pressure would be beneficial to the structural behaviour.

Comparison of test and simulation

This chapter compares the results of the physical test and the simulation described in the previous chapters, with focus on the deformation of the arch. A comparison was made between a symmetric and a asymmetric arch, in order to gain insights in the effect of asymmetry on the arch.

Comparison of start situation

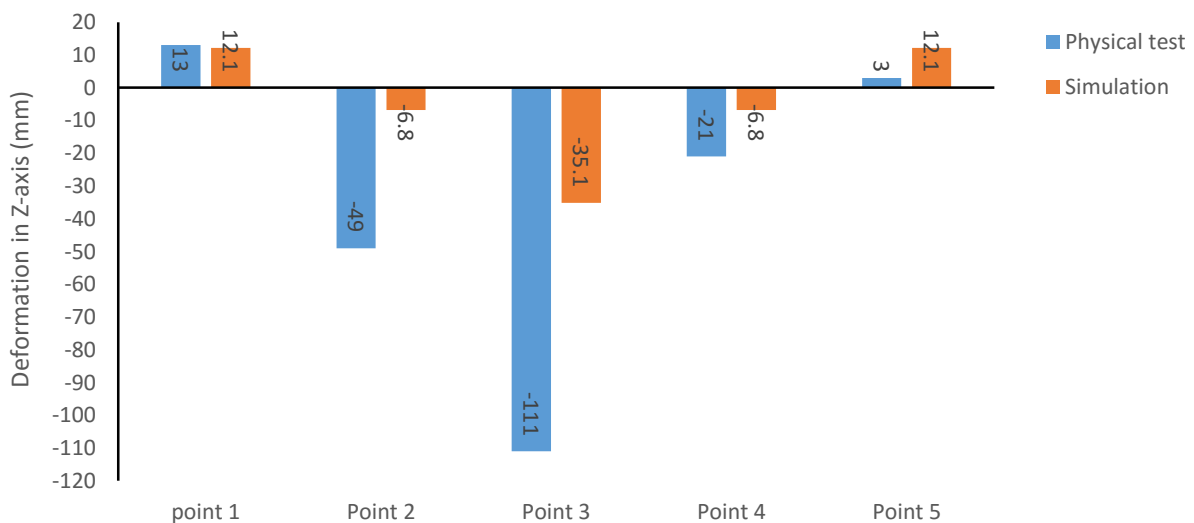
Graph 8 shows the difference in height of the arch between the test situation and the simulation. It can be concluded that the arch in the test situation was overall higher than the arch in the simulation. It has to be noted that an inaccuracy in measuring in the physical test situation exists, which could enlarge these differences. This is discussed in the chapter “Testing of Tensairity arch”. The beam in the test situation was also asymmetrical, creating a large deformation at point five.



Graph 8: Height bottom compression element start situation

Comparison of test one

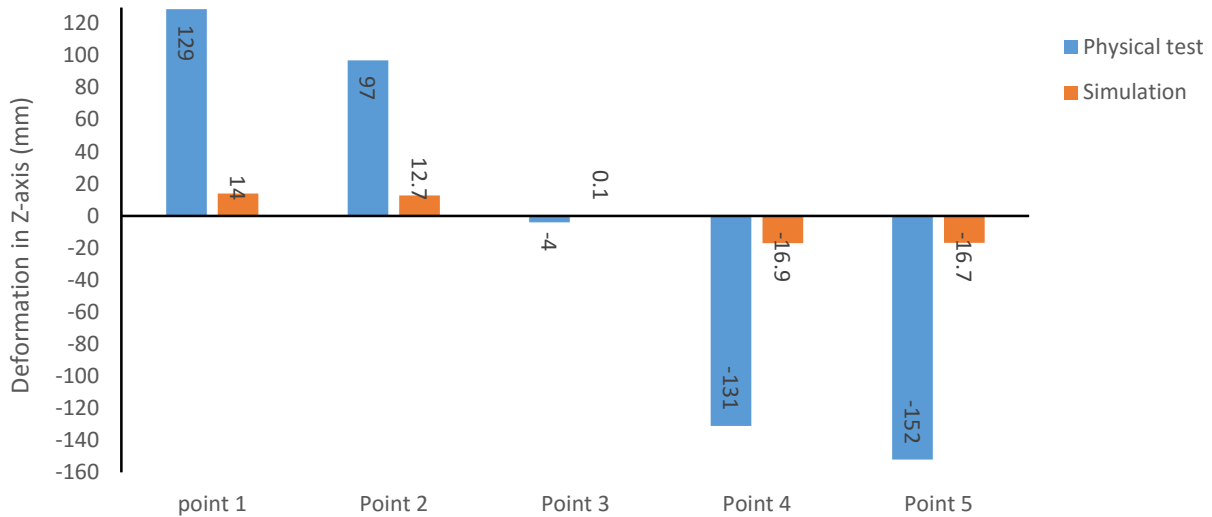
There were large differences between the simulation and the physical test (Graph 9). The deformation of point one was almost equal, while the deformation in point five gave noticeable differences. This was an unexpected result, due to the fact that points two, three and four gave a larger deformation in the physical test compared to the simulation. As mentioned in the chapter “Testing of Tensairity arch”, this is probably due to asymmetry of the arch. Also a minor deviation in the position of the load was a possible cause. The plastic deformation was only present in the test situation, which was quite determining in the results of the following tests.



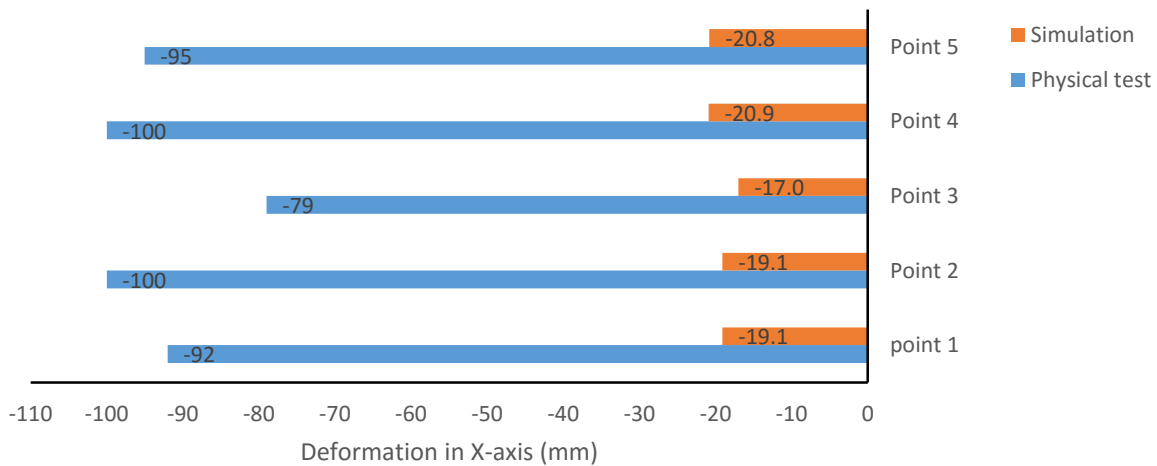
Graph 9: Comparison of physical test and simulation of test one

Comparison of test two

Large differences were present between the results of physical test and the simulation in the second test (Graph 10 and Graph 11). Both deformations showed the same type of deformations, but the physical test vertically deformed approximately 7.5 to 9 times more than the simulation. It also deformed approximately 5 times more horizontally. It is likely that the deformation in the test situation was enhanced by the plastic deformation of test one. Also the fact that the physical arch was asymmetric enhanced the deformation. The physical arch showed a plastic deformation in the second test which was not visible in the simulation.



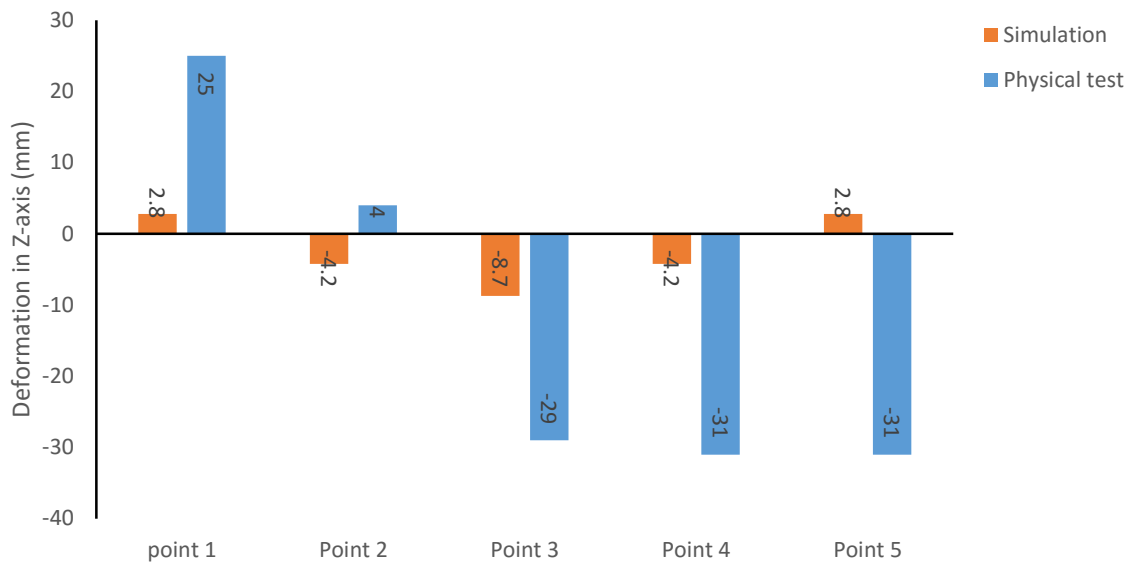
Graph 10: Comparison of physical test and simulation of test two (vert. deformation)



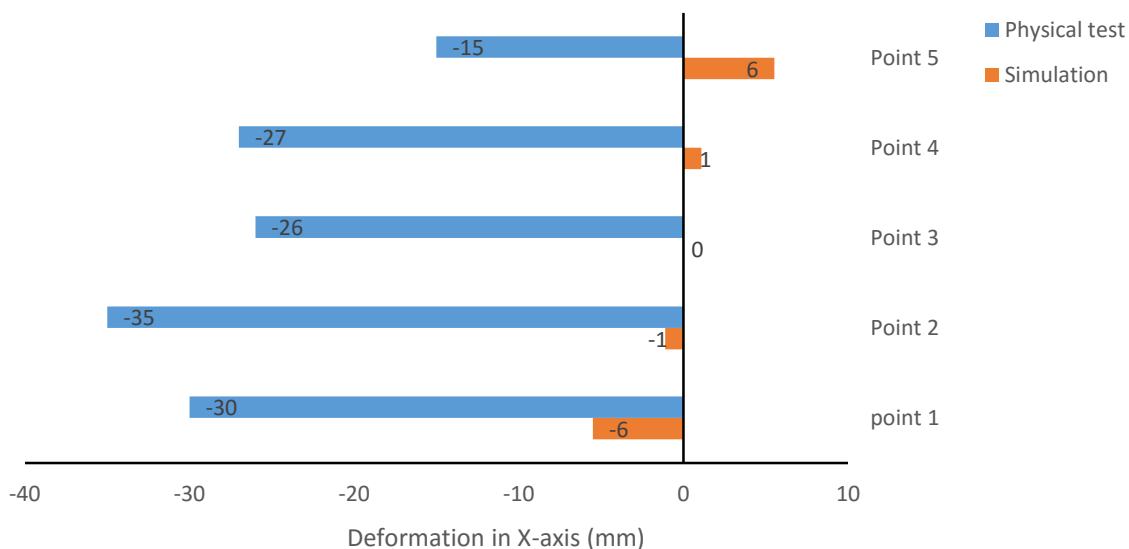
Graph 11: Comparison of physical test and simulation of test two (hor. deformation)

Comparison of test three

Differences in deformation between the test situation and the simulation were present in test three (Graph 12 and Graph 13). The simulation showed an upward deformation in points one and five, and a downward deformation in the middle three points, with a maximum downward deformation in point three. The physical arch on the other hand showed a large upward deformation in point one, a minor upward deformation in point two, and a large downward deformation in the other three points. Differences in the horizontal deformation was also noticeable. The physical arch had deformations towards point one, while the simulation showed that point one and two were opposites of point four and five. These differences were the result from the plastic deformation from the first two tests and the fact that the arch was asymmetric.



Graph 12: Comparison of physical test and simulation of test three (vert. deformation)



Graph 13: Comparison of physical test and simulation of test three (hor. deformation)

Verifying effect asymmetry of beam on test results

The asymmetry of the beam is appointed as one of the main causes of the high differences in deformation between the physical test and the simulation. An additional simulation test was performed, in order to verify this conclusion (Appendix N). This test consisted of a single aluminium arch, which was symmetric in the first situation and asymmetric in the second. A vertical point load in the middle of the arch was introduced in both situations.

The symmetric arch showed a uniform deformation, while the asymmetric arch showed a non-uniform deformation. The asymmetric arch showed larger deformations compared to the symmetric version.

Although the asymmetry of this arch was not the same as the asymmetry of the Tensairity arch, it can be concluded that the asymmetry of the arch had a noticeable effect. This verified the conclusions made earlier, which stated that the differences in deformation between the physical test and the simulation was partially caused by the asymmetry of the beam.

Conclusion and Discussion

Conclusions are drawn in this chapter on the following subjects:

- Design of the tent structure,
- Design, production and end result of the arch,
- Test Results,
- Simulation results,
- End conclusion.

Recommendations will be given after conclusions are drawn.

Design of the tent structure

The final tent structure has a lot of potential. It is possible to change the appearance of the structure, creating multiple functions for the tent. It is also possible to scale the tent, creating even more options. Unfortunately it is not a modular system, reducing possible aesthetic options. The fact that the Tensairity arches are placed in one direction and have the same length is preferable, but the detailing of the imposition will be difficult. Building the physical arch has shown that the steel imposition gave lots of problems during construction. Having three impositions on each side of the arch that are able to rotate will make it much harder, making different detailing necessary. Steel cables in transverse direction are necessary, in order to meet the regulations.

Design, production and end result of the arch

The final variant of the detailing of the arch contained several problems. The detailing looked promising, due to the fact that the aluminium compression elements only had to be shoved in the fabric sleeves and everything could be transported in a small package. The sleeve concept started out with one single piece of fabric, which became five pieces per sleeve because it was not possible with one piece. It became clear that the sleeve detail was very complex and took too many production hours. Three detailing / production errors caused a lot of wrinkles in the arch: inaccuracies in the fabric patterns, uneven stretching of the fabric during stitching/welding and too tight detailing of the fabric sleeve, preventing the compression element from being able to slide within the sleeve. These wrinkles partially disappeared after inflation. Another problem during construction was the insertion of the compression elements in the imposition. At first they wouldn't go in, and the next moment they were in too far. This problem was caused by the fact that the fabric sleeves were too long and eventually created a barrier.

Tensile strength tests were performed during the fabrication, which made clear that the stitched connections were not very strong. The final tests had to point out if the connections were strong enough.

The design and the end result of the arch contained lots of errors and is far from perfect. It was however functioning in the end, and it was a good prototype for the final testing. A different design has to be made that is less complex, is less time consuming to produce and has stronger connections. A more demountable design has to be made, which would likely result in special extruded keder-profiles instead of simple tube profiles. The connections would also be solely made by welding instead of stitching.

Test Results

Four tests have been done: 1; load in the middle, 2; load at a quarter, 3; load distributed over five points, 4; the same as test one, but with the main purpose to check the plastic deformation and to see the effect of higher loads on the arch. The asymmetry of the arch was further enhanced by the tests. The vertical and horizontal displacement was measured before, during and after the test using a Laser Distance meter on five predefined fixed points. The deformation of the arch gave expected results for test one and two although there were some effects visible from the asymmetry of the arch. Test three on the other hand gave less expected results. This was partially due to the asymmetry of the arch, but mostly due to the plastic deformation as a result of test one and two. Test four verified the results of test one that the arch showed a noticeable plastic deformation starting at 500 kg. The deformation at 500 kg between test one and four were however not equal. This is probably due to the fact that the arch was already plastically deformed in the fourth situation.

The plastic deformation of the Tensairity arch was caused by the plastic deformation of the aluminium compression elements. Friction between the inflatable bags and the fabric hull was also accounted as a cause. The inflated bags did not go back to their original position after the load was released. Deflation and re-inflation of the bags showed that the arch went back a little to its original state.

The plastic deformation of the compression elements could occur due to the fact that the compression elements were probably too stiff. A less stiff compression element would deform more, but plastically deform later. A good balance has to be found between stiffness and load bearing capacity.

The third test performed in this study was compared to the testing of a Tensairity arch created by Maffei. Despite the fact that there were quite some differences in dimensions and detailing, there were also quite some similarities. The type of deformation matched, and both arches were asymmetric. The arch from this study however had a higher load bearing capacity. This was due to the fact that bigger compression elements were used and a triangular web was used instead of a vertical web. This comparison verified that asymmetry had a noticeable effect on the load bearing capacity of an arch.

The second and third test performed in this study was compared to the testing of a Tensairity arch created by Crettol et al. Both arches deformed the same way, but the arch from Crettol et al performed overall better. This was mostly caused by the much higher internal pressure in the arch from Crettol et al. The optimization of the arch in vertical direction led to better structural integrity during the performed tests. The arch from this study is likely better able to withstand out-of-plane forces. The difference in stiffness of the aluminium compression elements was most likely the cause of the dissimilarities in plastic deformation. Interesting to see was the fact that FEM-analyses showed that a constant hull diameter resulted in the optimal shape. It is likely that the sides of the arch benefit from a constant hull diameter. This should be investigated further in combination with triangular webbed Tensairity arches.

Simulation results

Designing of the arch in Oasys GSA was very complex. Many problems had to be dealt with during the design phase, like unconstrained elements or elements drawn among the wrong axes. Comparisons were made between a start situation and situations with alterations in several properties of the web material and in the permanent loads of the start situation. The effect of changing the internal pressure was noticeable, while the effect of changing the web material had very little effect. This was due to the fact that the changed values were still too high to show noticeable differences. The self-weight of the arch had a negligible effect on the results of the arch. These results were all quite expected, although the extent of the effects were somewhat surprising for some comparisons.

The first three tests of the physical arch were simulated with Oasys GSA, in order to verify the results and to gain insights in the forces acting in a Tensairity arch. The deformations were at a maximum at the location of the load. At the points of the load, the forces in the weft direction of the fabric increased a little for the outer layer and the horizontal web, while it decreased in the diagonal web. This was due to the deformation of the section at that location. The forces in the warp direction of the fabric were overall lower at the point of the load. This is due to the fact that the arch expands more at the rest of the beam, introducing large forces at those points. The bending stress in the compression elements were opposites for the location of the load and the rest of the arch, showing large difference. These differences can be explained by the fact that the stress at the load was very local, while for the rest of the arch the stress spread over its entire length. There was a relatively small difference in bending stress between the top and bottom compression elements, which can be explained by the fact that the fabric web transferred a lot of load from the top to the bottom.

A fourth test compared the first test with an arch that had an internal pressure of 200 mbar, instead of 100 mbar. This comparison gave somewhat unexpected results. There were minor differences in deformation, while large increases in the 2D-forces (N_x and N_y) occurred. The large increases in the 2D-forces are explained by the fact that the internal pressure pushed harder onto the fabric. Further research should be done, in order to verify the reliability of the simulations.

Comparison of test and simulation

The physical test and the simulation both showed the same type of deformation for the first two tests. The physical tests however showed larger deformations than the simulation. The plastic deformation from the first test was noticeable in the second test, due to the fact that the difference in amount of deformation was even larger than in test one. Test three showed differences in amount of deformation and in positive and negative horizontal and vertical deformations.

The differences in amount of deformation was partially due to the asymmetry of the arch and the plastic deformation after each test. It is also possible that there were significant wrinkles in the fabric webs of the actual arch, reducing the capacity of the webs to function properly. Question marks can be placed with Oasys GSA as well. The exact material properties of the fabric was unknown and it was not verified that the halve arch would give the same results as a full arch. It is likely that Oasys GSA is not advanced enough to simulate Tensairity projects. Further research should be done in order to gain certainty of the cause of the differences in deformation. This includes a thorough investigation of the current model, the development of a new model in Oasys GSA and the development of a new model in another simulation program.

End conclusion

Beside the flaws in the design and the errors during fabrication/construction, it could be stated that the project was a success. Attention points became clear regarding the design of the beam. The tests gave enough insight in the structural behaviour of the arch and showed the bottlenecks of detailing Tensairity projects. These results will be beneficial for future designs. More research and development has to be done in order to create the perfect arch.

Bibliography

- Architen Landrell. (2010, March 10). *Using PTFE Glass Cloth*. Retrieved from Architen Landrell: <http://www.architen.com/articles/using-ptfe-glass-cloth/>
- Ascent Roofing LTD. (N.D.). *Home*. Retrieved from Asent Roofing LTD - From the simplest of repairs o the most complex of projects: <http://ascentroofingltd.co.uk/>
- Attwoolls Manufacturing. (N.D.). *590g/m² Flame Retardant PVC Coated Polyester. Width: 250 cm*. Retrieved from Attwoolls Manufacturing: <http://www.attwoollsmanufacturing.co.uk/fabrics/pvc-fabric/500g-m-flame-retardant-pvc-coated-polyester-width-250cm/>
- Big Span structures, L. (N.D.). *Air Supported Structures*. Retrieved from World Wide Diversity in... Fabric Architecture: http://www.bigspanstructures.com/air_dome.php
- Birdair. (N.D.). *Estadio Ciudad de la Plata*. Retrieved from Birdair: <http://www.birdair.com/projects/estadio-ciudad-de-la-plata>
- Buitink Technology. (2011). *ETFE Informatiefolder*. Duiven: Buitink Technology.
- Buitink Technology. (N.D.). *Advanced Lightweight Structures*. Retrieved from Buitink Technology: <http://www.buitink-technology.com/nl/>
- Buitink Technology. (N.D.). *Demontabele tensairity overkapping*. Retrieved from Buitink Technology - advanced lightweight structures: <http://www.buitink-technology.com/nl/innovatie/demontabele-tensairity-overkapping/>
- Buitink Technology. (N.D.). *Duurzaamheid & Milieu*. Retrieved from Buitink Technology - Advanced Lightweight Structures: <http://www.buitink-technology.com/nl/duurzaamheid-milieu/>
- Crettol, R., Gauthier, L., Luchsinger, R., & Vogel, R. (2010). *Tensairity Arches. Proceedings of the International Association for Shell and Spatial Structures Symposium*. Shanghai.
- Detail inspiration. (N.D.). *Roof over Parking Area in Montreux*. Retrieved from Detail inspiration: <http://it.detail-online.com/inspiration/roof-over-parking-area-in-montreux-103599.html>
- Dieterle, F. (2008, October 2). *Tensairity-Bridge*. Retrieved from Google+: <https://plus.google.com/photos/+FlorianDieterle1984/albums/5222431723397063297>
- EMPA. (N.D.). *Tensairity - technology*. Retrieved from EMPA, Center for Synergetic Structures: http://www.empa.ch/plugin/template/empa/*/107063
- Empa. (N.D.). *Tensairity Principle*. Retrieved from Empa - a Research Institute of the ETH Domain: http://www.empa.ch/plugin/template/empa/*/107063
- Empa. (N.D.). *Tensairity; The new lightweight structure*. Retrieved from Empa - a Research Institute of the ETH Domain: http://www.empa.ch/plugin/template/empa/*/107059
- European Committee For Standardization. (2005, November). *NEN-EN 13782 ; Temporary structures - Tents - Safety*. Brussels.
- Forsstrom. (N.D.). *TX 200-500*. Retrieved from Forsstrom: http://www.forsstrom.com/pages/default_uk.asp?sectionid=281
- Heslop, A. (2010, March 10). *Basic Theories of Tensile Fabric Architecture*. Retrieved from Architen Landrell: <http://www.architen.com/articles/basic-theories-of-tensile-membrane-architecture/>
- Kroonenburg, H. v. (1974). *Methodisch ontwerpen. de Ingenieur, nr. 47*.

- Lakes, R. (N.D.). *Mean of Poisson's ratio*. Retrieved from <http://silver.neep.wisc.edu/~lakes/PoissonIntro.html>
- Luchsinger, R., & Crettol, R. (N.D.). *The role of fabrics in Tensairity*. CH-8600 Duebendorf, Switzerland: Empa, Center for Synergetic Structures.
- Luchsinger, R., Pedretti, A., Steingruber, P., & Pedretti, M. (N.D.). *Light Weight Structures with Tensairity*. Biasca, Switzerland: Airlight Ltd.
- Maffei, R. (2010-2012). *Sheltering in Emergency: Processes and Products*. Milan: Politecnico Di Milano.
- NingBo High-MeiYong International Trading CO.,LTD. (N.D.). *3732-130P1 PTFE Coated Fiberglass Fabrics*. Retrieved from NingBo High-MeiYong International Trading CO.,LTD: <http://www.glass-fibers.com/ptfe-fabric/1162731.html>
- Oasys. (1985-2015). *Oasys GSA Help Guide*. London, England. Retrieved from <http://www.oasys-software.com/>
- Pedretti, A., Steingruber, P., Pedretti, M., & Luchsinger, R. (N.D.). *The new structural concept Tensairity: FE-modeling and applications*.
- Pedretti, M. (2004). *Tensairity*. Biasca, Switzerland: Airlight Ltd.
- Pronk, A., Maffei, R., & Martin, H. (2009). *Research on the combination of water and membranes as a structural building material*. Valencia: Proceedings of the International Association for Shell and Spatial Structures (IASS) Symposium .
- R.H. Luchsinger, A. P. (2004). *The new structural concept Tensairity: Basic principles*. London: Taylor & Francis Group.
- Reynolds, P. (2011, Februari 1). *Waitomo Visitor Centre*. Retrieved from Architecturenow: <http://architecturenow.co.nz/articles/waitomo-caves/#img=0>
- Ropex Industrie-Elektronik GmbH. (N.D.). *Cirus*. Retrieved from Thermoplastic film sealing particulary foils: <http://www.ropex.de/cirus.php>
- Seidel, M. (2007). *Tensile Surface Structures: A Practical Guide to Cable and Membrane Construction*. Vienna: Ernst & Sohn.
- Son, M. E. (2007). *The design and analysis of Tension Fabric Structures*. Cambridge: Massachusetts Institute of Technology.
- Technet Alliance. (N.D.). *Roof over Parking Area in Montreux*. Retrieved from TechNet Alliance - Your Global CAE-Partner: http://www.technet-alliance.com/uploads/tx_caeworld/Art_Opz_4_DETAIL.pdf
- Technical commission CEN/TC 250. (2011). *NEN-EN 1 991 -1 -4*. BrisWarehuis.
- University of Cambridge. (N.D.). *Definition of Young's Modulus*. Retrieved from University of Cambridge: <http://www.doitpoms.ac.uk/tlplib/thermal-expansion/young-mod-def.php>
- University of Toronto. (N.D.). *Shear Modulus*. Retrieved from <http://faraday.physics.utoronto.ca/IYearLab/WilberforceRefShear4of8.pdf>
- Vink, F. (1998). *Mechanica; toepassing in de bouw en waterbouw*. Delft, Netherlands: Delft University Press.
- Wever, T. (2008). *Tensairity; The effect of internal stiffeners on the buckling behaviour of an inflatable column*. Delft: Delft University of Technology.

- Wever, T., Plagianakos, T., Luchsinger, R., & Marti, P. (2010). *Effect of fabric webs on the static responses of spindle shaped Tensairity columns*. Switzerland: Empa.
- Wilson, A. (2013, February). *ETFE Foil: A guide to design*. Retrieved from Architen Landrell: <http://www.architen.com/articles/etfe-foil-a-guide-to-design/>
- World in a Shell. (N.D.). *Facts and Figures*. Retrieved from The World in a Shell; Art & Science, People & Heritage: <http://www.worldinashell.net/index.html>
- Young, H., Freedman, R., & Bhathal, R. (2010). *University Physics: Australian edition*. Frenchs Forest: Pearson Australia.
- Zeiler, W. (2014). *Basisboek Ontwerpen*. Groningen/Houten: Noordhoff Uitgevers bv.

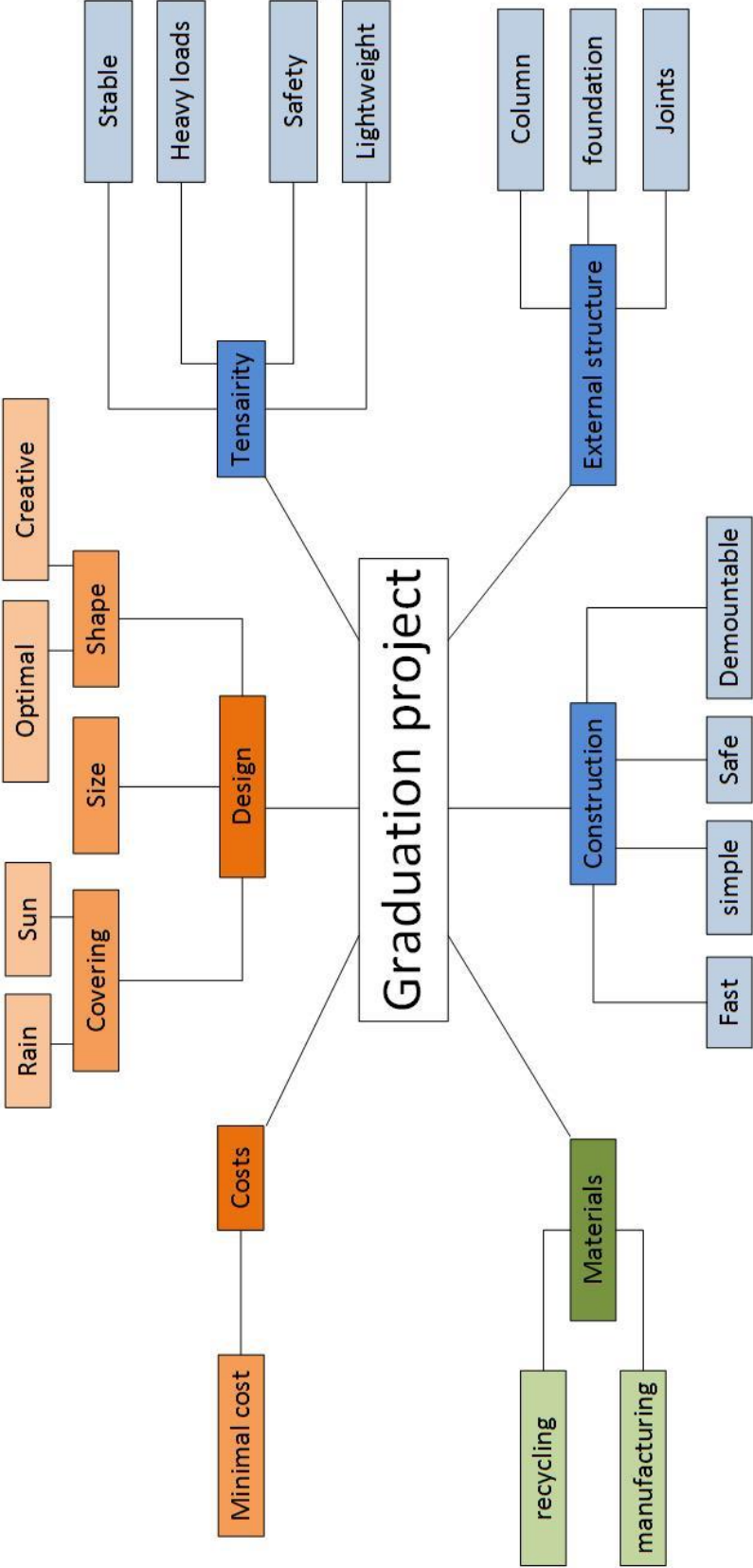
Appendix A

Research methodology

Phase 1	<i>Analysis</i>	Conduction of literature study. Important information is gained. Creation of a graduation plan, containing: problem definition, goal, (sub) research questions, methodology and time planning.
	<i>Synthesis</i>	Development of program of requirements, containing all demands and requirements of the project. Development of morphological scheme. Variants for the requirements and functions from step three are developed.
	<i>Selection</i>	Evaluation of the morphological scheme and creation of combination of the designed variants.
		Development of sketches based on the combination of variants. Evaluation of the sketches.
Phase 2	<i>Designing</i>	Development of the Tensairity arch. Simulation of the Tensairity arch.
		<i>Construction</i>

Appendix B

Mind map



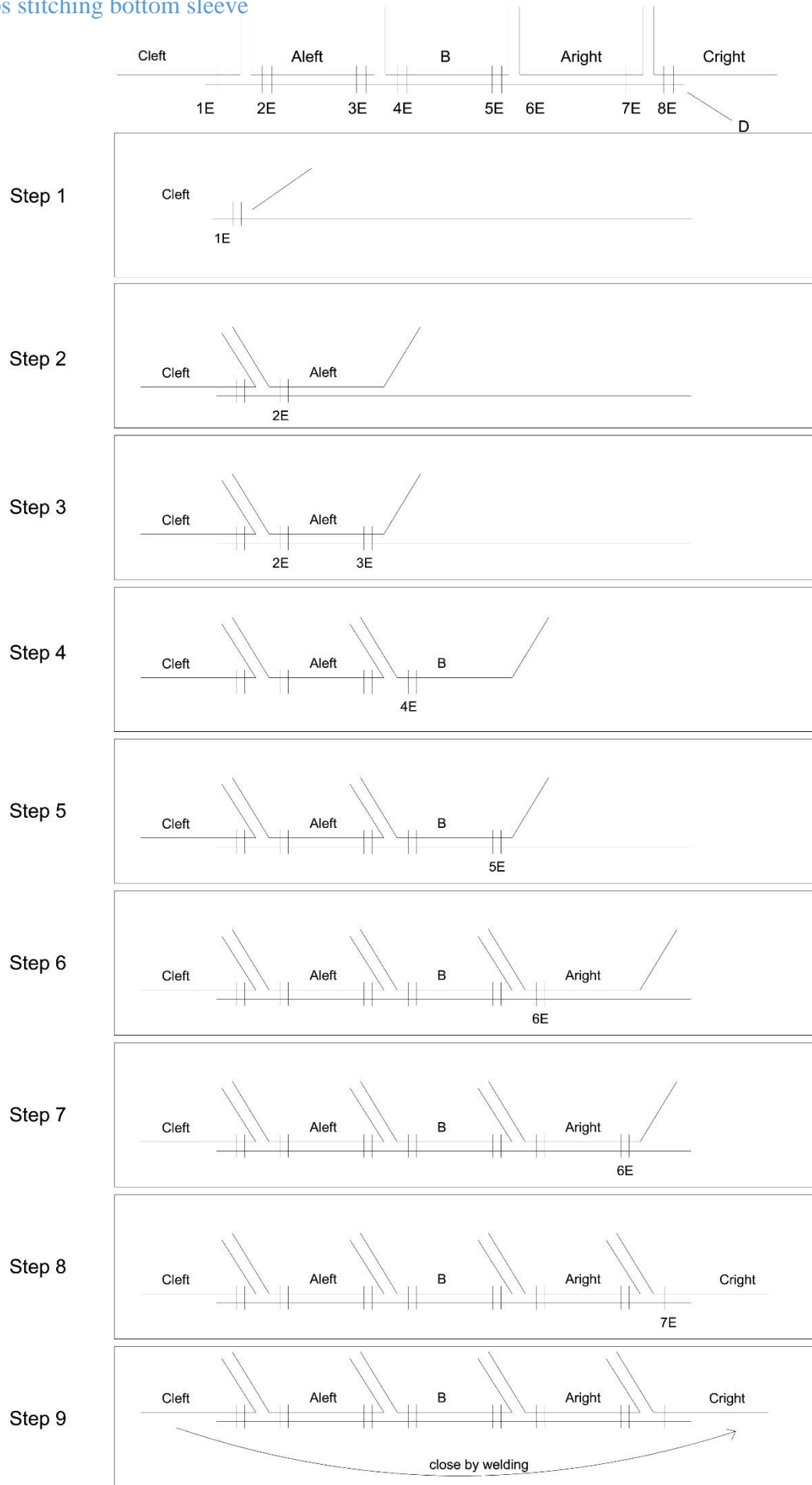
Appendix C

Program of requirements

Requirements	<i>Tensairity</i>	<p>The Tensairity structure must be strong and stable and lightweight.</p> <p>The connection of the Tensairity with the external structure must be as strong as possible.</p>
	<i>External structure</i>	<p>The external structure has to be optimized. Dimensions of the structure must be minimized without losing the required structural properties.</p> <p>The external structure must be strong and stable. It should have good structural joints and good materials.</p>
	<i>Design</i>	<p>The design must contain creative aspects and be optimized on the usage of space.</p> <p>The structure must protect the user from rain and sun, but also create a light environment.</p> <p>The structure has to meet the safety regulations on: constructive, use, and fire safety.</p>
	<i>Construction</i>	<p>The structure has to be demountable. The structure must be transported as small as possible.</p> <p>The structure must be erected in a simple and fast way. It should contain the least actions possible. Heavy labour should be prevented.</p> <p>The safety of the builders should be ensured when constructing the structure.</p>
	<i>Sustainability</i>	<p>It must be attempted to use as sustainable materials as possible.</p> <p>The construction should occur as sustainable as possible.</p>
	<i>costs</i>	<p>The project must have minimal costs. Considerations have to be made between costs, sustainability and structural properties.</p>

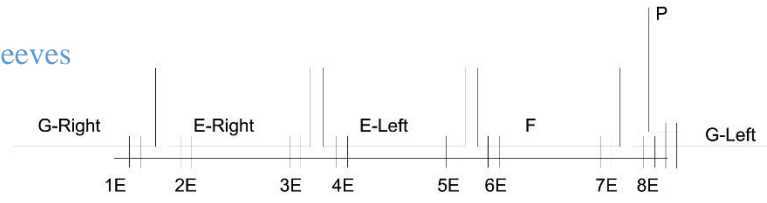
Appendix D1

Steps stitching bottom sleeve



Appendix D2

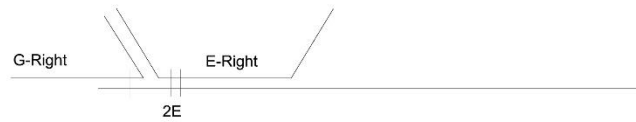
Steps stitching top sleeves



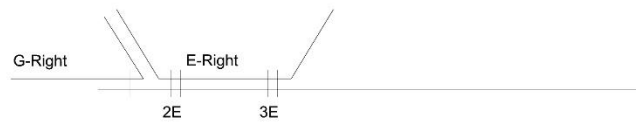
Step 1



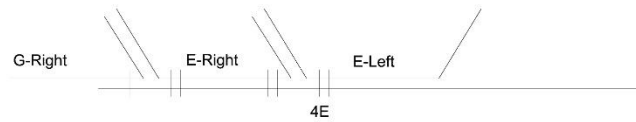
Step 2



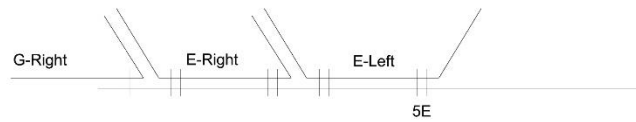
Step 3



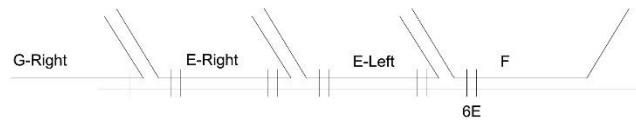
Step 4



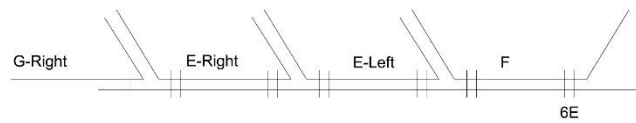
Step 5



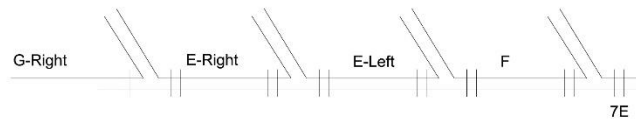
Step 6



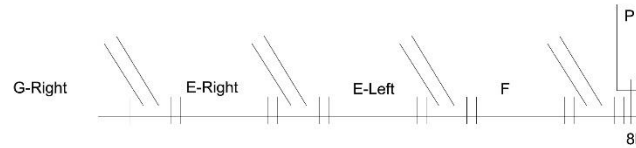
Step 7



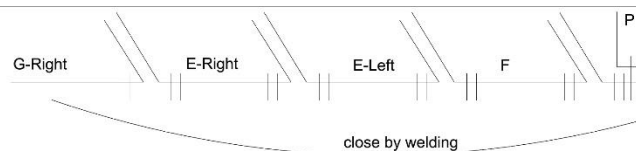
Step 8



Step 9

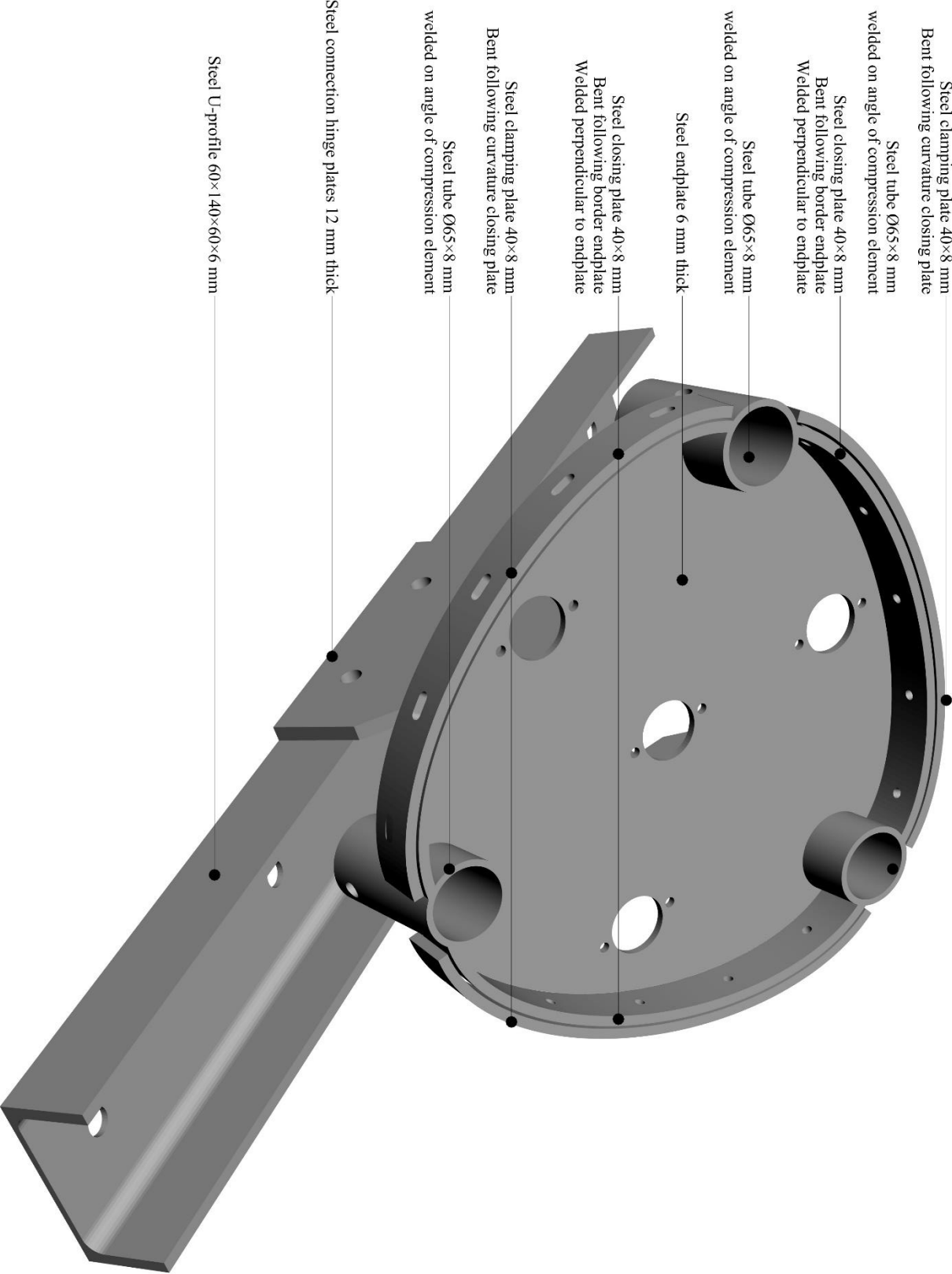


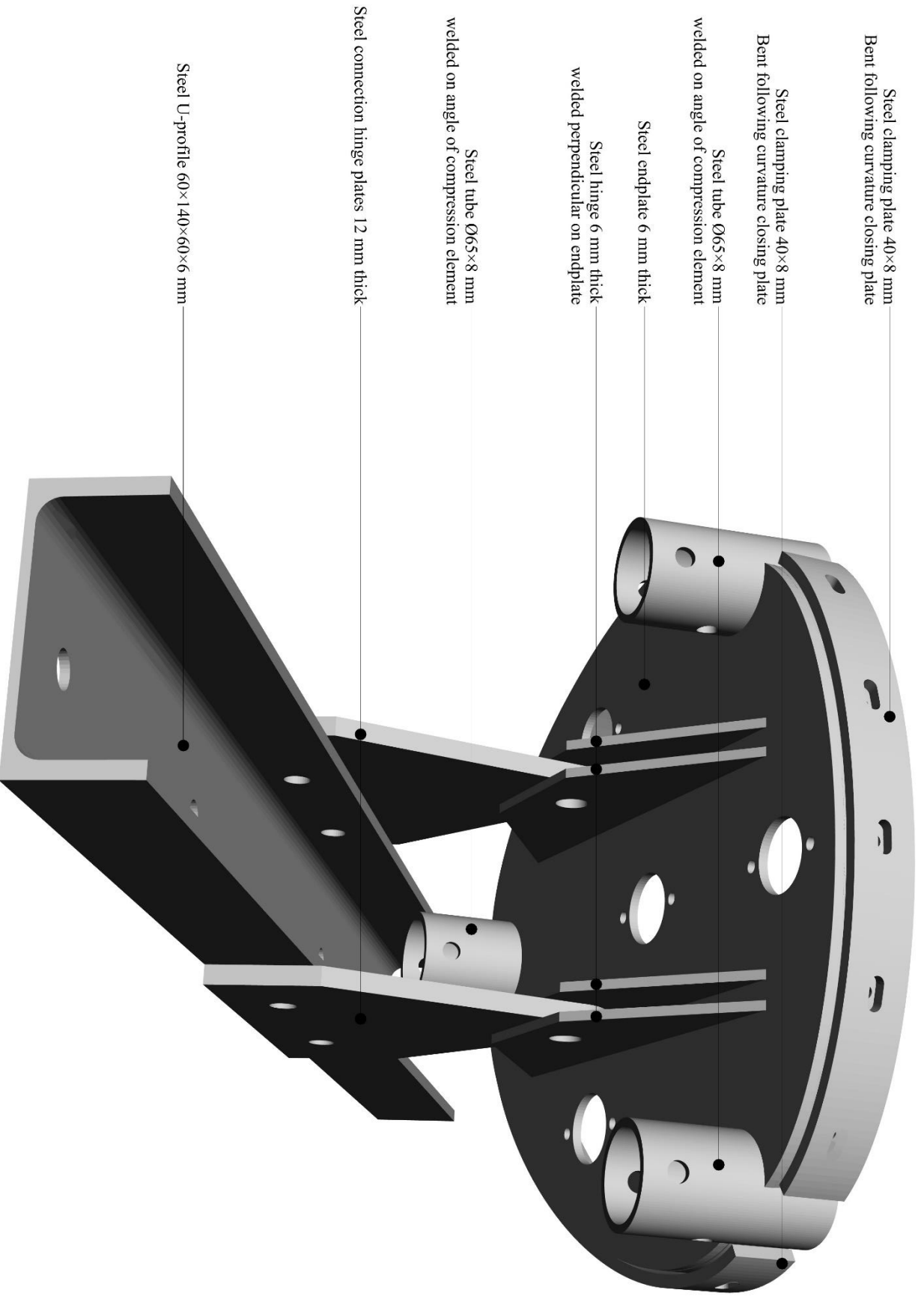
Step 10



Appendix E

Detail steel imposition





Aluminium

Aluminium (AW-606 T66)	
Diameter:	50 mm
Wall thickness	3 mm
Weight	1,22 kg/m ¹

Dimensions Tensairity beam:	
Span:	11000 mm
Height:	5000 mm
Length (top):	14860 mm
Length (bottom):	14080 mm

weight compression element (top):
 $1,22 \times 14,86 = 18 \text{ kg}$

weight compression element (bottom):
 $1,22 \times 14,08 = 17 \text{ kg}$

Total weight aluminium: 53 kg

Steel

Steel (E235+C) tube	
Diameter:	42 mm
Wall thickness	5 mm
Weight:	4,56 kg/m ¹

- 3 Pieces of aluminium compression element
- 2 Pieces of steel connector
- 0,3 m¹ long steel connectors

Weight steel connector:
 $4,56 \times 0,3 = 1,37 \text{ kg}$

Total weight steel: 8,2 kg

Fabric

Material fabric outer layer:	PVC coated polyester	→	0,75 kg
Material fabric web:	PCV coated aramid	→	1,00 kg
Material fabric sleeves:	PVC coated polyester	→	1,00 kg

Area fabric outer layer:

Area fabric web:

Area fabric sleeves

Total Area Tensairity hull:

$25,2 \text{ m}^2$
 $15,9 \text{ m}^2$
 $29,2 \text{ m}^2$
 $54,4 \text{ m}^2$

Weight fabric outer layer:

Weight fabric web:

Weight fabric sleeves

Weight tendons fabric sleeves

Total weight fabric hull

$= 25,22 \text{ m}^2 \times 0,75 \text{ kg/m}^2 = 18,9 \text{ kg}$
 $= 15,87 \text{ m}^2 \times 1,00 \text{ kg/m}^2 = 15,9 \text{ kg}$
 $= 29,16 \text{ m}^2 \times 0,75 \text{ kg/m}^2 = 21,87 \text{ kg}$
 $= 43,80 \text{ m}^1 \times 0,18 \text{ kg/m}^1 = 7,665 \text{ kg}$
 $64,3 \text{ kg}$

Total

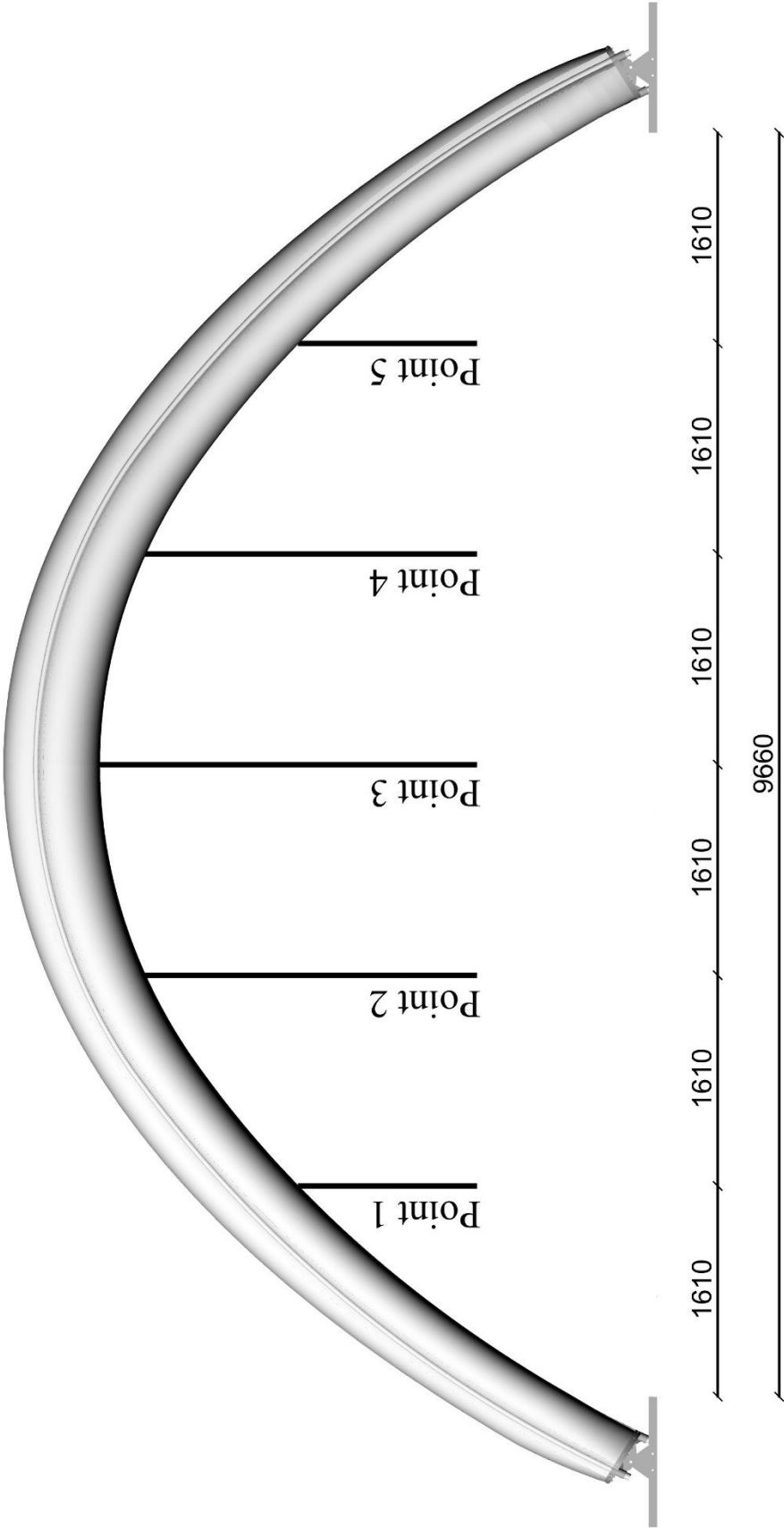
Weight aluminium compression elements 53 kg
 Weight steel connectors 8 kg
 Weight fabric hull 64 kg +
 Total weight Tensairity beam 126 kg
 Weight Tensairity beam per meter: 8,5 kg/m¹

Appendix F

Self-weight Tensairity arch, without bolts nuts and impositions

Appendix G

Distribution of suspension points



Appendix H1

Test one; load on middle suspension point (top=100 kg, mid=300 kg, bottom 500 kg)



Appendix H2

Test two; load on quarter suspension point (top= 100 kg, mid=200 kg, bottom=300kg)



Appendix H3

Test three; load distributed on five suspension points (top=150 kg, mid=300 kg, bottom=500 kg)



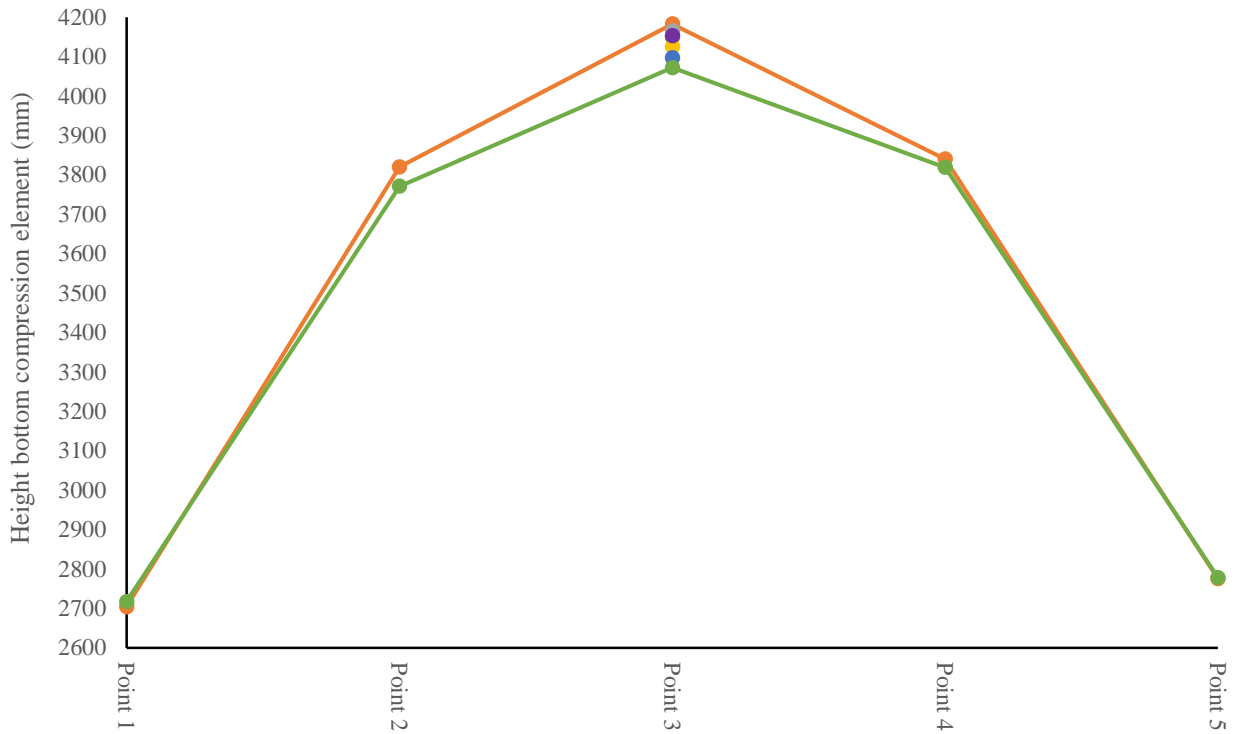
Appendix H4

Test four; load on middle suspension point (top=100 kg, mid=600 kg, bottom=800 kg)



Appendix I

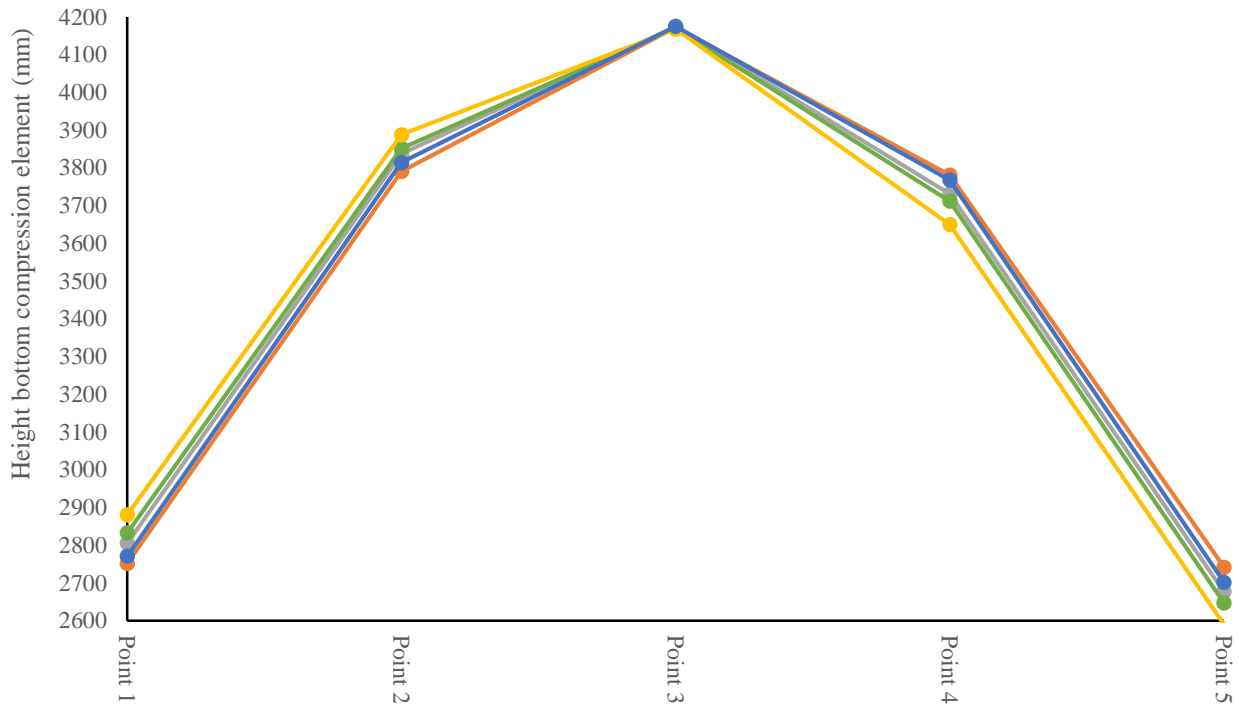
Graph test one: load in middle (height bottom compression element)



	Point 1	Point 2	Point 3	Point 4	Point 5
0 kg	2704	3820	4183	3840	2775
100 kg	-	-	4165	-	-
200 kg	-	-	4149	-	-
300 kg	-	-	4125	-	-
400 kg	-	-	4097	-	-
500 kg	2717	3771	4072	3819	2778
0 kg	-	-	4153	-	-

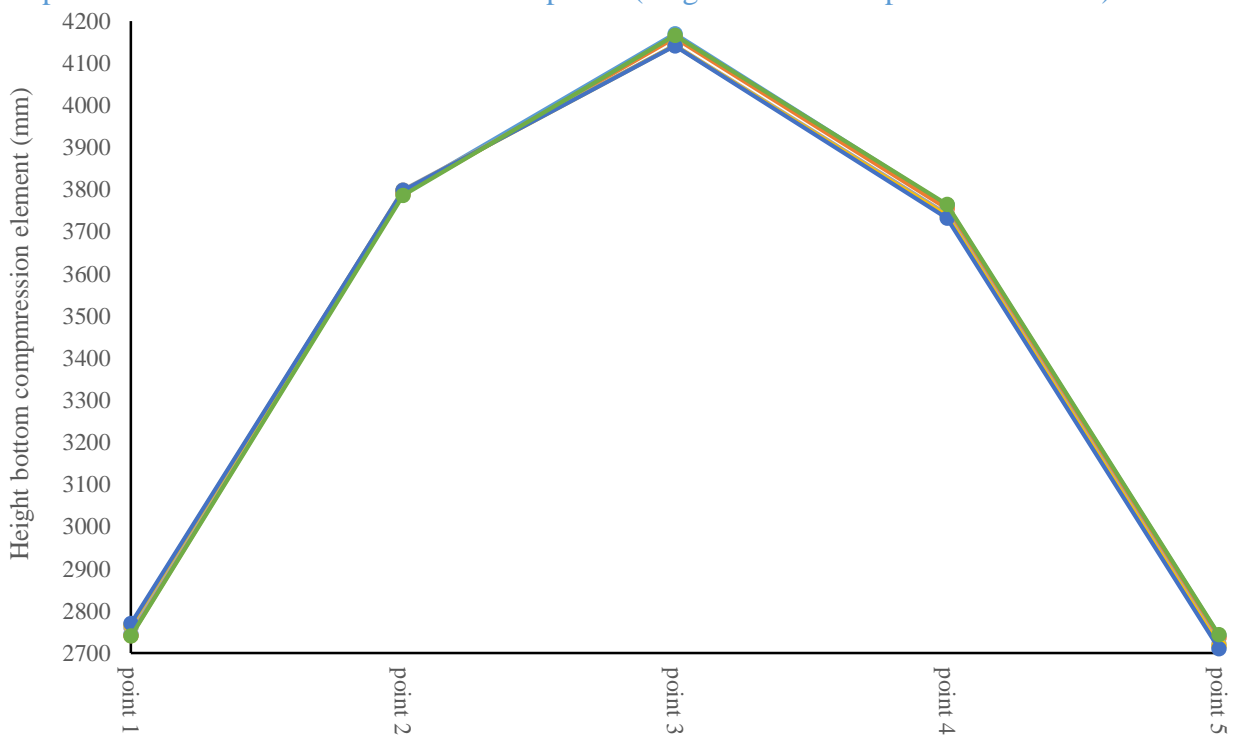
	Point 1	Point 2	Point 3	Point 4	Point 5
0 kg	2704	3820	4183	3840	2775
100 kg	-	-	4165	-	-
200 kg	-	-	4149	-	-
300 kg	-	-	4125	-	-
400 kg	-	-	4097	-	-
500 kg	2717	3771	4072	3819	2778
0 kg	-	-	4153	-	-

Graph test two; load at a quarter (height bottom compression element)



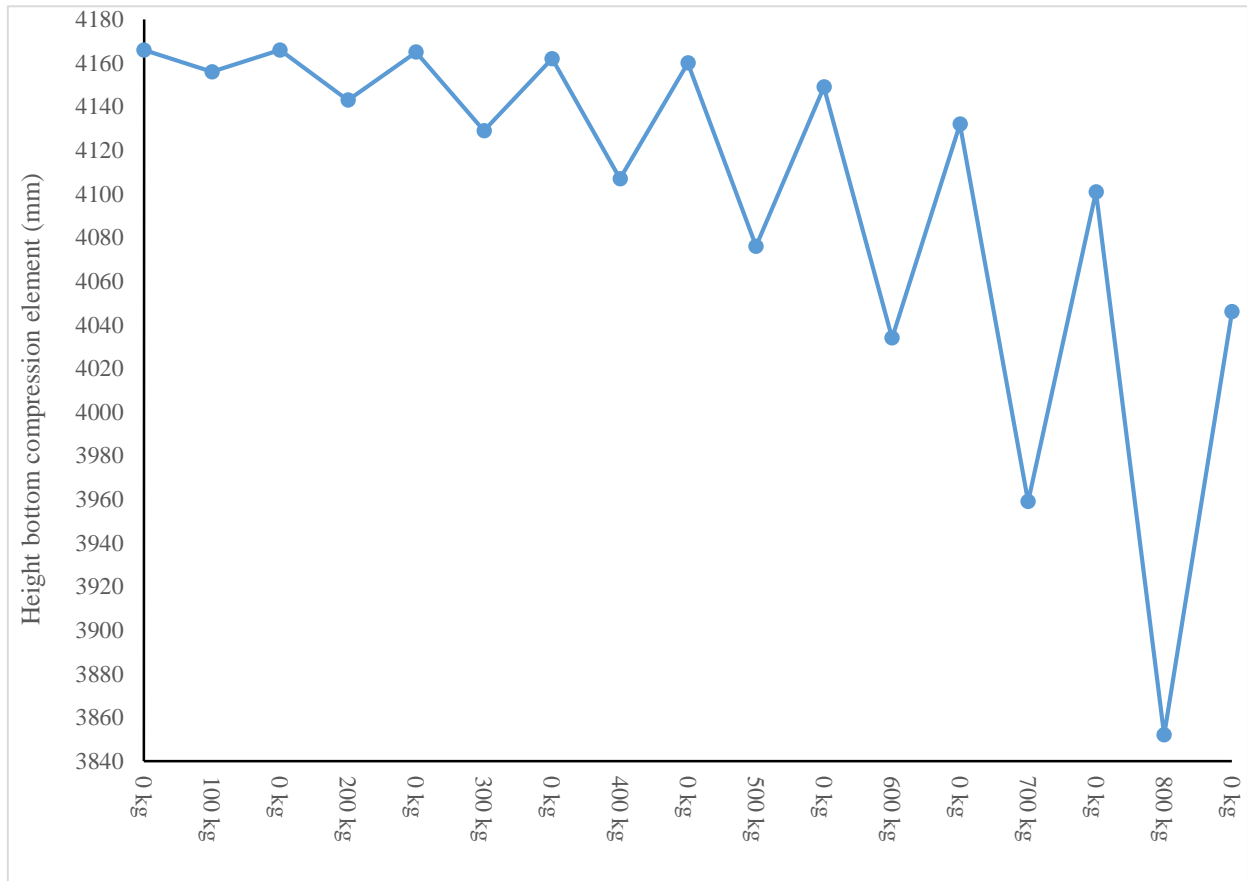
	Point 1	Point 2	Point 3	Point 4	Point 5
0 kg	2752	3791	4172	3781	2742
100 kg	2806	3837	4174	3731	2677
200 kg	2833	3852	4171	3712	2647
300 kg	2881	3888	4168	3650	2590
0 kg	2771	3814	4175	3768	2702

Graph test three: load distributed over five points (height bottom compression element)



	Point 1	Point 2	Point 3	Point 4	Point 5
0 kg	2745	3794	4170	3763	2741
150 kg	2741	3789	4160	3755	2736
300 kg	2760	3799	4143	3742	2721
400 kg	2767	3797	4142	3738	2716
500 kg	2770	3798	4141	3732	2710
0 kg	2740	3786	4166	3765	2743

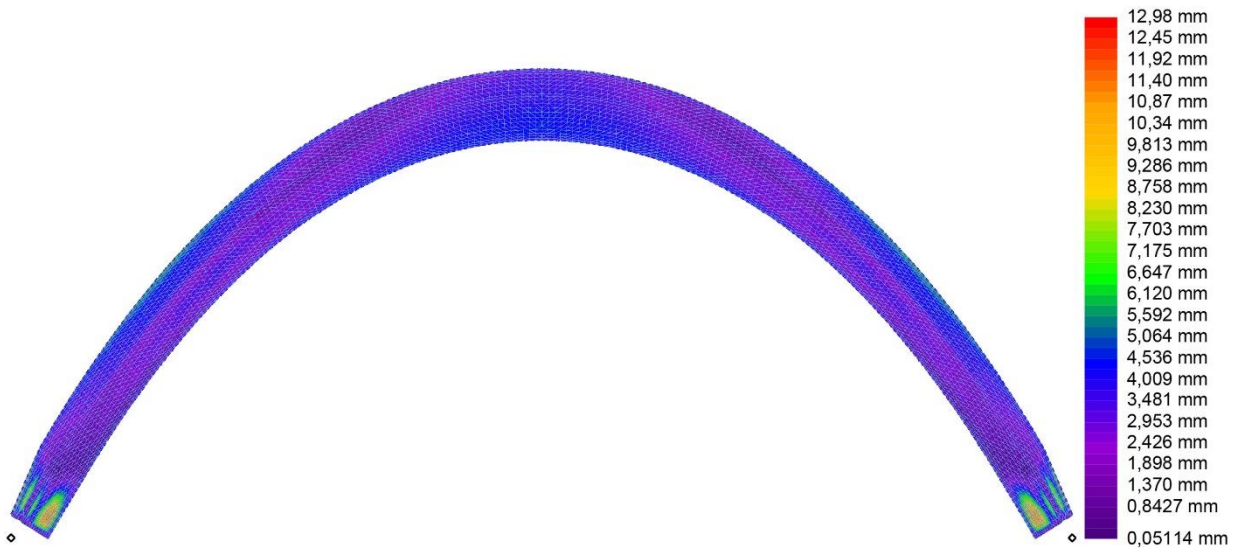
Graph test four: load in middle (height bottom compression element)



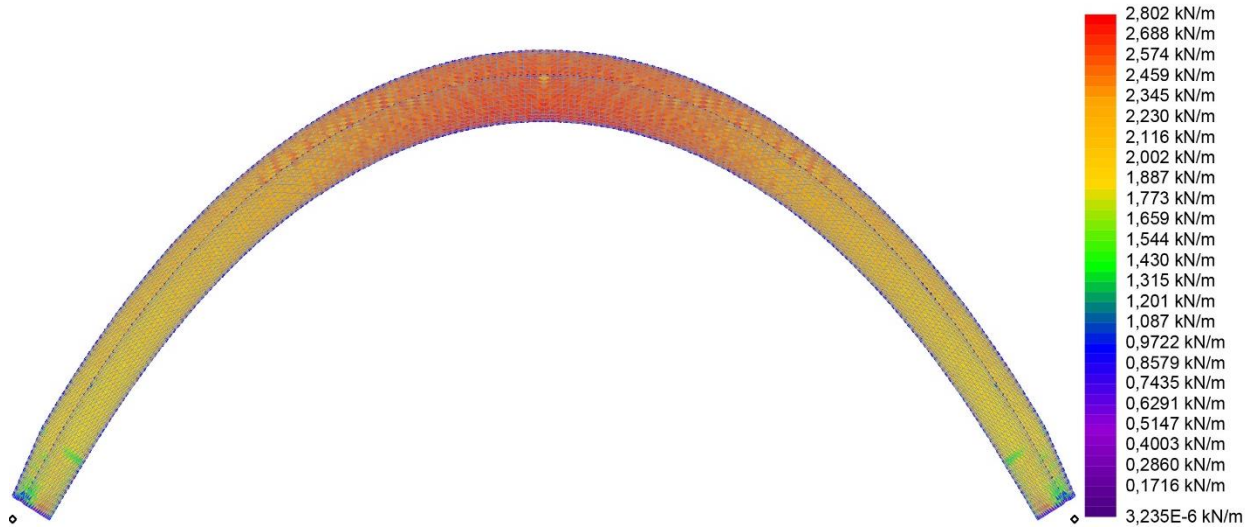
Point 3	
0 kg	4166
100 kg	4156
0 kg	4166
200 kg	4143
0 kg	4165
300 kg	4129
0 kg	4162
400 kg	4107
0 kg	4160
500 kg	4076
0 kg	4149
600 kg	4034
0 kg	4132
700 kg	3959
0 kg	4101
800 kg	3852
0 kg	4046

Appendix J

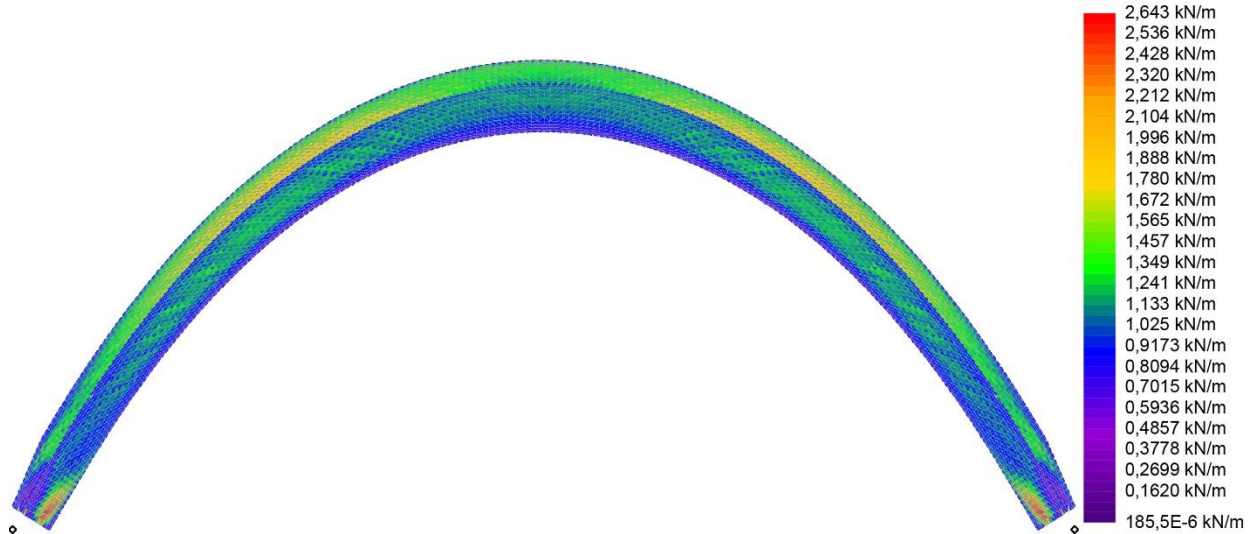
Start simulation (Resolved Element Translation)



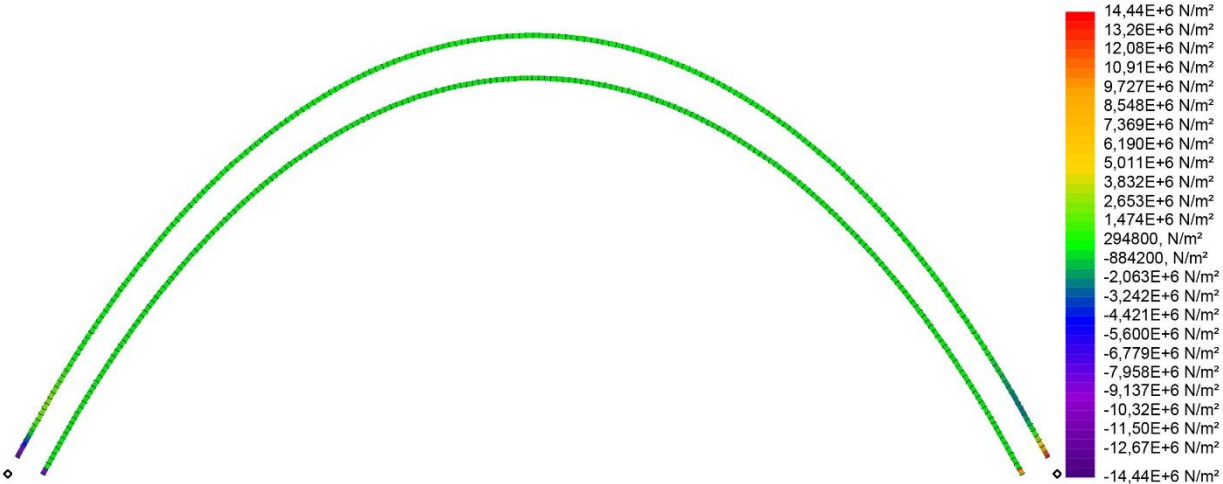
Start simulation (2D force Ny)



Start simulation (2D force Nx)



Start simulation (bending stress Bz + ve y)



Appendix K1

Comparison of start situation and altered variables (resolved element translation in mm)

Alteration in self-weight

	Bottom	Top
Start situation	-4,061	-2,367 = -1,694
Without self-weight	-3,985	-2,234 = -1,751

Alteration in internal pressure

	Bottom	Top
Start situation (100 mbar)	-4,061	-2,367 = -1,694
Lower internal pressure (50 mbar)	-2,344	-1,275 = -1,069
Higher internal pressure (200 mbar)	-7,424	-4,417 = -3,007

Alteration in Poisson ratio

	Bottom	Top
Start situation (0.4)	-4,061	-2,367 = -1,694
Lower Poisson ratio (0.3)	-4,346	-2,494 = -1,852
Higher Poisson ratio (0.5)	-3,760	-2,252 = -1,508

Alteration in Warp modulus

	Bottom	Top
Start situation (850 kN/m)	-4,061	-2,367 = -1,694
Lower warp modulus (700 kN/m)	-4,150	-2,457 = -1,693
Higher warp modulus (1000 kN/m)	-3,984	-2,288 = -1,696
Lower warp modulus (100 kN/m)	-4,823	-3,252 = -1,571

Alteration in Weft modulus

	Bottom	Top
Start situation (600 kN/m)	-4,061	-2,367 = -1,694
Lower weft modulus (400 kN/m)	-3,940	-2,248 = -1,692
Higher weft modulus (800 kN/m)	-4,110	-2,436 = -1,674
Lower weft modulus (50 kN/m)	-0,603	-2,604 = 2,001

Alteration in Shear Modulus

	Bottom	Top
Start situation (45 kN/m)	-4,061	-2,367 = -1,694
Lower shear modulus (30 kN/m)	-4,608	-2,919 = -1,689
Higher shear modulus (60 kN/m)	-3,631	-1,934 = -1,697
Lower shear modulus (5 kN/m)	-5,979	-4,314 = -1,665

Appendix K2

Comparison of start situation and altered variables (2D-force N_y in fabric outer layer)

Alteration in self-weight

	Bottom	Top	Average
Start situation	2,767	2,416	2,592
Without self-weight	2,767	2,417	2,592

Alteration in internal pressure

	Bottom	Top	Average
Start situation (100 mbar)	2,767	2,416	2,592
Lower internal pressure (50 mbar)	1,376	1,197	1,287
Higher internal pressure (200 mbar)	5,522	4,864	5,193

Alteration in Poisson ratio

	Bottom	Top	Average
Start situation (0.4)	2,767	2,416	2,592
Lower Poisson ratio (0.3)	2,762	2,421	2,592
Higher Poisson ratio (0.5)	2,772	2,411	2,592

Alteration in Warp modulus

	Bottom	Top	Average
Start situation (850 kN/m)	2,767	2,416	2,592
Lower warp modulus (700 kN/m)	2,767	2,416	2,592
Higher warp modulus (1000 kN/m)	2,767	2,416	2,592
Lower warp modulus (100 kN/m)	2,768	2,410	2,589

Alteration in Weft modulus

	Bottom	Top	Average
Start situation (600 kN/m)	2,767	2,416	2,592
Lower weft modulus (400 kN/m)	2,767	2,420	2,594
Higher weft modulus (800 kN/m)	2,767	2,414	2,591
Lower weft modulus (50 kN/m)	2,782	2,504	2,643

Alteration in Shear modulus

	Bottom	Top	Average
Start situation (45 kN/m)	2,767	2,416	2,592
Lower shear modulus (30 kN/m)	2,769	2,416	2,593
Higher shear modulus (60 kN/m)	2,765	2,416	2,591
Lower shear modulus (5 kN/m)	2,776	2,417	2,597

Appendix K3

Comparison of start situation and altered variables (2D-force N_y in fabric web)

Alteration in self-weight

	Bottom	Top	Average
Start situation	1,028	1,683	1,356
Without self-weight	1,016	1,686	1,351

Alteration in internal pressure

	Bottom	Top	Average
Start situation (100 mbar)	1,028	1,683	1,356
Lower internal pressure (50 mbar)	0,500	0,847	0,673
Higher internal pressure (200 mbar)	2,102	3,358	2,730

Alteration in Poisson ratio

	Bottom	Top	Average
Start situation (0.4)	1,028	1,683	1,356
Lower Poisson ratio (0.3)	0,988	1,692	1,340
Higher Poisson ratio (0.5)	1,070	1,674	1,372

Alteration in Warp modulus

	Bottom	Top	Average
Start situation (850 kN/m)	1,028	1,683	1,356
Lower warp modulus (700 kN/m)	1,029	1,683	1,356
Higher warp modulus (1000 kN/m)	1,027	1,682	1,355
Lower warp modulus (100 kN/m)	1,098	1,715	1,407

Alteration in Weft modulus

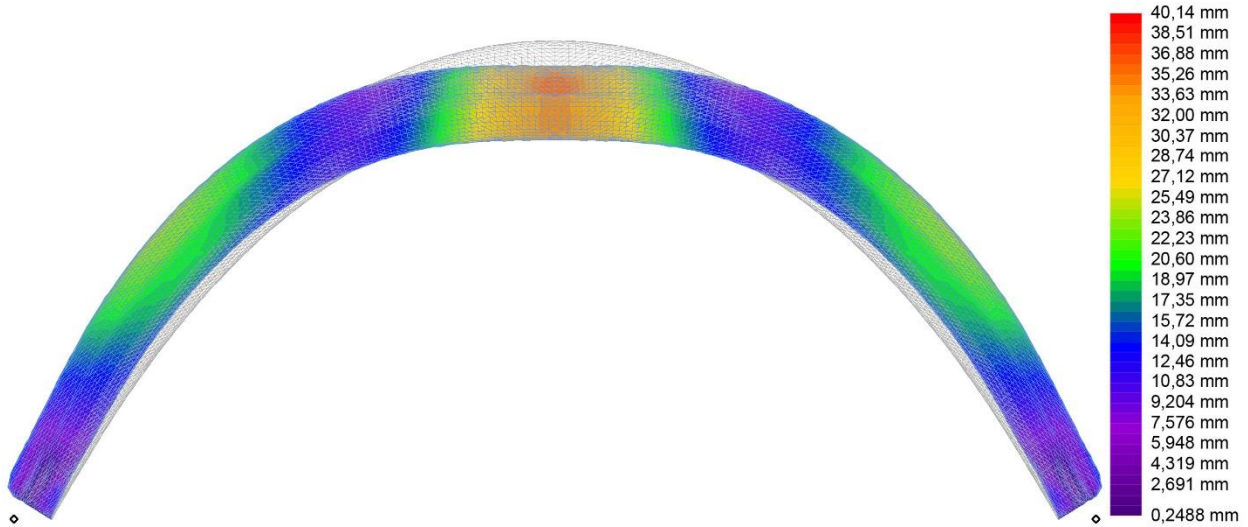
	Bottom	Top	Average
Start situation (600 kN/m)	1,028	1,683	1,356
Lower weft modulus (400 kN/m)	0,974	1,701	1,337
Higher weft modulus (800 kN/m)	1,057	1,672	1,365
Lower weft modulus (50 kN/m)	0,582	1,710	1,146

Alteration in Shear modulus

	Bottom	Top	Average
Start situation (45 kN/m)	1,028	1,683	1,356
Lower shear modulus (30 kN/m)	1,003	1,685	1,344
Higher shear modulus (60 kN/m)	1,048	1,681	1,365
Lower shear modulus (5 kN/m)	0,946	1,689	1,317

Appendix L1

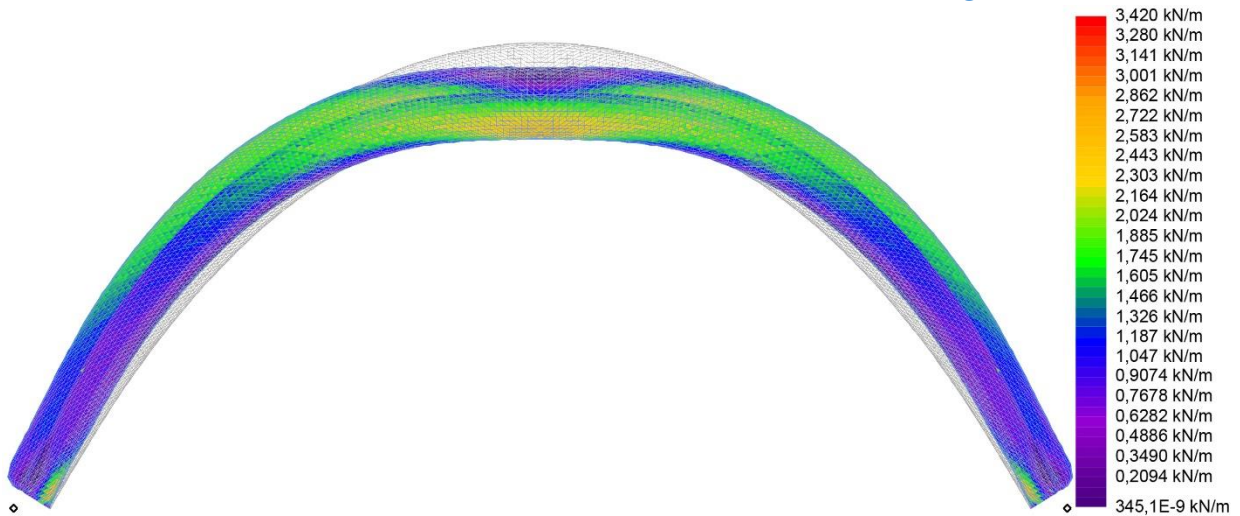
Simulation results with a load in the middle (Resolved Element Translation, deformation magn. x8)



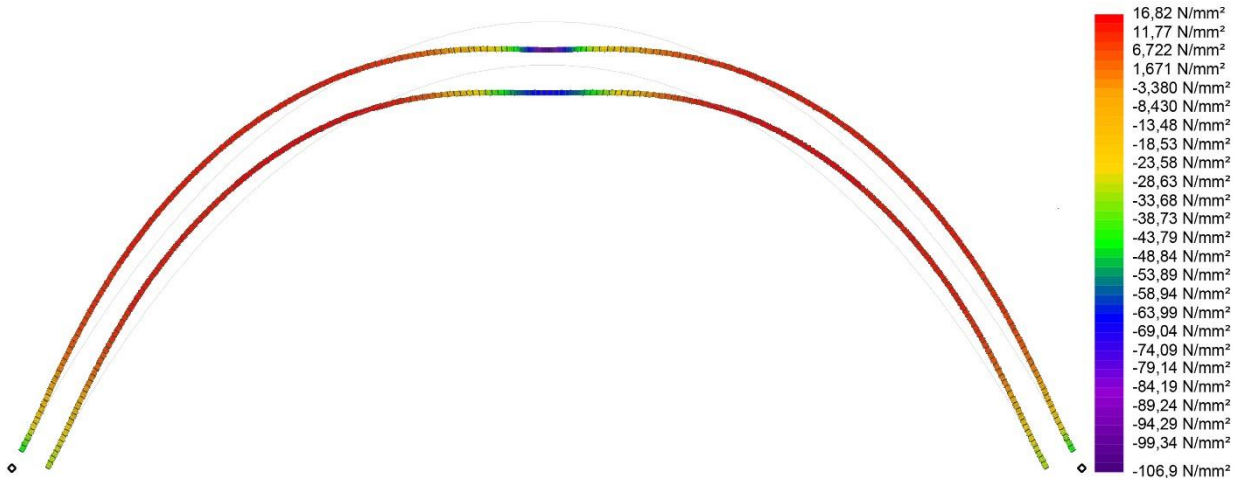
Simulation results with a load in the middle (2D-force Ny, deformation magn. x8)



Simulation results with a load in the middle (2D-force Nx, deformation magn. x8)

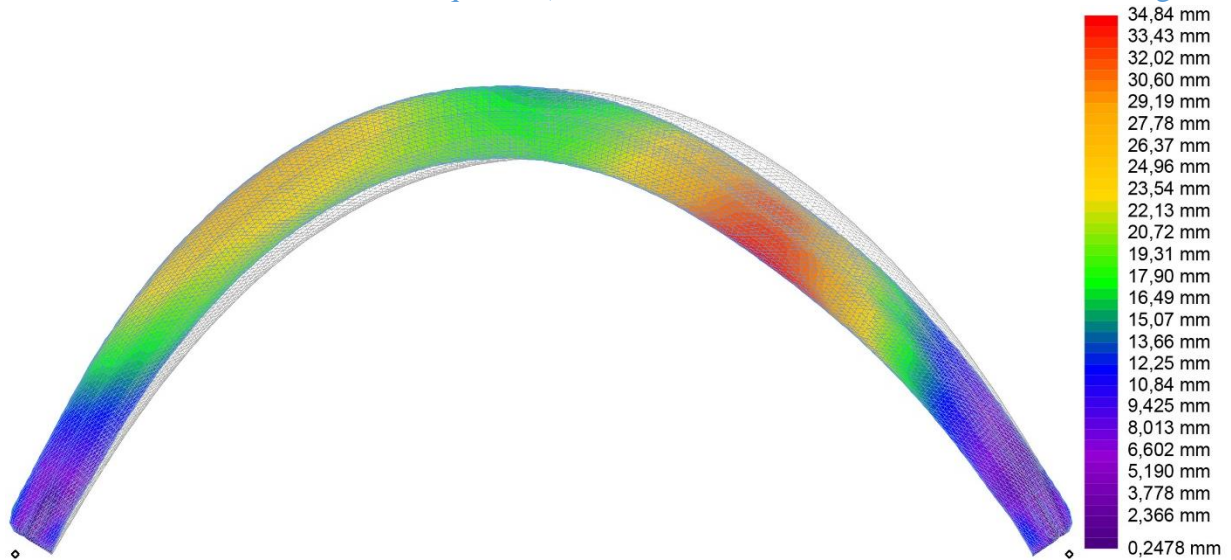


Simulation results with a load in the middle (Bending stress Bz +ve y, deformation magn. x8)

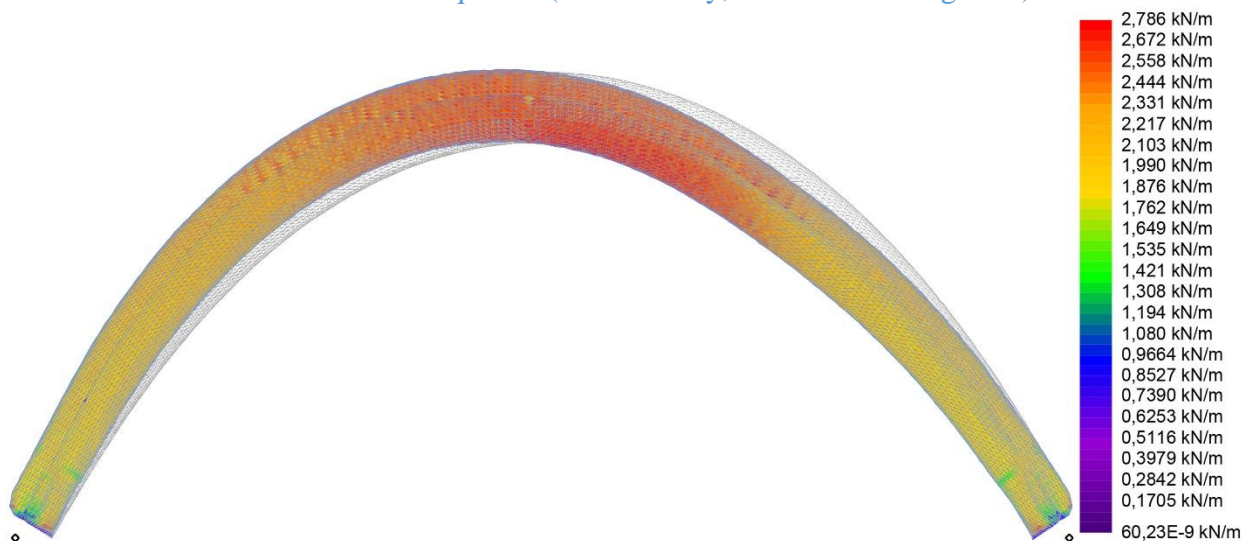


Appendix L2

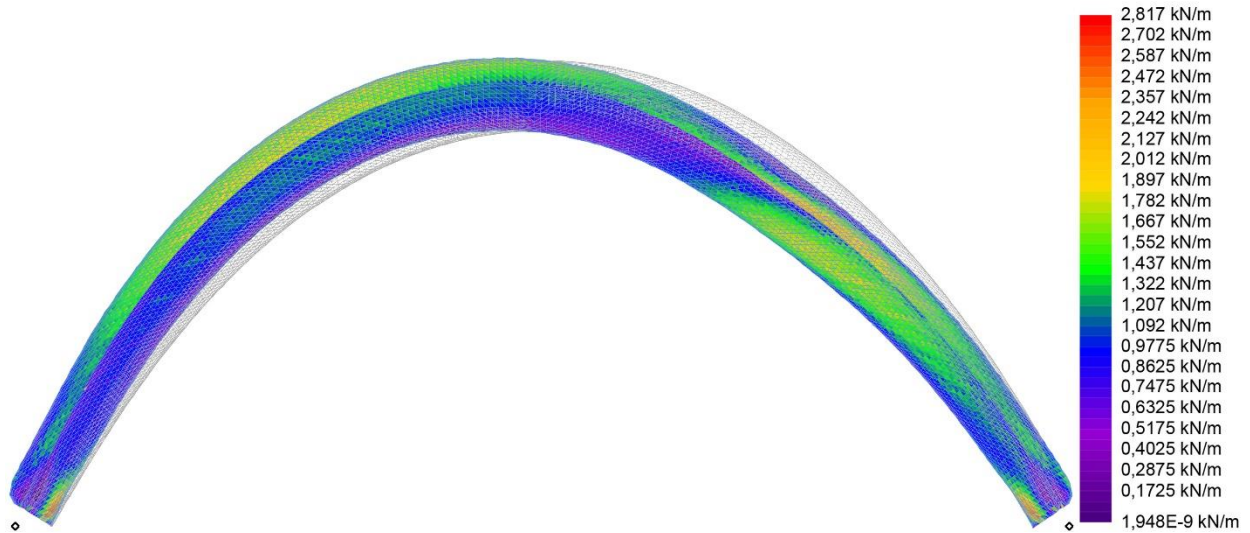
Simulation results with a load at a quarter (Resolved Element Translation, deformation magn. x8)



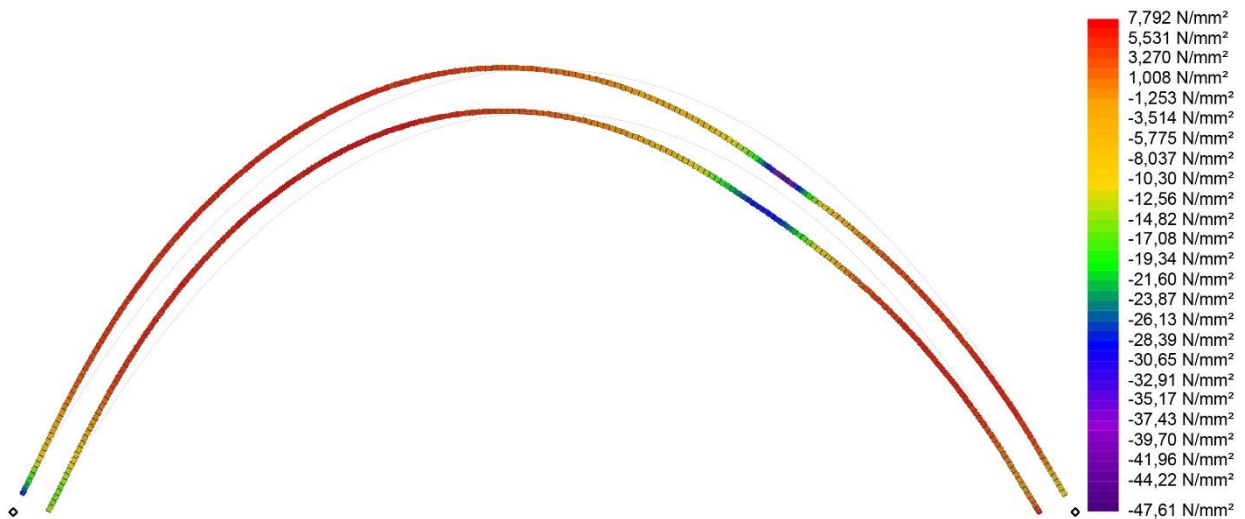
Simulation results with a load at a quarter (2D-force Ny, deformation magn. x8)



Simulation results with a load at a quarter (2D-force Nx, deformation magn. x8)

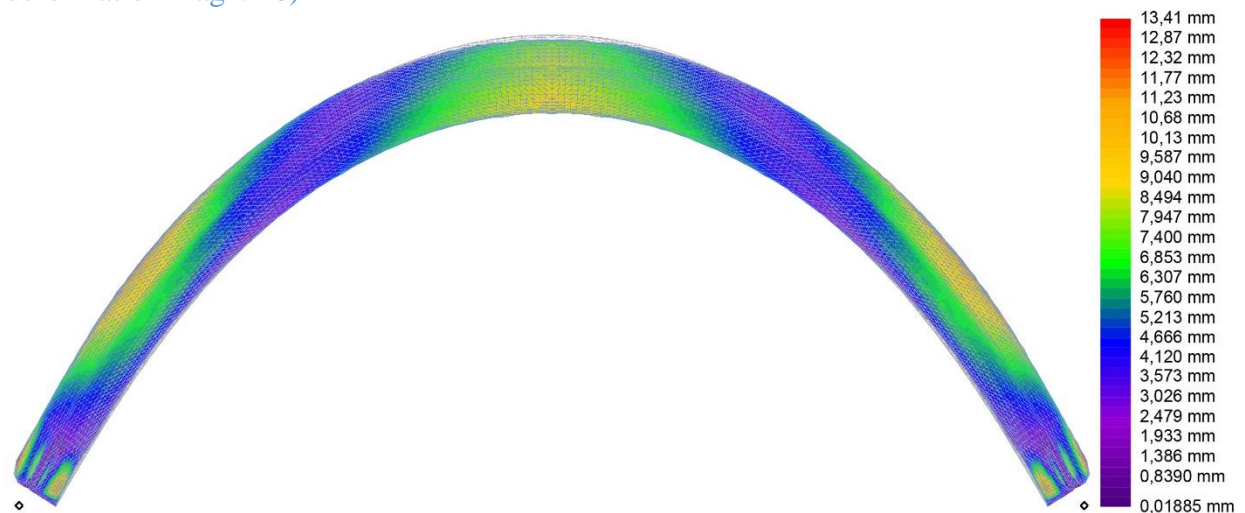


Simulation results with a load at a quarter (Bending stress Bz + ve y, deformation magn. x8)



Appendix L3

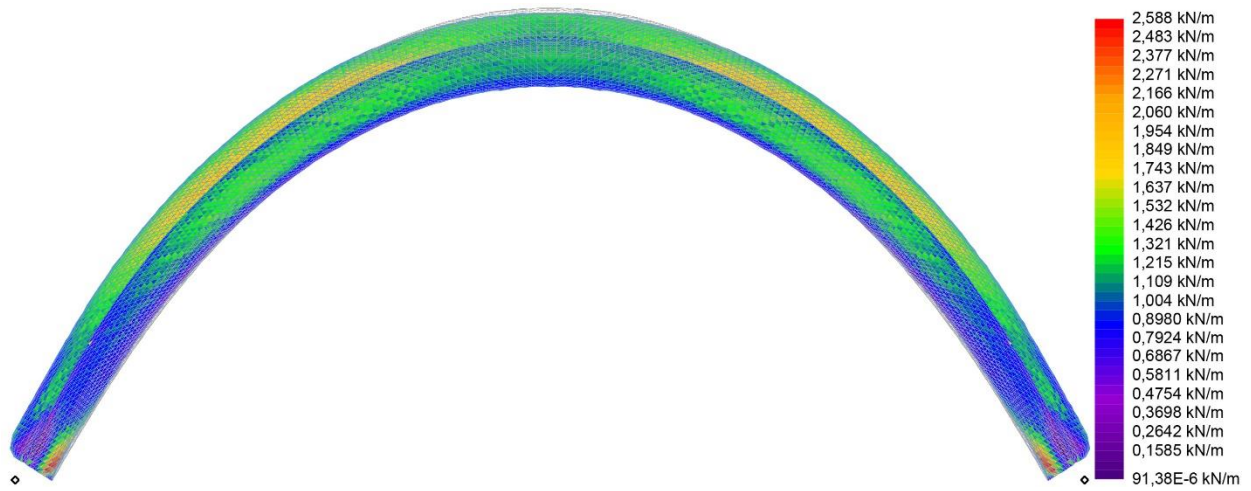
Simulation results with a load distributed over five points (Resolved Element Translation, deformation magn. x8)



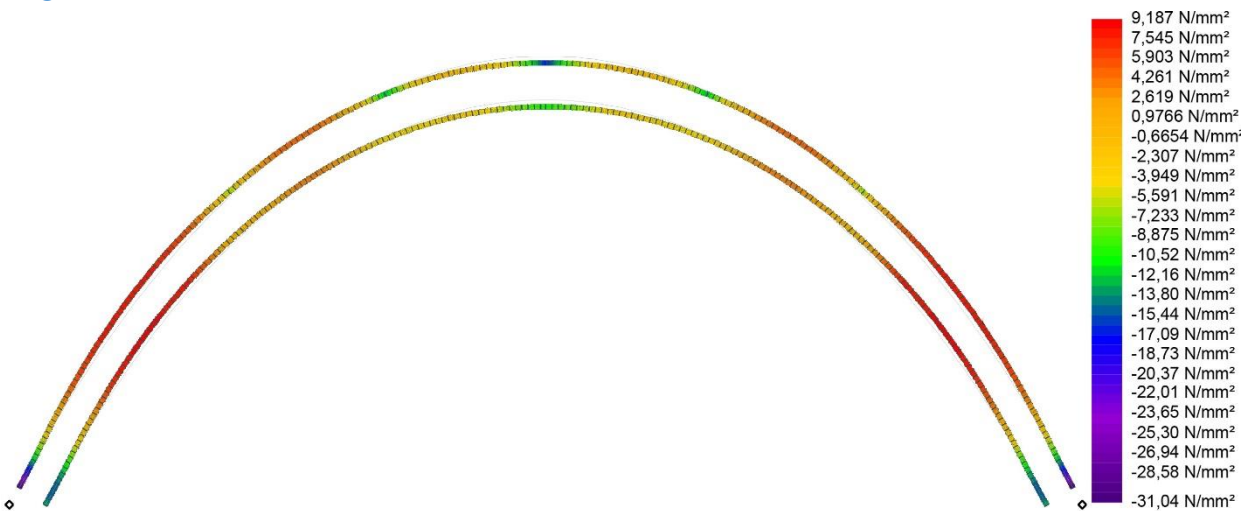
Simulation results with a load distributed over five points (2D-force Ny, deformation magn. x8)



Simulation results with a load distributed over five points (2D-force Nx, deformation magn. x8)

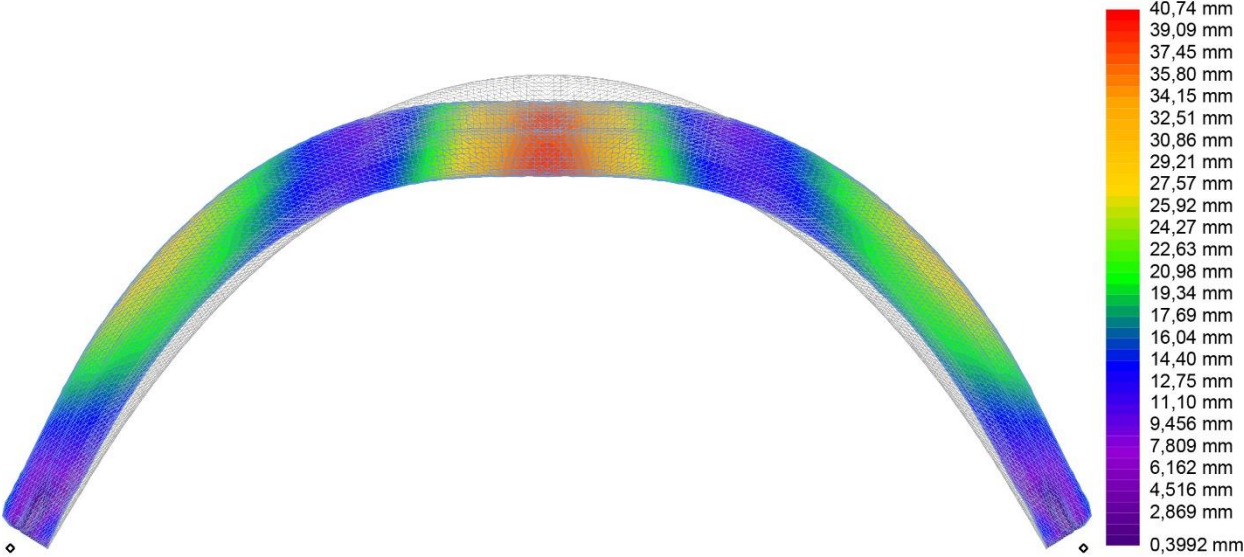


Simulation results with a load distributed over five points (Bending stress Bz + ve y, deformation magn. x8)

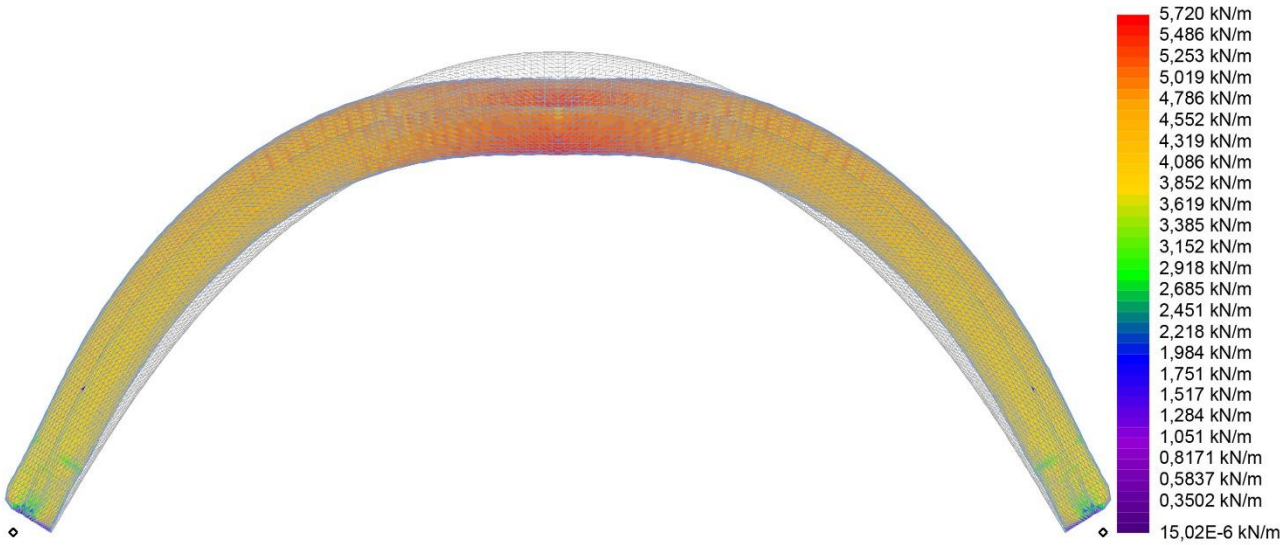


Appendix M

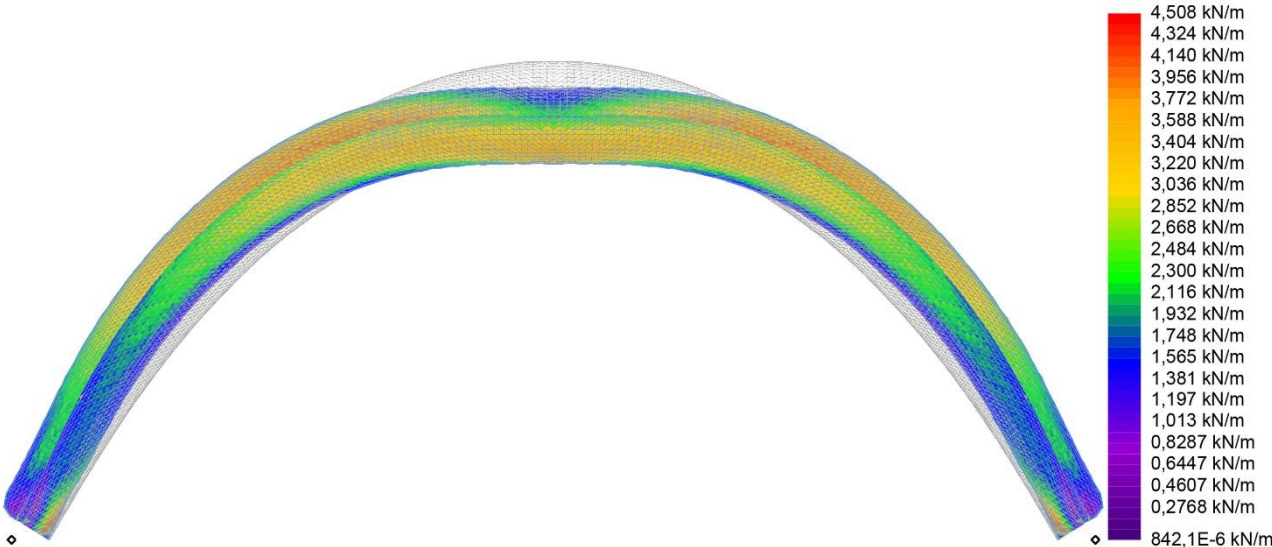
Simulation results with a load in the middle and a higher internal pressure (Resolved Element Translation, deformation magn. x8)



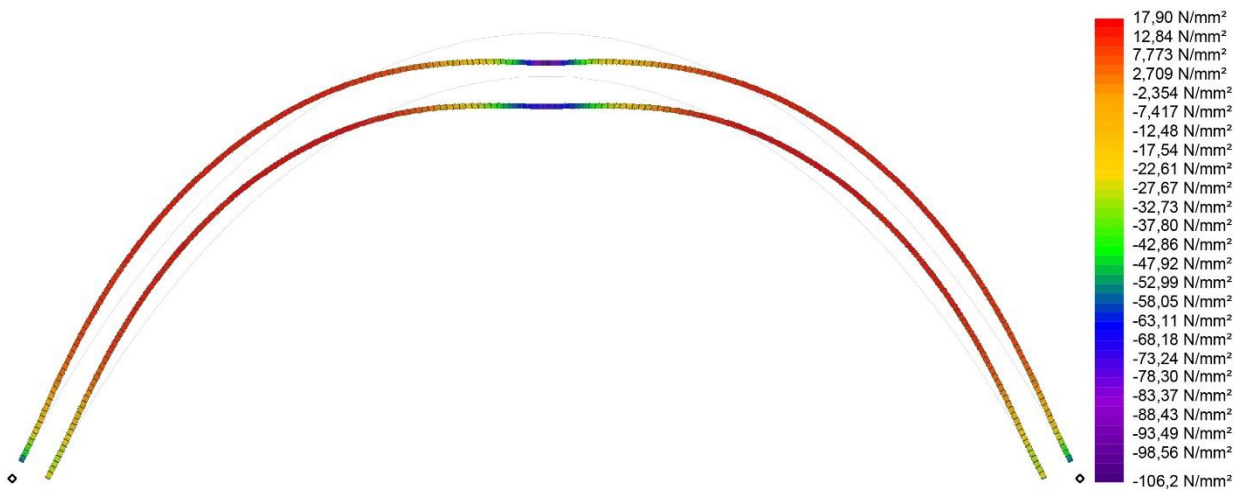
Simulation results with a load in the middle and a higher internal pressure (2D-force N_y , deformation magn. x8)



Simulation results with a load in the middle and a higher internal pressure (2D-force Nx, deformation magn. x8)

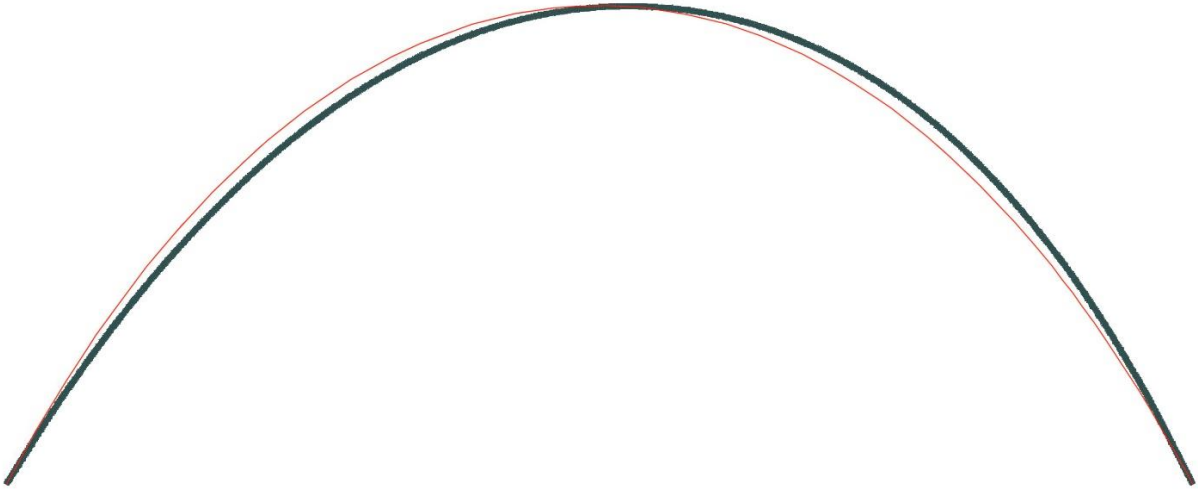


Simulation results with a load in the middle and a higher internal pressure (Bending stress Bz +ve y, deformation magn. x8)

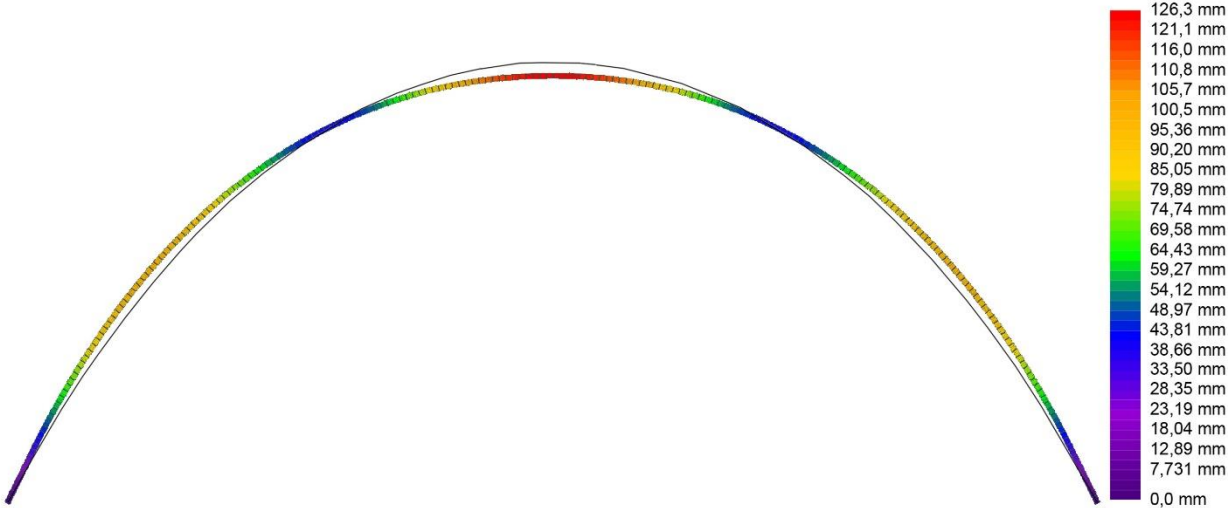


Appendix N

Asymmetry test: start situation (red = symmetric, black = asymmetric)



Asymmetry test: symmetric version with point load in middle



Asymmetry test: asymmetric version with point load in middle

